INTEGRATION OF THE MICROCIRCUITRY OF THE DEEP CEREBELLAR NUCLEI INTO CANONICAL CEREBELLAR CIRCUITS

by

Gregory James Wojaczynski

B.A., University of California at Berkeley, 2011

Submitted to the Graduate Faculty of

The Kenneth P. Dietrich Graduate School of

Arts and Sciences in partial fulfillment

of the requirements for the degree of

Doctor of Philosophy

University of Pittsburgh

2016

UNIVERSITY OF PITTSBURGH

DIETRICH SCHOOL OF ARTS AND SCIENCES

This dissertation was presented

By

Gregory James Wojaczynski

It was defended on

March, 28th 2016

and approved by

Peter Strick, Ph.D., Professor

Linda Rinaman, Ph.D., Professor

Alan Sved, Ph.D., Professor

Christiaan de Zeeuw, M.D., Ph.D., Professor

Dissertation Advisor: J. Patrick Card, Ph.D., Professor

INTEGRATION OF THE MICROCIRCUITRY OF THE DEEP CEREBELLAR NUCLEI INTO CANONICAL CEREBELLAR CIRCUITS

Gregory James Wojaczynski, Ph.D.

University of Pittsburgh, 2016

Defining the anatomical organization of cerebellar circuits has been the pursuit of neuroanatomists for over a century. The regular, repeated cytoarchitecture across the entire extent of the cerebellar cortex has led to an alluring promise that by understanding how a small patch of cortex processes information, we can generalize this finding to understand how the cortex functions as a whole. While great progress has been made to characterize cortical circuits, there has been a relative paucity of studies examining the microcircuitry of the deep cerebellar nuclei. Recent studies have shown that the deep nuclei are not passive relays of cortical processing but rather are highly sophisticated nodes within the cerebellum that have the capacity to both store memory traces and function without cortical input. The local network of the deep nuclei consists of at least six cell types and to date little information is known as to how these cells are synaptically linked, and how the cortex feeds into this network. The heterogeneity of the deep nuclei and the limitations of monosynaptic tracing techniques have hindered efforts to fully define the microcircuitry that supports nuclear processing. The advent of viral transneuronal tracing gives us the opportunity to probe the multisynaptic networks that are so characteristic of cerebellar circuits. The studies in this dissertation were designed to define the microcircuitry of the deep nuclei by utilizing monosynaptic and viral transneuronal tracing.

First we provide evidence for largely non-collateralized projections from Purkinje cells onto principal or nucleo-olivary projection neurons using a dual viral tracing paradigm. In the

second study we combine classical and viral tracing to provide strong evidence supporting the longstanding hypothesis that the inferior olive and cerebellum form a series of parallel, closed-loop circuits. Lastly we demonstrate, using monosynaptic tracing, a novel excitatory nucleo-cortical projection from the parvocellular interpositus nucleus targeting the Purkinje cell layer of the paraflocculus. Our studies, while confirming some aspects of cerebellar dogma, cast serious doubt onto the long held assumptions that the deep cerebellar nuclei are relay nuclei. These new findings suggest a substantial revision to cerebellar functional theories is necessary.

TABLE OF CONTENTS

LIST OF FIGURES

PREFACE

All of the work presented here would not have been possible in the least without the emotional and material support of many individuals, and in particular, my mentor J. Patrick Card, Ph.D. and lab manager Karina Steren, MPH. Dr. Card provided me with the means and freedom to explore cerebellar circuits using viral transneruonal tracers as a graduate student; more importantly, however, he taught me how to be a scientist. He helped to focus my mind from that of a naïve, fresh-out-of-college, first-year graduate student to one of a discerning, deliberate investigator. I know that years from now I will still be incorporating his guidance into my work and I cannot thank him enough for giving me the chance to learn from him. Karina Steren has been my friend and partner in lab since I joined in 2012. Without her help, I would not know the first thing about the vast majority of the lab procedures I employed over the course of my graduate career. She patiently taught me the technical skills necessary to complete these experiments and was always more than willing to help out whenever I fell behind. Pat and Karina, I am eternally indebted to you.

I'd like to thank my committee members Linda Rinaman, Ph.D., Alan Sved, Ph.D., and Susan Sesack, Ph.D. who helped to keep me on track to actually complete my dissertation in a reasonable amount of time. Without them I would have been conducting additional experiments for years in order to satisfy my own scientific curiosity. My committee chair, Peter Strick, Ph.D., provided me with the intellectual expertise necessary to investigate the cerebellum using

transneuronal viral tracing and gave me some of the best advice I have ever received. I also want to sincerely thank my outside examiner Christiaan de Zeeuw, M.D., Ph.D. Having Dr. de Zeeuw serve as my outside examiner was truly an honor as his work has deeply influenced and inspired my own. Speaking with him about my work was such a rewarding and challenging experience and I consider it a privilege to have had that opportunity.

Additionally, many others have lent me their invaluable technical assistance during my stay at the University of Pittsburgh. I want to thank Tom Harper for teaching me how to operate the confocal and electron microscopes; without his help I would not have been able to conduct many of the analyses present here. Thank you to David Volk, M.D., Ph.D. and Elizabeth Sengupta for teaching me *in situ* hybridization, which was more than a generous undertaking. Over the course of my graduate studies I have had seven undergraduates that helped me both complete technical aspects of my experiments and gave me an opportunity to develop my own mentoring techniques. In order of their joining of the lab: Timothy Ohlsen, Michelle Richard, Sasha Safonova, Niaz Khan, Michael Oltman, Margaret Jia, and Lee Harkless. Their individual contributions are too numerous to list here and so I will simply say thank you so much for the immense support you all have given me.

Finally, I'd like to thank my friends and family for all the love and support they provided. My parents, Alicia and Dave, and my siblings, Brittany and Scott, have always had my back and encouraged me whenever I waivered. My friends and roommates Kristine Ojala and Randy Lee, thank you so much for the emotional support to make it through to the end of graduate school. Without you two my final days would have been filled with more stress than I could have handled. To everyone listed here, and to everyone else I could not fit but helped me nonetheless, from the bottom of my heart, thank you!

List of Abbreviations

BDA	biotinylated dextran amine
Cb	calbindin
ChAT	choline acetyltransferase
CTβ	cholera toxin, beta subunit
DAO	dorsal accessory olive
DCN	deep cerebellar nuclei
dlh	dorsal lateral hump
DM	dorsal medial group of the inferior olive
FG	Fluorogold
GABA	gamma-aminobutyric acid
GAD67	glutamic acid decarboxylase
GFP	green fluorescent protein
IO	inferior olive
IP	interpositus nucleus
MAO	medial accessory olive
MLI	molecular layer interneuron
NC	nucleo-cortical
NeuN	neuronal nucleus (protein)
NOPN	nucleo-olivary projection neuron
OCNO	olivo-cortico-nucleo-olivary
PC	Purkinje cell

pcIP	parvocellular interpositus
PO	principal olive
PPN	principal projection neuron
PRV	pseudorabies virus
PT	Purkinje cell targeting
RFP	red fluorescent protein
RN	red nucleus
TH	tyrosine hydroxylase
μm	micrometer
μl	microliter

1.0 GENERAL INTRODUCTION

"It should be obvious already that the cerebellum has nothing to do with conscious or other higher order activities" (Ramón y Cajal, 1995). Santiago Ramón y Cajal's singular genius led us to the neuron doctrine and a solid first grasp of the organization of the brain, but he failed to appreciate the versatility of the cerebellum. A growing literature now clearly demonstrates that the cerebellum participates not just in adaptive motor control (Taylor and Ivry, 2014) but also in associative learning (Thompson and Steinmetz, 2009), higher-order cognitive processes (Bostan et al., 2013; Schmahmann, 2004; Strick et al., 2009), affect (Dolan, 1998; Schmahmann, 2010), autonomic regulation (Dietrichs and Haines, 1989; Haines and Dietrichs, 1989), and a variety of neurological disorders including Autism Spectrum Disorders (D'Mello and Stoodley, 2015; Reeber et al., 2013). All of these computations are supported by a set of four heterogeneous deep cerebellar nuclei (DCN) surrounded by an elegant, virtually uniform cerebellar cortex. Due to the crystalline organization of the cerebellar cortex, the prevailing theories on cerebellar function posit that its functional diversity arises by virtue of a mosaic of its afferent innervation by climbing fibers from the inferior olive and mossy fibers from the pontine nuclei and the medullary reticular formation (Cerminara et al., 2013; Pijpers et al., 2006; Pijpers et al., 2005; Witter and De Zeeuw, 2015). These two classes of afferent projections delineate a series of parasagittal zones called modules, which span the cortex and are thought to represent the cerebellum's basic computational unit (Ruigrok, 2011). Purkinje cell phenotypic markers such

as zebrin II (Ahn et al., 1994; Brochu et al., 1990), HSP25 (Armstrong et al., 2009; Armstrong et al., 2001) and HNK-1 (Marzban et al., 2004) recapitulate these modules, marking stripes of PCs that run perpendicular to the lobular folding of the cortex.

In contrast to the exquisite detail in which the cortex has been parceled, the synaptology and functional organization of the DCN, which convey cortical processing to extracerebellar effector nuclei, is only understood in general principles (Uusisaari and De Schutter, 2011). With the exception of a relatively small projection to the vestibular nuclei (Shin et al., 2011) and the locus coeruleus (Schwarz et al., 2015), the deep cerebellar nuclei are the sole synaptic targets of Purkinje cells in the cortex. This positions the DCN as the gate through which the cerebellum communicates with the rest of the brain. Understanding the unique microcircuitry of the deep cerebellar nuclei will be critical for ascertaining how differences among the nuclei enable a cytoarchitecturally uniform cerebellar cortex to support a multitude of different behaviors.

1.1 A MODEL BEHAVIOR FOR CEREBELLAR FUNCTION

In order to fully appreciate and understand the organization of neural circuits, it is important to place them in a functional context. One of the most well studied behaviors supported almost entirely by the cerebellum is eyeblink conditioning (Thompson and Steinmetz, 2009). In this behavioral paradigm experimental animals are exposed to two types of stimuli: neutral and aversive. The neutral stimulus is typically a tone (Halverson and Freeman, 2010a), light (Halverson and Freeman, 2010b), or tactile simulation (Carrel et al., 2012; Flaten and Blumenthal, 1998) that normally does not generate a reflexive movement (conditioned stimulus; CS). The aversive stimulus is either an airpuff onto the cornea (Heiney et al., 2014b) of the

animal or a small electric shock to the periorbital region (Horiuchi and Kawahara, 2010). Both of these aversive stimuli cause a reflexive blinking of the eye (unconditioned stimulus; US). If the stimuli are presented randomly, then the animal never changes its responses to each stimulus (no response for CS; blink for US). But if the US is always presented at the end of the CS, such that the CS is predictive of the US, the animal learns this association. This learning is observed as the animal blinking in response to the CS, even if no US is actually present. Eyeblink conditioning is taken as one of the simplest learned sensorimotor associations and is used as a proxy to study how different components of cerebellar circuitry support different aspects of both this and more complex behaviors.

Efforts to map the key nodes of the neural pathways supporting eyeblink conditioning have yielded great success. Numerous studies have shown that all of the necessary circuits for eyeblink conditioning lie either within the cerebellum, or its corresponding sensory input and motor output pathways (for review see (Thompson and Steinmetz, 2009)). For example, tracing studies have established that the muscle that closes the eyelid (orbicularis oculi muscle) is innervated by the dorsal lateral facial nucleus, which receives input from the dorsal lateral red nucleus, a direct target of the cerebellum (Gonzalez-Joekes and Schreurs, 2012; Morcuende et al., 2002). These studies and a number of behavioral, pharmacological and electrophysiological studies have further demonstrated that the critical region within the DCN controlling conditioned eyeblinks is the anterolateral anterior interpositus nucleus (Chen and Evinger, 2006; Heiney et al., 2014b). Although initial attempts to localize the region(s) within the cerebellar cortex that support conditioning pointed to part or all of the simplex lobules (HVI), it has now been established that a micro-region within the base of the lobule HVI is one of the primary cortical regions participating in eyeblink conditioning (Heiney et al., 2014a; Steinmetz and Freeman,

2014). Input to this circuit stems from the dorsal accessory nucleus of the inferior olive and different subregions of the pontine nuclei depending on the modality of the conditioned stimulus (Halverson and Freeman, 2010a, b; Mauk et al., 1986). It has been further established that there is a somatotopic map within the IP such that the lateral IP supports conditioning in more rostral areas of the animal (i.e., eyelids) and the medial IP supports conditioning in the caudal aspects of the animal (i.e., hind limb; (Mojtahedian et al., 2007)). With the major nodes of the eyeblink conditioning circuit established, the next step forward is to understand how the local circuitry within these nodes, and the synaptology of the connections *between* the nodes is organized in order to support eyeblink conditioning.

1.2 THE CANONICAL CIRCUIT

Over the course of the late 19th and early 20th centuries, much of the cortical cerebellar circuitry was established, largely due to the pioneering anatomical work of Santiago Ramon y Cajal (Ramón y Cajal, 1995). The vast majority of input to the cerebellum stems from two parallel afferent systems: the mossy fiber/parallel fiber circuit and the climbing fiber circuit. Recording studies have established that during eyeblink conditioning, the mossy fiber system is responsible for the transmission of CS signals to cerebellum (Halverson and Freeman, 2010a, b). In fact conditioning can take place with direct stimulation of the pontine nuclei as a replacement for an external CS and lesioning mossy fiber sources prevents this type of associative learning (Campolattaro and Freeman, 2008; Steinmetz et al., 1989).

Mossy fibers originate from a variety of extracerebellar sources, such as the pontine nuclei (Oka et al., 1985) and the lateral reticular nucleus (Matsushida and Ikeda, 1976), and enter the

cortex to target granule and Golgi cells in the granular layer. Granule cells in turn issue ascending axons that bifurcate in the molecular layer and can course for well over a millimeter parallel to the axis of lobular folding. Across their entire extent, parallel fibers make excitatory synaptic contacts onto the distal dendrites of PCs. Due to the size of PC dendritic trees and the sheer number of granule cells (~80 billion in humans), PCs can receive up to 200,000 synapses from individual granule cells (Tyrrell and Willshaw, 1992). This gives each granule cell only weak influence on the overall activity of PCs, and therefore many must be active in order to initiate a spike from PCs.

Climbing fibers on the other hand are thought to convey information of the unconditioned stimulus. These fibers fire in a rhythmic fashion, typically firing one action potential per second (1 Hz; (Llinás, 2011)). When the US is presented to the animal however, climbing fibers will fire in response, signaling what has been theorized as an error signal (Popa et al., 2016; Schweighofer et al., 2013). For example once the animal learns to blink in response to the CS, thus protecting its eye from the puff, climbing fibers will stop firing in response to the puff. Consequently substituting directly electrical stimulation of climbing fibers for a US is still sufficient to drive learning (Mauk et al., 1986).

The anatomy of the climbing fibers differs dramatically from the mossy/parallel fiber system. Climbing fibers originate solely from the inferior olive (IO) and directly innervate PCs through a powerful series of several hundred synapses from a single axon onto its dendritic tree (Sugihara et al., 1999). A single climbing fiber will collateralize to innervate approximately 7 PCs that span across lobules but are all within the same parasagittal strip, which closely aligns with the parasagittal strips stained for Zebrin II (Sugihara and Shinoda, 2004). Importantly each PC is innervated by one and only one climbing fiber. This, combined with its density of synaptic

contacts, gives the climbing fiber complete control of the PC such that if the climbing fiber fires an action potential, the PC necessarily follows suit (Eccles et al., 1966).

The canonical circuit virtually ends at the PC. Once both mossy and climbing fiber signals have been integrated by the PC, it projects into the deep cerebellar nuclei where it directly controls output neurons. In this view, the deep nuclei have been regarded as relay stations, simply reversing the sign of PC action potentials (Marr, 1969). However, PCs are not the only source of afferent input to PPNs. Both the climbing fiber system (De Zeeuw et al., 1997; Shinoda et al., 2000) and the mossy fiber system (Mihailoff, 1994; Shinoda et al., 1992) issue direct collaterals into the DCN, bypassing the cortex. These collaterals allow the DCN to function, albeit non-optimally, without an intact cortex (Garcia and Mauk, 1998; Luque et al., 2014). For example when large parts of Lobule HVI were aspirated, but spared the DCN, animals are still able to slowly learn new conditioned responses (Lavond and Steinmetz, 1989). The fact that the DCN can function without the considerable processing taking place in the cortex demonstrates that the DCN play a much more involved role in cerebellar behaviors than would be expected of simple relays of cortical signals.

1.3 THE DEEP CEREBELLAR NUCLEI

The cerebellar nuclei have largely been regarded as mirrors of cerebellar cortical processing, reversing the inhibitory signal of Purkinje cells to an excitation of the thalamus and other premotor pathways. In terms of eyeblink conditioning and other cerebellar behaviors, the entirety of the deep nuclei is often boiled down to a single cell type: the principal projection neuron (PPN). PPNs are large excitatory neurons that provide the main projection system

through which the cerebellum interacts with other levels of the neuraxis. PPNs primarily target the red nucleus, which then directly drives motoneurons, and the thalamus, which, in turn projects to many regions of the cerebral mantle (Bostan et al., 2013; Gonzalez-Joekes and Schreurs, 2012; Kelly and Strick, 2003; Morcuende et al., 2002; Ruigrok and Teune, 2014; Sun, 2012). Recording studies have consistently shown that PPNs are activated when movement occurs, suggesting that they contribute to maintaining ongoing behaviors (Heiney et al., 2014b). However, PPNs are also able to directly drive motor output, as optogenetic dis-inhibition of PPNs has been demonstrated to be sufficient for driving facial movements, including eyeblinks (Heiney et al., 2014a).

The dis-inhibitory control of PPNs by the cortex (Ito et al., 1964) has been a key piece of the prevailing theory of cerebellar function: the Marr-Albus-Ito model (Albus, 1971; Ito, 1984; Ito and Kano, 1982; Marr, 1969). This model theorizes that PPNs are activated by PCs briefly silencing their output to the deep nuclei. Since PPNs have a resting membrane potential that lies above threshold for action potential generation, they are constitutively active without synaptic input (Uusisaari and Knöpfel, 2012). The cortex is thought to provide constant suppression PPN firing via GABAergic PC synapses onto PPNs, whereas relaxtion of this inhibitory drive briefly allows PPNs to fire. Indeed, while parts of this model hold true, recent work has increasingly called the validity of this theoretical framework into question. For example, many Purkinje cells actually *increase* their firing rates during movements, instead of briefly pausing (Miller et al., 2002), and synchronized PC input to PPNs has been shown to robustly drive PPNs to fire (Person and Raman, 2012a, b). Furthermore, the depression in PC firing is theorized to be driven by climbing fiber responses to error signals. Support has been found for this, with recording studies demonstrating that when a climbing fiber fires on a trial, the probability that it fires again

during the same time period on the next trial decreases (Medina and Lisberger, 2008). A recent report challenged this theoretical framework by demonstrating that climbing fibers may initially convey error messages, but late into conditioning convey the *expectation* of error (Ohmae and Medina, 2015). In support, climbing fibers initially respond to an aversive airpuff, but over the course of training climbing fibers lose this response and instead fire in response to the predictive conditioned stimulus. Since the precise timing of climbing fiber input at the time of error is an essential feature of the Marr-Albus-Ito model, serious revisions are necessary in order to reconcile this theory with existing data.

Although the Marr-Albus-Ito model focuses heavily on how cortical processing affects the activity of PPNs, it is important to remember that the DCN are not composed of a single cell type. Within the DCN there exist at least six different phenotypes of neurons, with at least two being dedicated local interneurons (Uusisaari and Knöpfel, 2011; Uusisaari and Knöpfel, 2012). The second major projection system stemming from the cerebellum is the nucleo-olivary circuit. This system arises from very small GABAergic neurons that are distributed throughout the DCN and project exclusively to the inferior olive (Legendre and Courville, 1987; Ruigrok and Teune, 2014; Teune et al., 1995). Relatively little is known regarding the activity of nucleo-olivary projection neurons (NOPNs). Although the IO has been observed to be inhibited during movement, no recoding study has conclusively shown that NOPNs are actually active during this time period (Hesslow and Ivarsson, 1996). Given their small size (~10-15μm in diameter), NOPNs have been difficult to isolate in *in vivo* recordings, and to date only one report has been published detailing their activity under anesthesia (Giaquinta et al., 1999). Recently, NOPNs were recorded in slices for the first time, and their integration of PC input was assessed in relation to PPNs (Najac and Raman, 2015). Najac and Raman found that unlike PPNs, which

respond to synchronized PC input, NOPNs are strongly depressed by PC inhibition and do not display robust rebound potentials as PPNs do. Such a stark contrast in responses to the same cortical input begs the question of from where exactly the cortical input to these two neurons arises.

The issue of how cortical input is anatomically integrated in different DCN neurons was explored in two highly influential electron microscopic reports. The first used immunocytochemistry to label all PC axons, GABAergic neurons and glycinergic neurons in the DCN (De Zeeuw and Berrebi, 1995a, b). The authors found that individual PC axons collateralize to innervate both GABAergic and unlabeled (putatively glutamatergic) neurons at a rate of approximately 3% in single sections; this rate increased to 9% in analyses of serial sections. However, there exists at least one GABAergic local interneuron in the DCN, so it was unclear whether or not this result could be generalized to inputs onto PPNs and NOPNs specifically. Accordingly, Teune and colleagues (1998) reported results from an impressive triple tracing study that labeled PPNs and NOPNs with retrograde tracers and PC axons with an anterograde tracer. In areas of DCN where all three labeled profile could be found, they reported that approximately 2.5% (9 of 367 profiles) of PC axons collateralize to innervate both NOPN and PPN populations (Teune et al., 1998). From these data the authors concluded that it is likely that all or most Purkinje cells collateralize to innervate both cell types, though they do leave open the possibility that subsets of PCs innervate only one class of cells. This report, while convincingly demonstrating that PCs *can* collateralize onto both PPNs and NOPNs, is difficult to generalize to the entire projection system throughout the DCN, due to the narrow scope inherent in ultrastructural analyses. It is currently unclear whether or not the collateralization seen by Teune and colleagues is the exception or the rule. It is often posited that the activity of NOPNs

can be assumed to be similar to PPNs, if indeed they are under the exact same influence from Purkinje cells (Uusisaari and De Schutter, 2011; Uusisaari et al., 2007; Uusisaari and Knöpfel, 2012). However, given the data from Raman and colleagues demonstrating opposite responses to the same pattern of PC input, it is worthwhile to question whether or not they do receive the same inputs.

Apart from defining the exact targets of PCs in the DCN, another important goal is to characterize the local circuit networks that integrate PC afferents into a coherent output. Currently there are six putative cell types in the DCN and only sparse data indicating how they might be wired to one another locally (Uusisaari and De Schutter, 2011; Uusisaari and Knöpfel, 2011). The most well documented synaptic connection in the DCN is from a glycinergic (possibly mixed GABAergic) interneuron synapsing onto PPNs. This connection is supported by ultrastructural analyses (De Zeeuw and Berrebi, 1995a, b), viral transneuronal tracing (Gonzalez-Joekes and Schreurs, 2012), and electrophysiological slice recordings (Husson et al., 2014). Inputs from other resident DCN neurons onto PPNs are entirely unknown to date. The only other suggested synaptic connection is a recurrent collateral from PPNs onto NOPNs. However, evidence for this synapse is weaker, as the anatomical study showing this connection used Golgi impregnations that can only distinguish between large and small neurons (Chan-Palay, 1973a, b, c, d; Matsushida and Iwahori, 1971). The only other data supporting this connection are that inhibition of the inferior olive can be elicited by antidromic stimulation of PPNs, suggesting that there exists some short circuit (presumed monosynaptic) connecting PPNs to NOPNs (Svensson et al., 2006). Depending on both their innervation patterns from the cortex and from local circuits, DCN neurons could have vastly different responses than those predicted by theoretical models that do not incorporate these considerations. In order to build accurate models of

cerebellar nuclear activity it is essential that we work to determine the wiring patterns of the diverse neuronal elements resident within the DCN.

1.4 THE OLIVO-CORTICO-NUCLEO-OLIVARY LOOP

One major component of the modular projections to the cortex and DCN is a putative closed loop circuit that links the cortex, deep nuclei and inferior olive (De Zeeuw et al., 1994; De Zeeuw et al., 1998; Pijpers et al., 2005; Ruigrok, 2011; Sugihara and Shinoda, 2004, 2007; Sugihara et al., 1999; Voogd et al., 2013). These trisynaptic loops originate in the inferior olive, project to the cortex in the form of climbing fibers that synapse upon PCs, and also issue collaterals to the DCN. PCs then project directly onto neurons in the DCN, which in turn issue an inhibitory feedback projection to the same inferior olive neurons that began the loop. The nucleo-olivary (NO) projection is GABAergic and specifically targets the regions of IO dendrites where they are electrotonically linked via gap junctions (De Zeeuw et al., 1989; Fredette and Mugnaini, 1991). This unique anatomical arrangement led Rodolfo Llinas to theorize that the nucleo-olivary projection shunts electrical conductance across gap junctions, thereby de-coupling IO neurons (Llinás, 1974). This was an intriguing theory that would allow the DCN to dynamically regulate the formation or dissolution of transient ensembles of coupled inferior olive neurons, but it was difficult to prove. Lefler and colleagues (2014) were able to directly assess this theory using optogenetic stimulation of NOPN axons in the IO while measuring current conductance across gap-junction coupled IO neurons. They were able to confirm Llinas's theory, demonstrating that conductance between IO neurons is shunted when the NO projection is active (Lefler et al., 2014). It was further demonstrated that the NO projection works to shape

and synchronize the IO's responses to incoming somatosensory inputs (Hogri et al., 2014). Thus, the DCN have considerable control over the manner in which incoming sensory signals from the IO enter the cerebellar circuit.

A key component of the olivo-cortico-nucleo-olivary (OCNO) loop theory is that the loops are topographically closed, such that a series of parallel, largely non-interacting modules bridge discrete cell groups in the IO, DCN and cortex. In order to determine if this is the case, it must be known at the level of single cells whether or not the loops are closed or open. Pijpers and colleagues, using injections of monosynaptic retrograde tracer into the DCN and a monosynaptic anterograde tracer into the inferior olive, were able to demonstrate the correspondence of labeled PCs and climbing fibers in the cortex (Pijpers et al., 2005). Although this study did provide evidence for closed OCNO loops, conclusive demonstration of closed loops was hindered due to the fact that they had to make separate injections of the DCN and IO. Given the precise nature of proposed OCNO loops, their two injection sites would have to be perfectly aligned within the circuit in order to fully test the closed-loop hypothesis. Furthermore, their focus was on the C1-3 zones of the cortex and so it is undetermined whether their results generalize to other cerebellar regions.

Without conclusive proof, the critical question of whether or not the OCNO circuit is a series of closed or open loops remains (Uusisaari and De Schutter, 2011). If each loop is closed, as has been postulated, cerebellar modules would perform as independent, non-interacting entities. This would imply that a given cerebellar module only controls olivary input within its own module. If they are open loops, i.e., not all connections in the circuit are reciprocal, then each cerebellar module would be able to affect the activity of neighboring modules. A very important point to consider when defining OCNO loops throughout the cerebellum is that the

DCN are not as homogenous as the cortex. Though the available experimental evidence points toward the ubiquity of closed OCNO loops, this has yet to be confirmed for the entirety of the DCN and its cortical and olivary counterparts.

1.5 THE DCN ARE HETEROGENEOUS STRUCTURES

As mentioned above, the cerebellar nuclei (the fastigial nucleus, posterior and anterior interpositus nuclei (IP), and the dentate nucleus) are not a homogenous set of structures (Beitz and Chan-Palay, 1979a, b; Chan-Palay, 1973a, b, c; Korneliussen, 1966; Matsushida and Iwahori, 1971). Each nucleus is cytoarchitecturally unique; allowing for quick identification at the light microscopic level. Unlike the cortex, which has the same circuit structure throughout, the potential organizational differences across the DCN imply specialization to support the myriad of different cerebellar-controlled behaviors. For example, the somatotopy observed within the IP during conditioning of either eyeblinks or hind limb flexion could be supported by the differences in neuronal organization of the lateral versus the medial IP (Mojtahedian et al., 2007). The dentate nucleus has also been shown with anatomical studies in monkey to contain both motor and non-motor domains which could be in part supported by the cytoarchitectonic and phenotypic differences observed between the dorsal and ventral sections of the nucleus (Dum et al., 2002; Kelly and Strick, 2003). Within the fastigial nucleus there is a ventral subregion that contains glycinergic projection neurons that target the vestibular nuclei (Bagnall et al., 2009). This contrasts with the fastigial pressor response area of the caudal aspects of the nucleus that does not contain glycinergic projection neurons, and is involved in the regulation of blood pressure (Giuditta et al., 2009). It is reasonable to suggest then that the differences within

and across the DCN are necessary for their involvement in specific behaviors, and that understanding the organization of each may yield great insight into *how* each subnucleus participates in each behavior.

Within the posterior IP there is a subfield in the ventral aspect of the nucleus that appears to be cytoarchitectonically unique compared to the rest of the IP. This region has been reported to have a higher concentration of small cells generally (Chan-Palay, 1973b; Korneliussen, 1966; Matsushida and Iwahori, 1971), and more specifically a higher concentration of NOPNs (Giaquinta et al., 1999; Husson et al., 2014). Given the preponderance of small cells within this region, we will refer to this region as the parvocellular Interpositus (pcIP). Such a distinction from the rest of the DCN, where NOPNs are loosely distributed among numerous PPNs (Ruigrok and Teune, 2014; Teune et al., 1995), implies that the pcIP is specialized to support cerebellar behaviors that are distinct from behaviors supported by magnocellular aspects of the nucleus. In addition to the unique anatomical organization of its resident cells, the pcIP also receives a unique extracerebellar afferent: caudal raphe interpositus axons. Caudal Raphe Interpositus (CRI) area axons were discovered by Luo and colleagues, and were found to almost exclusively target the pcIP (Luo and Sugihara, 2014). This is the first known afferent of the cerebellum that does not target the cortex, but rather only targets one specific deep cerebellar nucleus. The hallmark of cerebellar anatomy has been the regularity and uniformity of the mossy and climbing fiber systems, which topographically target all aspects of the cortex and deep nuclei. The specificity with which CRI axons target the pcIP, and solely the pcIP, support the idea that the pcIP is an anatomically unique subnucleus of the DCN. With differences in resident neuronal populations and afferent connectivity it has become increasingly clear that the DCN are non-

homogenous entities and may be anatomically specialized to process inputs relating to the specific cerebellar activities they support.

1.6 NUCLEO-CORTICAL PROJECTIONS

In addition to the canonical circuit and the underexplored complexity of internal DCN wiring, there is one final piece of the cerebellar network: projections from the DCN back to the cortex. Nucleo-cortical (NC) projections were first discovered 40 years ago by two independent groups of researchers (Gould and Graybiel, 1976; Tolbert et al., 1976). Both of these groups reported a novel projection from the DCN back to the granular layer of the cortex that has a similar terminal morphology to mossy fibers and originates from all of the deep cerebellar nuclei. This was a large departure from the canonical circuit in the sense that the Marr-Albus-Ito theory assumes that cortical control of the DCN is unidirectional. However, feedback projections to the cortex could drastically alter the manner in which the cortex integrates extracerebellar afferents, and in turn, how that affects its control of output neurons in the DCN.

The majority of the NC projection is excitatory, and arises from the axon collaterals of PPNs (Houck and Person, 2015). A recent report demonstrated that optogenetically stimulating or inhibiting NC fibers from PPNs can amplify or dampen conditioned eyeblinks, respectively. The authors interpreted these projections as being an efference copy of DCN output that amplifies on-going cortical processing (Gao et al., 2016). In addition to excitatory NC projections, there have also been several reports of inhibitory projections back to the cortex. Inhibitory nucleo-cortical neurons were first identified in cats in 1989 using combined retrograde tracing and immunohistochemistry (Hámori and Takács, 1989). The authors further reported

GABA positive NC terminals at the ultrastructural level targeting glomeruli in the granular layer (Hámori et al., 1990). The presence of inhibitory NC neurons was subsequently confirmed in rats (Batini et al., 1989; Batini et al., 1992). After these initial reports, the presence and function of inhibitory NC projections was not assessed again until the discovery, by Uusisaari and colleagues, of a glycinergic neuron in the dentate nucleus that projects solely to the cortex and not to extracerebellar targets (Uusisaari and Knöpfel, 2010). This group then demonstrated optogenetically that this NC neuron targets Golgi cells in the cortex, directly inhibiting them (Ankri et al., 2015). Though this projection has not been tested behaviorally, the authors suggest that this projection could work to recruit cortical processing by dis-inhibiting granule cells via Golgi cells. In this way it may behave similarly to the excitatory NC projection tested by Gao and colleagues (Gao et al., 2016). Whether the collaterals of PPNs and glycinergic NC axons represent the entirety of the NC projection has not been firmly established, and this becomes particularly important when considering the unique anatomical properties of the pcIP. Further investigation is needed to determine whether or not the pcIP is reciprocally connected with the cortex in the same manner as other subdivisions of the DCN.

1.7 OUTSTANDING EXPERIMENTAL QUESTIONS

Though many aspects of cerebellar circuit have been mapped out there remain several critical questions pertaining to the microcircuitry of the cerebellum. The first question that will be assessed in this dissertation is whether or not the collateralization of PC axons onto PPNs and NOPNs reported by Teune and colleagues is generalizable to the entirety of the DCN (Teune et al., 1998). If PPNs and NOPNs are in fact under differential control by the cortex (i.e., single

PCs only innervate one type of projection cell), then this opens the door to new theoretical frameworks as to how the cortex regulates the output of its projection neurons. Being able to separately control principal and nucleo-olivary output could allow the cerebellum to dynamically tailor its output to different targets in order to best serve the demands of the task at hand. Answering this question is essential for our general understanding of how the DCN integrate cortical input and translate that into coherent output to target nuclei. The second question is whether or not OCNO loops are closed, down to the cellular level, throughout the entirety of the cerebellar circuit. There has been considerable evidence pointing to this arrangement, but it has been difficult to assess the circuit as a whole using classical tracing and electrophysiological techniques. Confirming the ubiquity of closed OCNO loops is a critical piece of evidence needed to solidify the theory that olivo-cerebellar modules represent the basic anatomical (and presumed functional) unit of the cerebellum. The final question is whether or not cytoarchitectonically unique subdivisions of the DCN likewise issue unique projections back to the cortex. It has been established that anatomically distinct regions of the DCN may issue unique projections to extracerebellar targets, and so it is critical to extend this question to nucleo-cortical projections stemming from unique subnuclei. Differences in interconnectivity with the cortex could reveal novel avenues for functional manipulation of these circuits in order to ascertain how such anatomical differences support the functional topography observed across the DCN.

1.8 VIRAL TRANSNEURONAL TRACING AS AN APPROACH TO INVESTIGATING CEREBELLAR CIRCUITS

The major hindrance to mapping the macro-architecture of cerebellar circuits, including OCNO loops, has been the use of monosynaptic tracers to map multi-synaptic networks. With the advent of viral tracing technologies, we can circumvent the limitations of past experimental methods to determine both the macro- and micro-circuitry of cerebellar circuits. A number of naturally occurring neurotropic viruses (e.g. alphaherpesviruses, rabies virus) have evolved to invade neurons preferentially through their synaptic connections (Card and Enquist, 1994, 2014; Card et al., 1993; Strick and Card, 1992, 2011; Zemanick et al., 1991). This trait can be devastating for individuals who develop viral encephalitis, but it proves to be invaluable for researchers attempting to map multisynaptic networks in animals (Dix et al., 1983a; Dix et al., 1983b). When injected intracerebrally, these viruses typically invade axon terminals and are retrogradely transported back to the parent neuron's nucleus. There the viruses replicate and then spread throughout the somatodendritic compartment, where they exit the infected neuron through its afferent synaptic connections to invade the next neuron in the circuit. There now exist several recombinant strains of these neurotropic viruses that are attenuated for virulence and spread either retrogradely (Card and Enquist, 2014) (e.g., pseudorabies virus; PRV), or anterogradely (Rinaman and Schwartz, 2004; Wojaczynski et al., 2015; Zemanick et al., 1991) (e.g., herpes simplex virus type 1 strain H129) through neural circuits. Some of these viruses have been engineered to express unique fluorescent reporters constitutively (Smith et al., 2000) or conditionally (Card et al., 2011a; Card et al., 2011b). A number of studies have used these viruses to study the output of PPNs via the thalamus to the neocortex (Kelly and Strick, 2003; Middleton and Strick, 1998, 2000, 2001) and the basal ganglia (Bostan et al., 2010; Bostan and

Strick, 2010; Hoshi et al., 2005), and via the red nucleus to motor circuits controlling conditioned eyeblinks (Gonzalez-Joekes and Schreurs, 2012; Morcuende et al., 2002; Sun, 2012). However, no studies to date have used these valuable reagents in dual labeling studies to assess NOPN output to the inferior olive, or to investigate how the NOPN and PPN outputs are controlled by the cerebellar cortex. We employ these viruses in combination with classical tracers to define the synaptology of cerebellar modules in terms of both their long range and local synaptic networks. We focus our analyses on the local synaptology of the deep cerebellar nuclei; specifically, how the interpositus nucleus integrates its afferent input from the cerebellar cortex and inferior olive to produce a coordinated outflow to its extracerebellar targets.

1.9 SUMMARY AND EXPERIMENTAL DESIGN

Over a hundred years' worth of scientific effort has been directed towards understanding the functional capacities of the cerebellar cortex. These endeavors have yielded a wealth of information on the cerebellum's ability to participate in behaviors ranging from classical conditioning to language processing. Yet there remains a persistent simplification in how we conceptualize the DCN. As of now the three DCN are treated as anatomically and computationally equivalent, yet growing evidence suggests that this is an over-generalized view. The studies in this dissertation were designed to probe the anatomical circuits through which the DCN integrate input from the cerebellar cortex and IO, and the circuits through which the DCN in turn project back to these input structures. **We hypothesize that the DCN are not simple relays, but rather that they integrate cortical input in a cell-type specific basis in order to**

coordinate the activity of PPN ouput to motor targets, NOPN output to the inferior olive, and NC output to the cortex.

The first study (Chapter 2) tested the specific hypothesis that single Purkinje cells collateralize to innervate both principal projection neurons and nucleo-olivary neurons. To accomplish this we injected two isogenic recombinants of PRV that each express a unique fluorescent reporter into red nucleus and the inferior olive. Allowing for retrograde transneuronal transport through the deep nuclei and back to PCs, we analyzed the expression of the reporters in order to determine the route(s) through which Purkinje cell input is directed onto projection neurons of the DCN. In the second study (Chapter 3) we aimed to confirm the long-standing hypothesis that the IO, cerebellar cortex and DCN form a series of parallel loop circuits that define the functional architecture of the cerebellum. We therefore injected a cocktail of a monosynaptic bidirectional tracer and pseudorabies virus into the inferior olive. We then mapped the distribution of retrogradely infected PCs and their correspondence with anterogradely labeled climbing fibers in order to determine the extent of closed vs. open loop networks. This study revealed a preponderance of NOPNs concentrated in the ventral portions of the interpositus, which became the focus of our third study (Chapter 4). In that study we tested the hypothesis that an anatomically unique subnucleus of the DCN, the parvocellular interpositus, is reciprocally connected with the cortex in the same manner as other subdivisions of the interpositus. We delivered a monosynaptic anterograde tracer into the parvocellular interpositus and analyzed the morphology, neurotransmitter content, and synaptology of nucleo-cortical fibers originating from this subnucleus. Our studies confirmed some aspects of canonical cerebellar circuitry, but also challenge key components of this circuitry. Our new findings underscore the further need for rigorous study of the anatomical connectivity of the

DCN, in order to understand how these nuclei contribute to the function of the cerebellum in both healthy and disease states.

2.0 PURKINJE CELLS DIFFERENTIALLY INNERVATE PRINCIPAL AND NUCLEO-OLIVARY PROJECTION NEURONS IN THE DEEP CEREBELLAR NUCLEI

2.1 INTRODUCTION

The uniform cytoarchitecture of the cerebellar cortex has led to a widely held belief that functional heterogeneity arises from a mosaic of afferent connectivity (Apps and Hawkes, 2009; Ito, 2006). The cerebellar afferents that define this mosaic have been extensively studied and form the foundation of a voluminous literature defining functional domains within the cerebellar hemispheres (Ruigrok, 2011; Sugihara and Shinoda, 2004, 2007; Voogd and Glickstein, 1998). This stands in stark contrast to understanding of the functional architecture of the deep cerebellar nuclei (DCN) (Sugihara, 2011; Uusisaari and De Schutter, 2011; Uusisaari and Knöpfel, 2008; Uusisaari et al., 2007). With the exception of direct projections to the vestibular nuclei, the DCN are the sole efferent synaptic target for Purkinje cells of the cerebellar cortex. The DCN are additionally innervated by collaterals of the two primary afferents to the cerebellar cortex, climbing fibers from the inferior olive and mossy fibers from diverse sources. Thus, the DCN occupy a point of convergence of cerebellar afferents and efferents, and there is a growing consensus that their integrative capacity contributes to motor function, cognition, and associative learning (Boyden et al., 2004; Strick et al., 2009; Thompson and Steinmetz, 2009). However,

despite the integral role of the DCN in cerebellar function, and the demonstration that at least six neuronal phenotypes – two of which are interneurons – are present within the DCN (Uusisaari and Knöpfel, 2011), detailed knowledge of the synaptology that determines the functional output of the cerebellum is lacking.

The vast majority of efferent projections from the DCN arise from two non-overlapping projection pathways: principal projection neurons (PPNs) innervating the red nucleus and thalamus, and GABAergic nucleo-olivary projection neurons (NOPNs) that terminate exclusively in the inferior olive (IO) (Ruigrok and Teune, 2014; Teune et al., 1995). The PPN projection is an effector pathway influencing cognition and motor function, while the nucleo-olivary feedback projection modulates electrotonic coupling of IO neurons and the temporal dynamics of IO responsiveness to sensory inputs (Hogri et al., 2014; Lefler et al., 2014; Llinás, 2013). Importantly, the way in which Purkinje cells feed into these functionally distinct projection pathways has been investigated but not fully defined. Several studies have established that Purkinje cells synapse upon PPN neurons, GABAergic NOPNs, and glycinergic interneurons (Chan-Palay, 1973c; De Zeeuw and Berrebi, 1995a, b; Najac and Raman, 2015; Person and Raman, 2012a), and ultrastructural analysis has shown that single Purkinje cell (PC) axons can synapse upon both PPN and NO projection neurons (Teune et al., 1998). Nevertheless, the degree to which PC afferents collateralize to innervate the NOPN and PPN efferent pathways within these channels, as well as the local circuit connectivity within the DCN, are only understood in general principles.

Transneuronal tracing with neurotropic viruses provides a powerful means of defining functionally distinct channels within neural networks (Boldogkoi et al., 2002; Callaway, 2008; Card and Enquist, 2014; Loewy, 1998; Song et al., 2005; Strick and Card, 1992, 2011).

Recombinants of viral tracers that express unique fluorescent reporters, either constitutively or conditionally, have been used effectively in a variety of systems to assess the degree of convergence and divergence of microcircuits within complex neural networks (Cano et al., 2004; Card et al., 2011a; Card et al., 2011b; Hettigoda et al., 2015; Wojaczynski et al., 2015). Application of this technology to define networks involving the cerebellum has revealed functionally distinct channels within the cerebellar cortex and deep nuclei that are linked to the basal ganglia (Bostan et al., 2010, 2013; Bostan and Strick, 2010), cerebral cortex (Dum et al., 2002; Dum and Strick, 2003; Kelly and Strick, 2003; Middleton and Strick, 1998, 2001), and facial motor neurons that innervate the orbicularis oculi muscle (Gonzalez-Joekes and Schreurs, 2012; Morcuende et al., 2002; Sun, 2012). However, to date, no study has employed dual infection approaches to define the degree to which PC afferents within the DCN collateralize to innervate PPN and NOPN neurons.

The current study tested the hypothesis that the majority of PC afferents to the DCN collateralize to innervate both PPN and NOPN DCN neurons in the rat. Using separate injections of isogenic, fluorescent recombinants of pseudorabies virus (PRV) into the red nucleus and IO we demonstrate that, although a small proportion of PC afferents collateralize to innervate PPN and NOPN neurons, the majority of PC afferents antecedent to these pathways are segregated. This finding strongly supports the conclusion that subpopulations of PCs independently modulate efferent effector and afferent sensory cerebellar circuitry.

2.2 MATERIALS AND METHODS

Animals and Regulatory Issues.

The University of Pittsburgh Institutional Animal Care and Use Committee, Recombinant DNA Committee, and the Division of Environmental Health and Safety approved all experiments. Adult male Sprague-Dawley rats (225-510 grams) were used in all experiments. Animals included in viral tracing studies were acclimated to a Biosafety Level 2+ (BSL2+) facility for a minimum of one day prior to the onset of experiments and lived in the facility through termination of the experiment. Animals used for Golgi impregnations were housed in a separate facility. The room temperature in both facilities was held constant between 22 and 25°C and the light/dark cycle in the facilities was 12 hours of light and 12 hours of dark (lights on at 0700). Access to food and water was provided ad libitum. A total of 26 rats were used in the study; 10 animals were used to interrogate the synaptology of PC projections to the DCN, 5 animals were used for control experiments that confirmed the ability of both recombinants to establish productive infections in individual neurons, 5 animals received individual injections of virus into the IO, and 6 animals were included in a Golgi analysis of the somatodendritic architecture of neurons in the interpositus nucleus.

Recombinant Viruses.

The recombinants used in this analysis were generated from the Bartha strain of PRV, an attenuated vaccine strain of virus that invades neurons and generates infectious progeny that travel exclusively in the retrograde direction through neural circuitry (Pickard et al. 2002; Card and Enquist 2012). Swine are the natural host of PRV but the virus has a broad host range, with

the capacity to infect essentially all mammals except primates. The genome of the virus has been sequenced (Klupp et al., 2004) and the genetic basis for virulence and directional spread of the virus through the nervous system has been studied extensively (Pomeranz et al., 2005). The recombinants used in this investigation are isogenic, with unique reporter genes inserted at the gG locus of the virus. Reporter expression in both recombinants is under the control of the cytomegalovirus immediate early gene promoter. PRV-152 expresses enhanced green fluorescent protein (EGFP; (Billig et al., 2000; Smith et al., 2000)) and PRV-614 expresses monomeric red fluorescent protein (mRFP; (Banfield et al., 2003)). The titer of PRV-152 was 1.24×10^9 plaque forming units per milliliter (pfu/ml) and the titer of PRV-614 was 3.04×10^8 pfu/ml.

Design of Viral Tracing Experiments.

Topographically organized subdivisions of the DCN and cerebellar cortex are known to be involved in the acquisition of conditioned responses, and the neural substrates essential for this learning have been well studied (Boele et al., 2010; Christian and Thompson, 2003; Freeman and Steinmetz, 2011; Medina et al., 2002; Thompson and Steinmetz, 2009; Yang et al., 2015). We therefore focused our analysis upon neural pathways integral to acquisition and execution of conditioned eye blink, a well-characterized model of cerebellar dependent associative learning (Figure 1). Injections of the red nucleus initially targeted the dorsolateral magnocellular subfield that innervates orbicularis oculi motor neurons in the facial nucleus that generate eye blink (Gonzalez-Joekes and Schreurs, 2012; Morcuende et al., 2002; Pacheco-Calderón et al., 2012; Sun, 2012). Similarly, injections of the IO initially targeted the dorsomedial group of the principal olive (DM) and the medial-most dorsal accessory (DAO) subfields that relay sensory information related to unconditioned stimuli. However, coordinates for both injection sites were

varied slightly to involve other subfields of the IO and RN in order to test the generalizability of the results described below. Although retrograde spread of the recombinants and CTβ from the red nucleus and the IO labeled neurons in all of the deep nuclei, in this report we focus our analysis primarily upon the interpositus nucleus (IP).

To assess the degree to which Purkinje cells collateralize to innervate both PPNs and NOPNs in this paradigm, we made separate injections of viral recombinants into the red nucleus and IO (n=10; Figure 1) and analyzed retrograde spread of infection from the injection sites to DCN projection neurons and their presynaptic PCs. In each case, PRV recombinants were injected as a cocktail with a 1% solution of CTβ (a classical tracer that does not cross synapses) in a 7:1 ratio (virus:CTβ) according to the approach developed by O'Donnell and colleagues (O'Donnell et al., 1997; Wojaczynski et al., 2015). The dual labeling of infected neurons with CTβ allowed us to distinguish first order projections labeled from the primary site of injection from neurons infected by transneuronal passage of virus. In two of the cases, the sites of recombinant injections were reversed to control for site-specific spread of virus. Although it is well documented that these recombinants can establish productive infections in the same neurons (e.g., (Adler et al., 2012; Asante and Martin, 2013; Cano et al., 2004; Hettigoda et al., 2015; Kampe et al., 2009; Kim et al., 1999)), we conducted control studies in which animals (n=5) received injections of a mixture of PRV-152 and PRV-614 into both the red nucleus and IO. The mixture contained equal volumes of each recombinant. The number of infected PCs expressing one or both reporters in both experimental paradigms was quantified according to the reporter proteins they expressed (detailed below). Because separate injections of recombinants into IO and red nucleus provided evidence of recurrent collaterals of PPNs contacting NOPNs in the DCN we sought further evidence of the existence of this local circuit through single injections of

a cocktail of PRV and CTβ into the IO (n=5; Figure 1). These experiments increased the number animals addressing the specific question of recurrent collaterals of PPNs but did so in a fashion that only involved retrograde transneuronal passage from the IO.

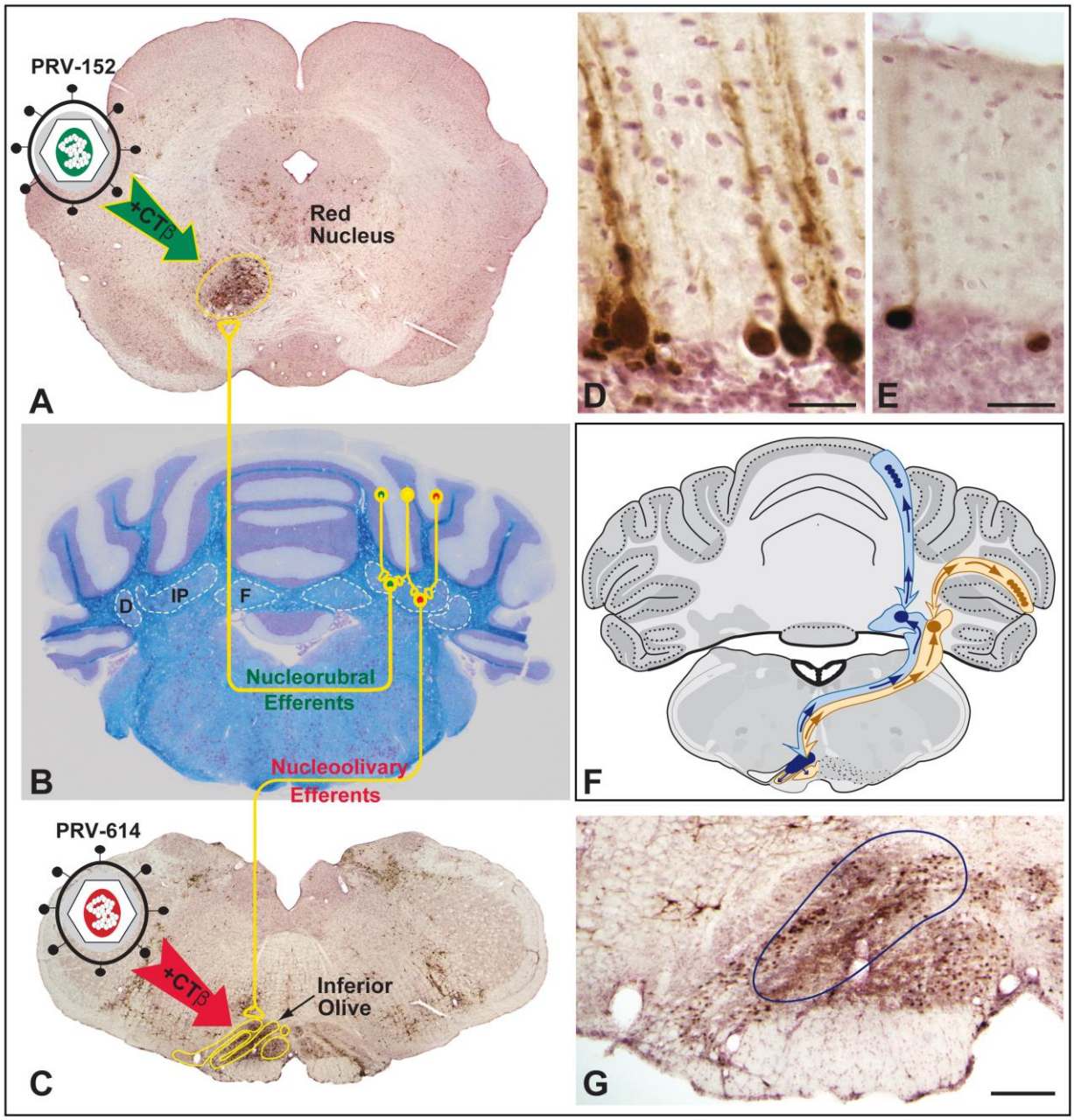
PRV-152
+CTβ
Red
Nucleus
A
D
E
D
IP
F
Nucleorubral
Efferents
Nucleoolivary
Efferents
B
F
PRV-614
+CTβ
Inferior
Olive
C
G

Figure 1. *Viral propagation through cerebellar circuits*

Injection sites typical of those achieved in dual injection paradigms (A, C, and G) and the circuitry through which tracers spread to cerebellar cell groups (B) are illustrated. Cocktails of virus and CTβ were injected into the red nucleus (A) and the inferior olive (C and G) of adult male rats, and the spread of tracers through synaptically connected neural networks was examined 48 hours later. Each injection consisted of an 80nl mixture of CTβ and PRV-152 (EGFP) or PRV-614 (mRFP). In two of the cases, the sites of recombinant injections were reversed to control for site-specific transport of virus. PRV spreads transneuronally in the retrograde direction from the injection sites to infect cerebellar networks presynaptic to the red nucleus and inferior olive. In contrast, CTβ only marks first order neurons retrogradely labeled from the injection site. Regions of overlapping expression of the two fluorescent reporters were quantified in the DCN and cerebellar cortex. The degree of collateralization of PCs synapsing upon principal projection neurons (PPNs) that innervate the red nucleus and nucleo-olivary projection neurons was assessed by determining the extent to which reporters of viral infection were present within the same PCs. Virus also spread from the primary site of injection (outline in blue in G) to other IO subfields. This secondary spread of virus within the IO led to temporally delayed infection of PCs linked to those subfields through synaptic connections in the DCN. The pathways through which primary and secondary infection of the cortex occurs is shown in F. The delayed temporal kinetics of viral spread to the cortex is reflected in the distribution of viral antigen within PCs. The longer duration of viral replication in PCs infected from the primary site of injection resulted in the spread of viral antigen throughout the somatodendritic compartment (D). In contrast, the delayed kinetics of infection resulting from infection of PCs via secondary spread of virus through the IO was reflected in the restricted concentration of viral immunoreactivity within nuclei and somata of infected PCs. See text for a detailed explanation. D = dentate nucleus, F = fastigial nucleus, IP = interpositus nucleus.

Stereotaxic Injections.

In all experiments, anteroposterior and mediolateral coordinates for injection of the red nucleus and IO were calculated from Bregma and dorsoventral coordinates were calculated from the dorsal surface of the brain using the stereotaxic atlas of Swanson (Swanson, 2004). The coordinates for injection of the red nucleus were anteroposterior (AP): -6.1 mm, mediolateral (ML): 1.0 mm, dorsoventral (DV): -6.7 mm in relation to Bregma with the incisor bar at -3.3 mm. The AP (-12.7 mm), DV (-9.7 mm) and incisor bar coordinates for injection of the IO were the same for each animal, but the ML coordinate varied (0.2-0.6 mm) in order to involve different IO subdivisions. The detailed procedures used for stereotaxic surgery of PRV in our laboratory have been published (Card and Enquist, 2014). Briefly, five animals received separate injections of the red nucleus and IO in a single surgery and five animals received the red nucleus injection 24hrs prior to the IO injection. The temporal separation of injections was performed to determine if the kinetics of viral spread of infection from the red nucleus and IO to the cerebellar hemisphere differed. Since no overt differences in these parameters were noted, only animals receiving injections in the same day were quantified (see below). All injections were made through beveled pulled glass pipettes with an internal tip diameter of ~40 μm. After drilling a hole in the cranium at the desired coordinates, the pipette was lowered into the brain and the tissue was allowed to decompress for 1 minute prior to pressure injection of 80 nanoliters of the virus-CTβ cocktail using a Picopump (World Precision Instruments, Inc., Sarasota, FL). The pipette was left *in situ* for ten minutes following each injection and then slowly removed. Craniotomies were filled with bone wax, incisions were closed with surgical staples, and a subcutaneous injection of the analgesic Ketofen (2 mg/kg) was administered. Animals were kept on a heating pad until they recovered consciousness and then returned to their home cage. The

animals lived within the BSL2+ facility for the balance of the experiment and received a daily injection of Ketofen during that period.

Tracer localizations.

Animals were deeply anesthetized by intraperitoneal injection of Fatal Plus (Vortech Pharmaceuticals, Dearborn, Michigan; 390 mg/ml sodium pentobarbital) and perfused transcardially with saline followed by 4% paraformaldehyde-lysine-periodate (PLP) fixative (McLean and Nakane, 1974) 48 to 72 hours following virus injection. Following cryoprotection in phosphate buffered sucrose solutions, sections were cut at 35 μm with a freezing microtome into six bins of cryoprotectant (section frequency of 210 μm/bin) and stored at -20°C until processed for immunocytochemical localizations or detection of reporter gene expression. Analysis of tissue was conducted in two stages. We first determined the extent of viral replication and spread from injection sites via dual immunoperoxidase localizations of PRV and CTβ, using rabbit polyclonal antibodies generated against acetone inactivated wild type PRV (Rb132, 133, 134; 1:10,000 (Card et al., 1990)) and a goat polyclonal antiserum generated against CTβ (List Biochemicals; 1:50,000). Viral antigens were identified using the brown reaction of diaminobenzidine (DAB) and CTβ was localized with the blue-black precipitate that results from nickel ammonium sulfate intensification of the DAB reaction product. These localizations did not discriminate between the recombinants, but did provide a permanent map of viral infection and CTβ transport that was used to direct the subsequent fluorescence microscopy analysis. We also determined the topographical distribution of first order projection neurons using tissue of an adjacent bin that was processed for immunoperoxidase localization of CTβ alone. Reporter gene expression was then evaluated in the next adjacent bin of tissue, using the native fluorescence of the reporters and immunofluorescence localization of CTβ to distinguish

first order neurons infected by retrograde transport of the two recombinants from the IO and red nucleus. Comparison of the pattern and extent of infected PCs as determined by immunocytochemical localization of viral antigens correlated with that of PCs expressing the reporters (GFP and mRFP) of infection. In each case, areas exhibiting viral infection in the immunoperoxidase localizations were analyzed for reporter gene expression. Additional localizations were conducted to precisely define injection sites and phenotypes of infected neurons. Consistent with prior studies (*e.g.*, (Card et al., 2006)) and detailed below, immunocytochemical localization of cells of monocyte lineage using a mouse monoclonal antibody to ED1 (Millipore; 1:100 (Collazos-Castro et al., 2005; Dijkstra et al., 1985; Rassnick et al., 1998)) allowed precise localization of pipette tracts and sites of primary virus injection. Phenotypically defined subpopulations of PCs concentrated in parasagittal bands were localized using a rabbit polyclonal antiserum generated against Zebrin II (Abcam; 1:100 ((Li et al., 2013)). Secondary antibodies conjugated to fluorophors (Alexafluor 488, Cy3, Cy5; Jackson ImmunoReseach Laboratories) were used for immunofluorescence localizations. Biotinylated secondary antibodies (Jackson ImmunoReseach Laboratories) and Vectastain *Elite* reagents (Vector Laboratories; Burlingame, CA) were used for immunoperoxidase localizations. The details of these procedures, as applied in our laboratory, have been published (Card and Enquist, 2014).

Data collection and analysis.

To precisely define primary sites of virus injection into IO and red nucleus subdivisions we localized virus, CTβ, and ED1 (a cytoplasmic antigen expressed by cells of phagocytic lineage (Dijkstra et al., 1985; Rassnick et al., 1998) in single sections using immunofluorescence. We have previously demonstrated that ED1 is a reliable marker of immune cell trafficking to areas of

damage (*e.g.*, cannula and pipette tracts) and viral infection (Card et al., 1993; Card et al., 2006; Rassnick et al., 1998; Rinaman et al., 1993). Consistent with these investigations we established objective criteria to precisely define the primary injection site and to map the extent of virus and CTβ spread from that site. Accumulation of ED1 positive cells along the pipette tract, and in an area at its termination coextensive with a dense concentration of neurons advanced in infection and labeled with CTβ, defined the site of first order uptake and replication of virus.

The distribution of first order projection neurons in the DCN was mapped using the bin of tissue processed solely for CTβ. Every section (7-8 per case) through the DCN was mapped at 40x magnification using a BX53F Olympus microscope equipped with a Ludl stage and StereoInvestigator image analysis software (version 8; MicroBrightfield, Inc.). Neurons were classified as either small cells (putative NOPNs) or large multipolar cells (putative PPNs). Classification of the projection targets of these first order neurons was determined in adjacent sections processed for detection of the natural fluorescence of the two unique reporters of PRV infection and by an extensive literature has defined the morphological features that distinguish PPNs from NOPNs (Chan-Palay, 1973b; Matsushida and Iwahori, 1971; Ruigrok and Teune, 2014; Uusisaari et al., 2007; Uusisaari and Knöpfel, 2012). The distribution of neurons replicating one or both of the recombinants was determined using an Olympus BX51 epifluorescence microscope equipped with filters specific for each of the fluorescent reporters (GFP excitation: 490±10nm; emission: 528±19nm; RFP excitation: 555±14nm; emission: 617±36.5nm). As noted above, areas previously identified to contain infected neurons in the immunoperoxidase localizations were analyzed for reporter gene expression. The interpositus nucleus and the cerebellar cortex of infected regions were scanned in sections at a frequency of 210 μm to identify neurons expressing reporters, either individually or in combination. All

infected neurons were photographed at 20x magnification for quantitative analysis using Adobe Photoshop software to determine the number of neurons expressing one or both fluorophors.

Viral infection of PCs from each injection site occurred entirely along the known topographic organization of cerebellar circuits (see results below). Thus, depending on the exact injection site within the red nucleus or the IO, infection of PCs from each injection site could be spatially segregated or overlapping. To accurately determine the degree to which PCs collateralized to synapse upon NOPNs and PPNs, we focused our analysis upon regions of the cortex that contained advanced stages of viral replication. This was an important element of our analysis since we also have demonstrated that virus spreads through IO subfields via gap junctions between IO dendrites and spines (Card et al., 2014). Thus, virus can reach PCs in the cerebellar cortex through direct uptake from the primary site of injection as well as indirectly via retrograde transneuronal spread through other IO or RN injection site subfields (figure 1F). PCs infected from the primary injection site therefore have a temporal advantage in the kinetics of viral transport from the IO or RN, a feature reflected in the distribution of viral antigens within the somatodendritic compartment of infected neurons. This is due to the sequence of gene expression from the viral genome in which immediate early gene expression produces the transcription factors necessary for the transactivation of early and late genes that express envelope glycoproteins and structural proteins (Pomeranz et al., 2005). Therefore, early replication is reflected in viral immunoreactivity being largely isolated to the cell nucleus and soma, and advanced replication generates a dense distribution of viral immunoreactivity throughout the somatodendritic compartment (Cano et al., 2001). This was reflected in our material, where PCs infected from the primary injection site were found in dense groups and exhibited extensive distribution of viral immunoreactivity throughout the somatodendritic

compartment (figure 1D). In contrast, retrograde transneuronal passage of virus through secondary spread of virus to other IO or RN subfields resulted in temporally delayed infection of sparsely distributed PCs in which viral immunoreactivity was largely restricted to the cell nucleus and soma (figure 1E).

Due to the aforementioned temporal kinetics of viral transport to the cortex we only quantified regions of cortex that contained groups of PCs advanced in infection. In every instance, these regions corresponded to the predicted zones of climbing fiber projections from infected IO subfields (Sugihara and Shinoda, 2004, 2007). This corresponded to that predicted by the spatial topography resulting from retrograde transneuronal infection from the red nucleus and IO. We used the approach for quantitative analysis defined by Ruigrok and Tuene which corrects for differences in the patterns of viral transport that may result from placement of injection sites that produce spatially separate populations of first order infected DCN neurons. The five cases included in our analysis produced PCs infected by both recombinants that fell within 250 μm of each other along the Purkinje cell layer (Ruigrok and Teune, 2014). The numbers and phenotypes of reporter gene expression of these groups of PCs were recorded. We counted approximately 15 sections per case; the exact number varied depending on the extent of viral spread and the degree of overlapping expression of recombinants within PCs. This approach focused the analysis upon areas of cortex synaptically linked to primary injection sites and excluded areas infected by secondary spread of virus.

Golgi impregnations.

The extent of dendritic fields of PPNs and NOPNs in the interpositus nucleus was an important consideration in determining the putative synaptic targets of PCs within the interpositus nucleus. We therefore sought to augment prior data addressing this issue through

Golgi impregnations of interpositus neurons (Matsushida and Iwahori, 1971). Six animals were included in this analysis, using an adaptation of the Golgi method developed by Angulo and colleagues (Angulo et al., 1996). Animals were deeply anesthetized with Fatal Plus and then perfused transcardially with physiological saline followed sequentially by 200 ml of 1.25% glutaraldehyde (GTA), 1% paraformaldehyde (PAF) in 0.15M sodium cacodylate buffer, and 200 ml of 6% potassium dichromate, 1.25% GTA, 1% PAF in double distilled H2O, both at pH 7.4 . The brain was removed and a 3 mm coronal slab of tissue containing the interpositus nucleus was bisected into left and right halves. Each half was wrapped in gauze and suspended in a jar containing 100 ml of chromation fluid (CF; 5% glutaraldehyde, 4% potassium dichromate in double distilled H2O). The pH of the CF was recorded at the outset of the incubation and on a frequent basis thereafter. When the pH had risen 0.7 units – typically 12 hours – the tissue was placed in fresh CF. Incubation times and the number of changes of CF varied among the tissue slabs in an effort to determine the optimal timing required to produce impregnated neurons against a clear background. Impregnated neurons were observed in all groups but the best results were achieved with 12-hour changes of CF over a 4 day period. Following chromation the tissue blocks were dipped in separate containers of 0.75% silver nitrate in double distilled H2O until all cloudiness was removed from the last solution. The blocks were then suspended in fresh silver nitrate solution for 24 to 48 hours. Thereafter, each block was washed in double distilled H2O and 100 μm sections were cut in the coronal plane using a vibratome. Sections were dried overnight on subbed slides, dehydrated in a series of ethanols, cleared in xylenes, and coverslipped with permount.

Each section through the interpositus nucleus was examined using a BX53F Olympus microscope equipped with a Ludl stage and Neurolucida image analysis software (version 8;

MicroBrightfield, Inc.) to identify impregnated neurons. Every neuron that was impregnated against a clear background was traced, and dendrites were traced and color-coded to signify branching order. Natural endings versus premature terminations caused by sectioning were also noted. The boundaries of the interpositus nucleus were recorded for each cell so that the disposition of the cell body and the orientation and extent of the dendritic field within interpositus was defined relative to nuclear boundaries. Each cell was also photographed with brightfield optics in several focal planes that revealed the cell body and different portions of the dendritic field.

2.3 RESULTS

Topography of recombinant spread to cerebellum.

The distribution of infected neurons in the IP and cerebellar cortex following injections into the red nucleus and IO was consistent with the topography demonstrated in prior studies using classical tracers (Daniel et al., 1987; Ruigrok and Teune, 2014; Sugihara and Shinoda, 2004; Teune et al., 1995). For example, injection of the dorsal magnocellular subfield of the red nucleus produced first-order labeling of PPNs that were concentrated in the anterolateral subfield of IP, while injections centered in the ventral magnocellular subfield labeled neurons in the medial IP subfield (Figures 2C and D). Similarly retrograde spread of virus and CTβ from the IO labeled small neurons that were topographically organized in a pattern consistent with prior reports (e.g., (Ruigrok and Voogd, 1990, 2000; Sugihara and Shinoda, 2004, 2007; Voogd et al., 2013)). For example, a case with an injection centered on the DM group of the principle olive with a small involvement of the rostral medial accessory olive resulted in first order infection of

small neurons concentrated in the dorsal lateral hump of the interpositus and the ventral parvocellular portion of the posterior IP (Figure 2A). Notably, in all cases that produced retrograde infection of the ventral parvocellular subfield of the posterior IP (pcIP), infected neurons were densely concentrated throughout this subfield (Figure 2A). In contrast, although large numbers of NOPNs were routinely observed in other subfields of the IP after injections involving other IO subfields, the packing density never approached that observed in the pcIP.

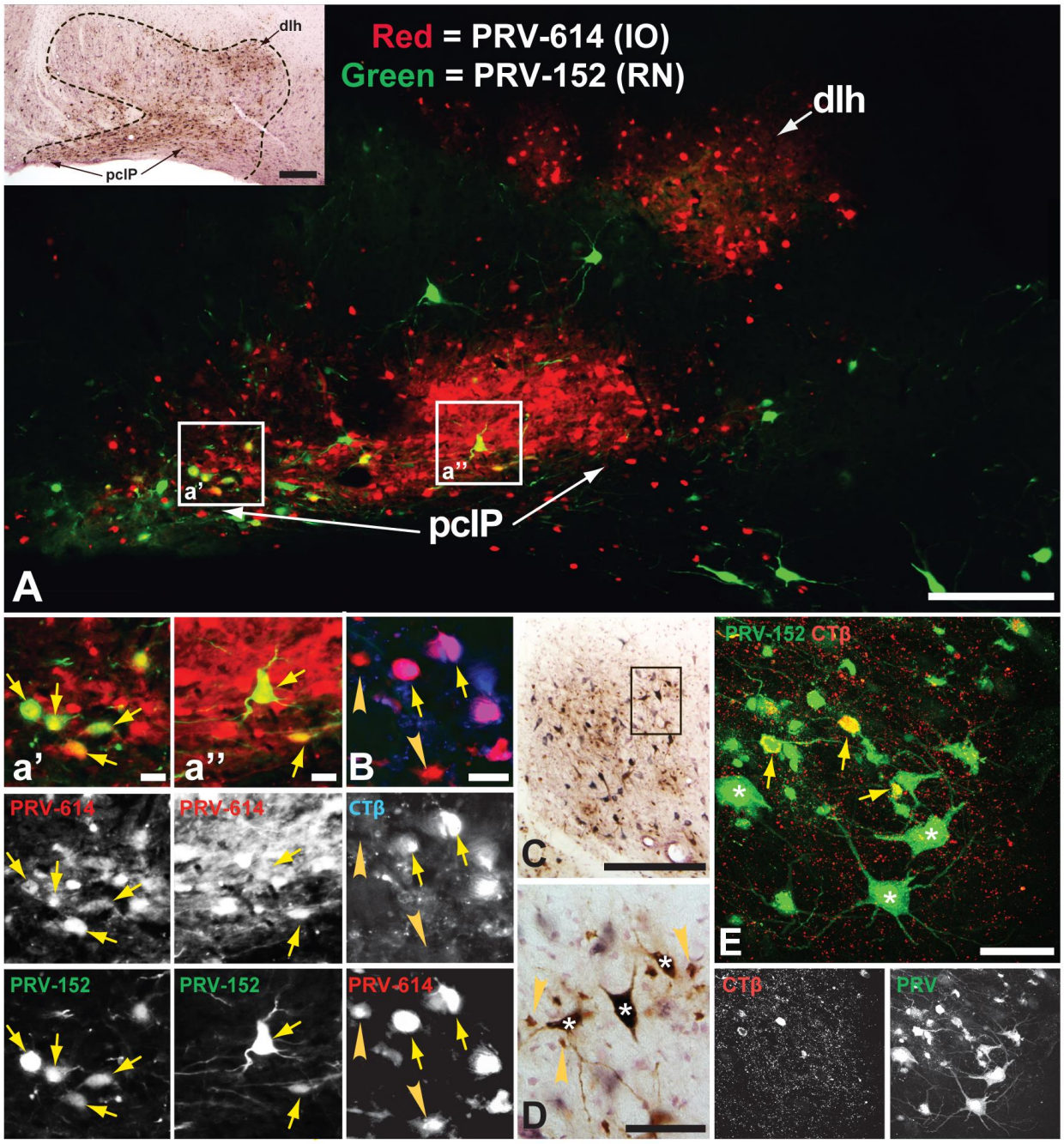
dlh
pclP
Red = PRV-614 (IO)
Green = PRV-152 (RN)
dlh
a'
a''
pclP
A
a'
a''
B
C
PRV-152 CTβ
E
PRV-614
PRV-614
CTβ
D
PRV-152
PRV-152
PRV-614
CTβ
PRV

Figure 2. *Virus spread through the DCN.*

Retrograde spread of virus from the IO (red fluorescence) and red nucleus (green fluorescence) to IP is illustrated. The inset in (A) shows the distribution of the two recombinants in the IP in an adjacent section stained for immunoperoxidase localization of viral antigens (brown; localizing both recombinants) and CTβ (black). Injection of virus centered in the DM subfield of IO produced differential concentration of infected NOPNs within the parvocellular (pcIP) and dorsal lateral hump (dlh) subfields of IP. The boxed areas in (A) are shown in higher magnification in (a') and (a''), with the individual channels for the fluorescent reporters of PRV-614 (red) and PRV-152 (green) infection shown below each figure. Evidence for infection of red nucleus PPNs via a recurrent collateral synaptically connected to NOPNs was present in dual infection experiments (a') and (a''). The arrows in panels (a') and (a'') identify dual infected PPNs resulting from injection of PRV-152 into the red nucleus and PRV-614 into IO. Panel (B) depicts transneuronal infection of small putative interneurons (arrowheads; PRV+/CTβ-) after first order infection of NOPNs (arrows; PRV+/CTβ+). Similarly, transneuronal infection of putative interneurons from first order infection of PPNs infected from the red nucleus is evident in (C) and (D). PPNs (asterisks) are labeled with both PRV (brown) and CTβ (black), while putative small interneurons are labeled only with PRV (arrowheads). Panel (E) demonstrates primary retrograde infection of NOPNs (arrows; PRV+/CTβ+) and transneuronal infection of PPNs (asterisks; PRV+/CTβ-) with PRV-152 in a case in which only the IO was injected. Anterograde transport of CTβ also labels collaterals of climbing fibers within IP. See text for more detailed description. Marker bars = 250 μm in (A) and (C); 25 μm in (a'), (a''), and (B); 50 μm in (D) and (E).

Correspondence of the location of labeled neurons within the DCN differed across cases due to small differences in the exact location of each injection site (Figure 3). Mapping the distribution of CTβ+ filled neurons revealed that some cases had both large and small projection neurons densely intermingled within the DCN (row D of cases 6, 7, and 8, Figure 3). Fluorescence analysis confirmed that these small and large projection neurons corresponded to NOPNs and PPNs, respectively (row E of Figure 3). Within these areas of dense overlap of the two viral recombinants, we found the greatest degree of dual labeled neurons indicating a short circuit synaptically linking PPNs and NOPNs (see section below). Other cases, such as cases 2 and 5, contained fewer regions of overlapping viral infection and correspondingly had fewer dual labeled neurons (row E of Figure 3). It is also important to note that the degree of spatial overlap of PPNs and NOPNs in the DCN was not directly proportional to the degree of spatial overlap of PCs infected via either the RN or IO projection pathways. In cases with both high degrees of spatial overlap (cases 6-8) and lower degrees of overlap (cases 2 and 5) we observed select regions of cortex that contained PCs infected from both pathways (row F of Figure 3; full description below). While the kinetics of viral spread to the cortex did vary among cases (rows F and G of Figure 3), all cases produced largely segregated patterns of infection of PCs. Importantly, this was true of the cases in which robust spread of infection to the cortex was present. Thus, the low numbers of dual infected PCs could not be attributed to inadequate viral spread through the DCN.

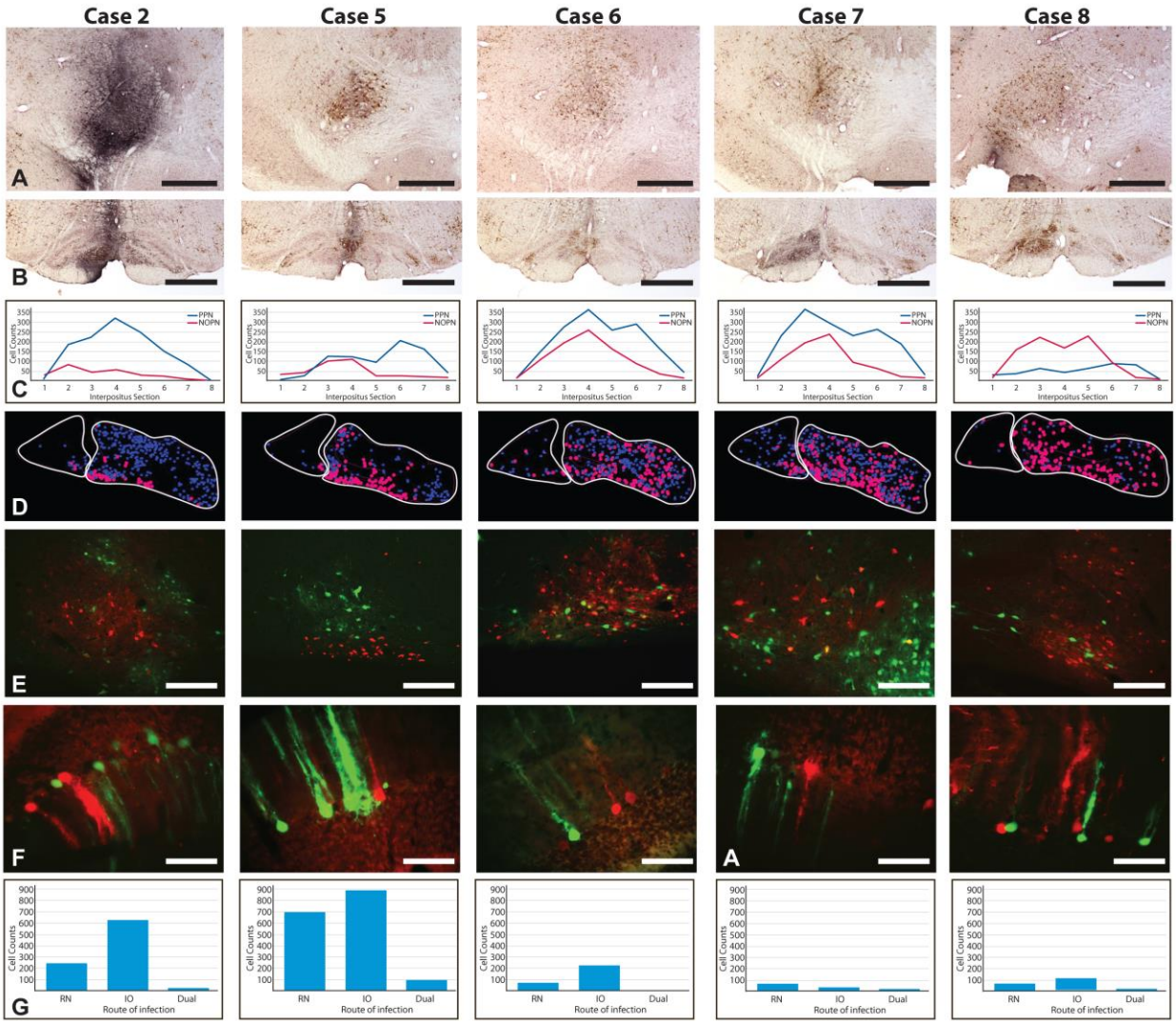

Figure 3. *Summary of quantified cases.*

Five columns document data for each of the viral tracing cases included in this report. Rows (A) and (B) show injection sites for the RN and IO, respectively on tissue processed for immunoperoxidase localization of viral antigen (brown) and CTβ (black) and counterstained with Neutral Red. Row (C) shows the rostrocaudal distribution of projection neurons retrogradely filled with CTβ (with the first section being the most caudal and the last section the most rostral extent of the DCN). Neurons were classified as small putative NOPNs or large putative PPNs based upon morphology. Row (D) shows the mapped distribution of projection neurons retrogradely filled with CTβ on a single section that contained the densest overlap of the two cell types. Small cells are shown as pink circles and large cells as blue squares. We confirmed the NOPN/PPN identity of these small/large cells in adjacent sections processed for the natural fluorescence of the recombinants (row E). Representative images of the differential infection of PCs via PPNs or NOPNs are shown in row F. Numbers of PCs infected from either the PPN pathway, NOPN pathway, or both are shown in row (G). Dotted lines in row (A) = approximate borders of the red nucleus and pararubral area; ml = medial lemniscus. Asterisks in rows (A) and (B) define the center of the primary injection site. Asterisks in row (D) indicate the area of the field shown in the photomicrographs in row (E). Marker bars = 750 μm in (A) and (B); 200 μm in (E); 100 μm in (F).

Golgi impregnations of IP neurons.

The implications of coextensive distribution of neurons for dual infection of PCs must include not only the degree of overlap of neurons retrogradely infected from the red nucleus and IO but also the dendritic fields of these neurons that are the synaptic targets of PCs. We therefore conducted Golgi impregnations of IP neurons in six animals. In each case, impregnated neurons were observed against a relatively clear background throughout the rostrocaudal extent of the IP, including the portions of IP that contained the majority of neurons retrogradely infected from the red nucleus and IO. Figure 4A shows a section through that portion of the nucleus stained with the Klüver-Barrera method. The yellow line defines the border of the IP and highlights large basophilic neurons (putative PPNs) and small pale staining (putative NOPNs). Figure 4B shows traces of the dendritic trees of 5 neurons in portions of the IP that contained the majority of infected nucleo-rubral and nucleo-olivary neurons. The traces of the dendritic tree are color coded to show the branching order of dendrites arising from the cell soma. In each case, the dendritic fields arising from each cell are extensive and extend through large regions of the IP. This was true of both small neurons (C, D, and E) and large neurons (F and G).

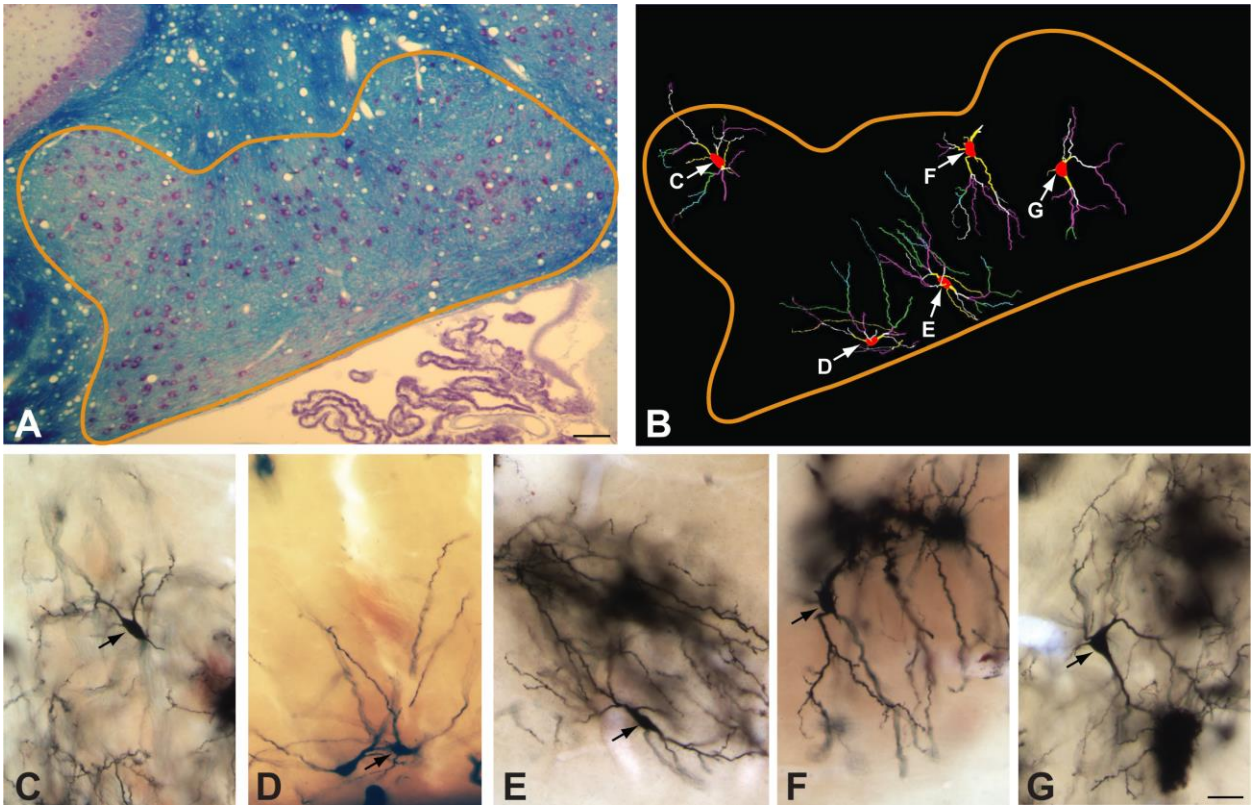

Figure 4. *Golgi impregnations of IP neurons.*

Panel (A) illustrates the portion of the IP that contained large concentrations of neurons infected from viral injections in the red nucleus and IO. The section is stained with the Klüver-Barrera method that stains myelin deep blue and incorporates a cresyl violet stain of neurons. Nuclear borders are marked by the orange line, and used in panel (B) to shown the location of 5 impregnated neurons as well as the extent and orientation of their dendritic fields within the IP. Dendrites are color coded to show the branch order of dendrites arising from the cell bodies. Panels (C – G) show photomicrographs of the cells marked in B. See text for detailed description. Marker bar in (A) = 100 μm; marker bar in (G) = 50 μm and (C – G) are the same magnification.

Recombinant spread within IP.

Viral replication and spread through local DCN circuitry was observed in all cases. Spread of virus from the IO infected both large neurons exhibiting PPN morphology as well as smaller neurons whose morphology conformed to small local circuit neurons. A consistent feature of the local spread of virus through the DCN was the presence of large multipolar neurons replicating both recombinants. A subset of these dual infected neurons also contained CTβ (triple labeled), confirming their identity as PPNs. When viral infection from the IO and red nucleus injections was extensive we found many examples of PPNs retrogradely infected from the red nucleus that also were infected by retrograde transneuronal passage of virus from IO (Figures 2a' and 2aa'). These dual infected neurons were always located in the immediate vicinity (<100 μm) of NOPNs containing CTβ, consistent with the existence of recurrent collaterals that link PPNs to NO projection neurons (Figure 2B). Retrograde infection of first order PPNs from RN injections also produced transneuronal spread of infection to small neurons in the immediate surround (arrowheads in Figure 2C and D), confirming previous studies demonstrating local interneurons that coordinate the activity of PPNs (Husson et al., 2014). Single injections of the virus and CTβ cocktail into the IO confirmed retrograde transneuronal passage of virus from NOPNs (PRV+/CTβ+ in Figure 2E) to PPNs (asterisks in Figure 2E).

Transneuronal Infection of Purkinje Cells.

Retrograde transneuronal spread of virus through the DCN routinely infected PCs in cerebellar cortex 48 hours post-inoculation. Infected PCs were present in subfields of cerebellar cortex known to be synaptically linked to the IO and red nucleus injection sites through the DCN. In all cases we observed largely segregated spread of the PRV recombinants to PCs in the cerebellar cortex (detailed below). Nevertheless, although a large literature has demonstrated the

capacity of neurons to replicate both of these recombinants in dual injection paradigms (e.g., (Adler et al., 2012; Asante and Martin, 2013; Cano et al., 2004; Hettigoda et al., 2015; Kampe et al., 2009; Kim et al., 1999; Stanley et al., 2010)), and we confirmed this for PCs in five animals that received injections of a mixture of the recombinants into the IO and red nucleus. In contrast to the results of separate injection of recombinants into IO and red nucleus, large numbers of dual infected DCN neurons (Figure 5A) and PCs (Figure 5B) were observed in in these animals. Quantitative analysis demonstrated that 3,433 of 6,504 PCs in these cases replicated both viruses. Dual infected PCs in individual cases ranged from 49.80% to 56.72%, with a mean of 53.21±1.51% (Figure 5C).

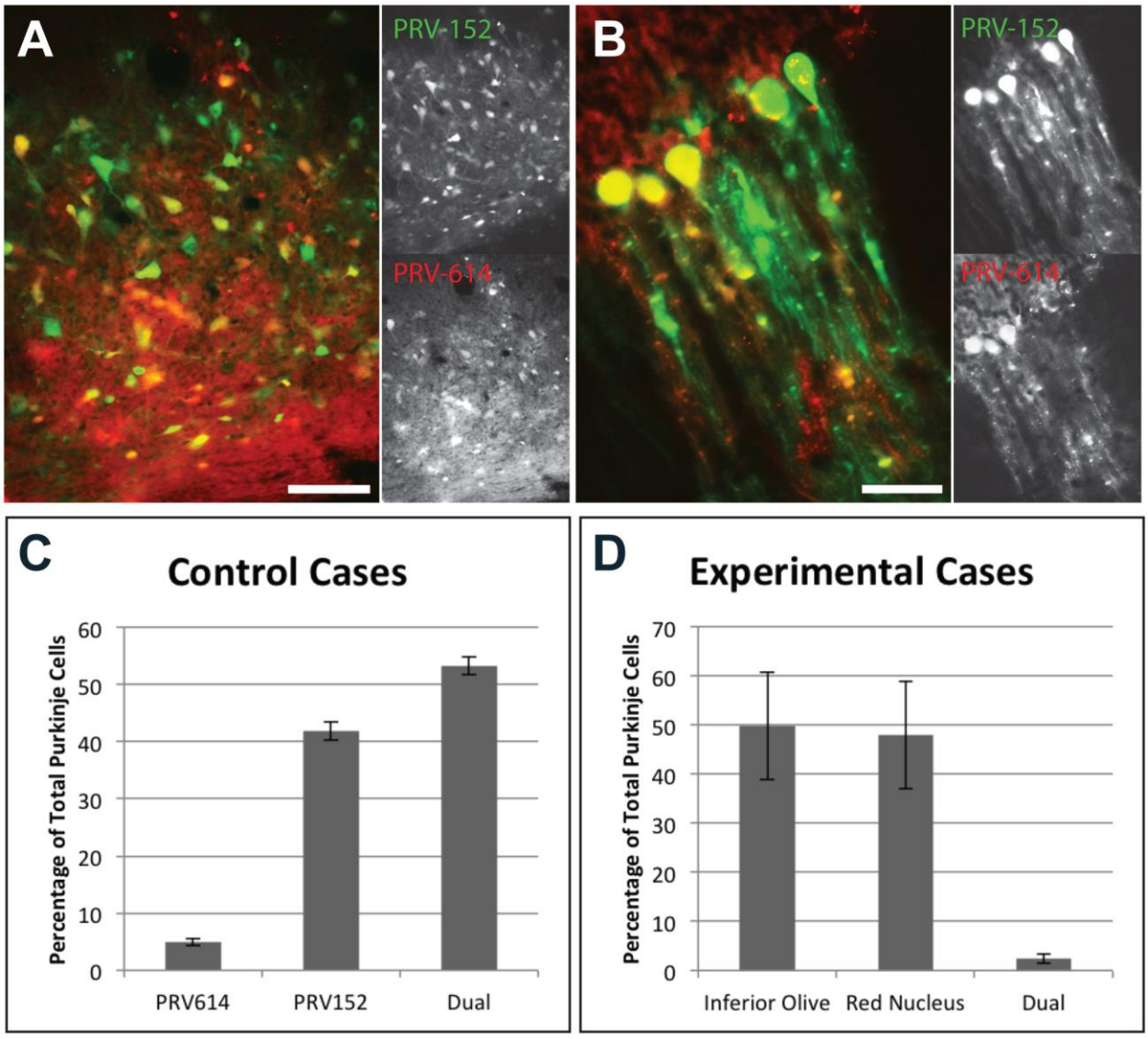

Figure 5. *Quantification of reporter expression.*

Extensive dual infection of neurons in the DCN (A) and cerebellar cortex (B) is reflected in the colocalization of the reporters of infection in both regions (yellow fluorescence). The images to the right of (A) and (C) show the channels for selective detection of EGFP (PRV-152) and mRFP (PRV-614). The mean percentage of neurons expressing one or both reporters in control and experimental cases are shown in figures (C) and (D), respectively. Percentages of neurons in each category for control experiments were: PRV-152 = 41.87±1.61%; PRV-614 = 4.93±0.61%; Dual = 53.21±1.51%. Percentages of neurons in each category for separate injections of viruses into IO and red nucleus were: inferior olive = 49.71±10.91%; red nucleus = 47.92±10.99%; Dual = 2.43±1.02%. Marker bars in (A) and (B) = 50 μm.

In animals receiving separate injections of PRV recombinants, large numbers of PCs in the cerebellar cortex differentially expressed either the EGFP or mRFP reporters of infection (Figure 5D and 6). These groups of single labeled PCs were found interdigitated amongst one another, such that a pattern of alternating GFP-only and mRFP-only profiles was seen in cortex infected from both PPN and NO pathways (Figures 6A-F). Depending on the location of injection sites in the RN and IO, this alternating pattern of single reporter expression was observed in the vermis (Figure 6A-D), paravermis (Figure 6B and E), hemispheres (Figure 6F) and/or floccular complex. PCs replicating both viral recombinants were also observed (Figure 6 arrows), a finding consistent with the prior ultrastructural demonstration that PC axons collateralize in the DCN to innervate both PPNs and NOPNs (Teune et al., 1998). These dual infected neurons were interspersed among the groups of individually infected neurons. Quantitative analysis confirmed the preponderance of neurons replicating only one viral recombinant. Of the 3,258 PCs counted across five cases, 3,121 expressed a single reporter and 137 (4.21%) expressed with both reporters. Individual cases ranged from 0.37 to 6.19% of PC profiles containing both reporters (mean: 2.44±1.02%), reflective of the differing degrees of transneuronal spread of virus to the cerebellar cortex (Figure 5D). Three cases with the most restricted infections contained virtually no dual labeled PCs (0.37-1.73%), but contained numerous groups of single labeled PCs intermingled with one another. Larger numbers of dual infected PCs were observed in the two cases that also exhibited larger percentages of single infected neurons: 2.80% and 6.19%. We interpret the correlation of dual infected neurons with more extensive spread of recombinants to the cerebellar cortex as a reflection of the synaptology of collateralized PC afferents within the DCN. The basis for this interpretation is detailed in the following paragraphs and in the discussion.

In one of the two cases with the most extensive transport of recombinants to the cortex, the IO injection site was concentrated in the rostral medial accessory olive, and the red nucleus injection site was concentrated in the centrolateral magnocellular subdivision. Consistent with prior circuit analyses with classical tracers, retrograde spread of the cocktail of virus and CTβ from the IO was concentrated in the ventral parvocellular and medial posterior subdivisions of the IP nucleus, while spread of virus and CTβ from the RN was concentrated in the lateral anterior subdivision of IP. Seventeen large putative PPNs expressed both reporters in the ventral parvocellular interpositus in this case, but the majority of infected neurons expressed only a single reporter of infection. Infection in the cortex was also largely segregated, with notable regions with extensive convergence of the two viral tracers. For example in the caudal vermis (lobules VIII-X) and in the paramedian lobule large numbers of intermingled PCs expressed one fluorescent reporter and small numbers of PCs expressed both reporters (Figure 6F). Quantitative analysis confirmed these qualitative observations, demonstrating that only 26 (2.80%) of 927 infected PCs contained both fluorescent reporters.

In the case with the most extensive spread of recombinants to the cortex, injection of the dorsal medial cell column of IO and the ventral magnocellular red nucleus labeled neurons in the medial most posterior and anterior subdivisions of IP as well as interstitial cell groups. In these areas the infection from the IO was always immediately ventral to the infection from the red nucleus. Infected neurons expressing one or both reporters were observed in vermis lobules VI-X, the copula pyramis, and the paramedian lobule (Figure 6A, C, and D). The large majority of these neurons expressed only one reporter, with only 6.19% expressing both reporters. As in other cases, the small numbers of dual labeled PCs were interleaved with larger groups of PCs expressing only one reporter (Figure 6 arrows). The appearance of dual labeled PCs only within

the context of large numbers of PCs expressing a single reporter is consistent with viral recombinants initially spreading through parallel circuits into the cerebellar cortex. PCs expressing both reporters likely were infected through via local circuits and therefore required a longer period of time for recombinants to spread to the cortex.

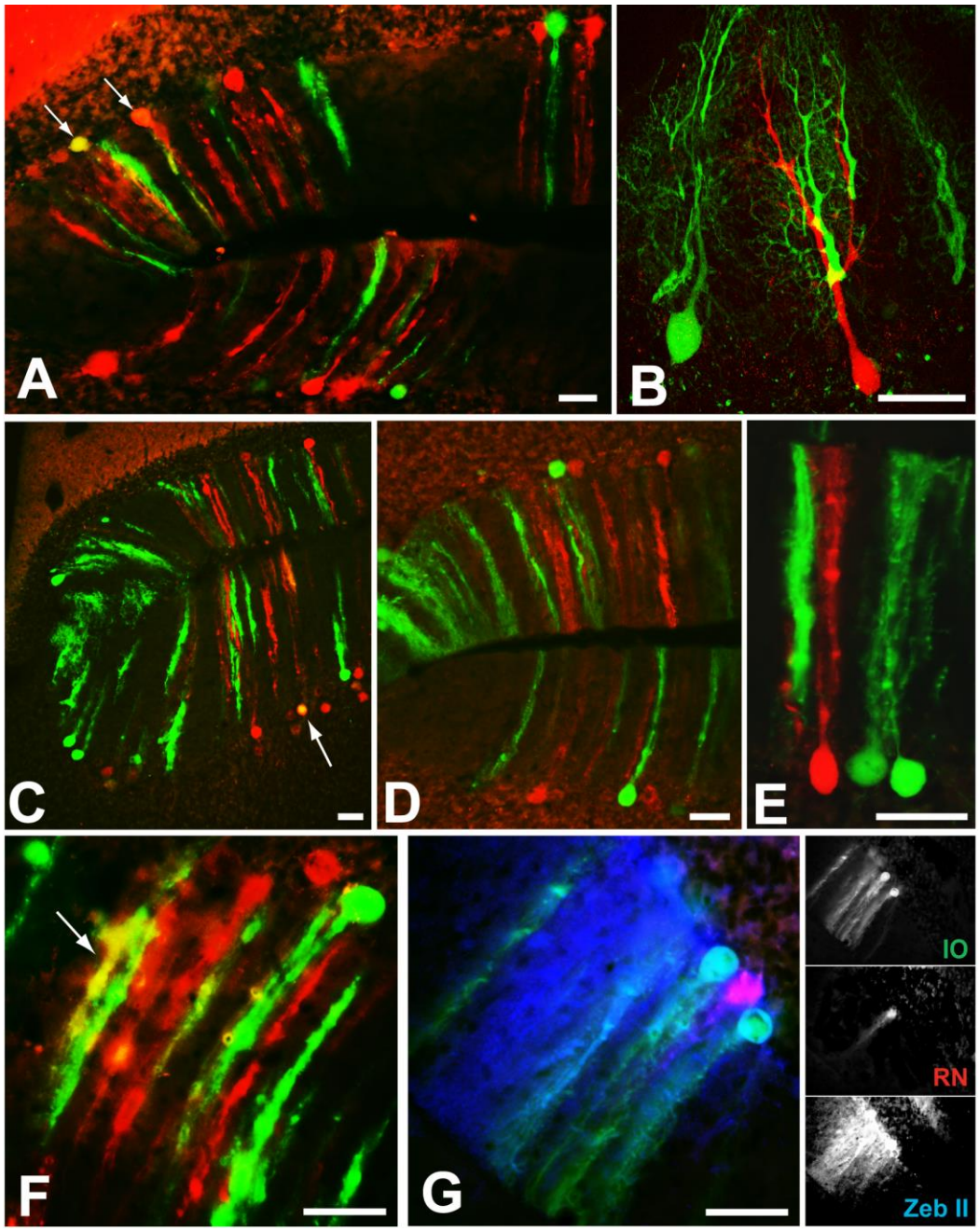

Figure 6. *Purkinje cells selectively innervate either PPNs or NOPNs.*

Sections through vermis lobules VIIIb and IXa (A, C and D), hemispheric lobule VI (B and E), and the paramedian lobule (F) reveal selective, projection-specific infection of PCs through NO and PPN neurons (red and green), and dual infected PCs synaptically linked to both projection pathways (yellow). The majority of PCs expressed only one reporter of infection and was interspersed between one another in localized groupings within lobules. Dual infected neurons were few in number and were interdigitated among projection-specific PCs (arrows). Zebrin II expression (blue) does not distinguish classes of PCs (G). All three classes were found within both zebrin positive and zebrin negative bands in all regions of cortex that contained infected PCs. Marker bars = 50 μm.

To further characterize the topography of PCs innervating either one or both projection pathways, we localized infected neurons in relation to zebrin II, a glycolytic isozyme (aldolase C) differentially expressed by PCs that defines parasagittal bands in cerebellar cortex distinguished by both function and by afferent and efferent projections (Ahn et al., 1994; Brochu et al., 1990; Graham and Wylie, 2012; Sugihara and Shinoda, 2007; Tsutsumi et al., 2015). Immunofluorescence localization of zebrin II with reporters of viral infection revealed PCs replicating one or both recombinants within both zebrin positive (Z+) and zebrin negative (Z-) bands with no preferential correlation. Additionally, we observed single and dual infected PCs within the same Z+ and Z- bands (Figure 6G), ruling out zebrin II as a defining factor for distinguishing PCs differentially linked to PPN or NO efferent projection pathways. Thus, although zebrin bands define topographically organized projections to the DCN, our data demonstrate that PCs within either Z+ or Z- bands differentially target PPN and NOPNs.

2.4 DISCUSSION

Contemporary literature has firmly established that the function of the cerebellum extends far beyond the control of movement. This is evident from the topographically organized, multisynaptic loops the cerebellum forms with both motor and non-motor targets (Reeber et al., 2013; Strick et al., 2009), as well as the presence of non-motor deficits in patients with cerebellar abnormalities (D'Mello and Stoodley, 2015; Desmond and Fiez, 1998; Schmahmann, 2004; Schmahmann and Schmahmann, 1998; Stoodley, 2014). The cerebello-cerebro-cerebellar loops that orchestrate these diverse functions arise solely from the principal projection neurons in the DCN, which target the red nucleus and the thalamus (Dum and Strick, 2003; Kelly and Strick, 2003; Middleton and Strick, 2001). Intermixed among PPNs in the DCN are nucleo-olivary projection neurons that give rise to the inhibitory feedback circuit between the cerebellum and the IO (Ruigrok and Teune, 2014; Teune et al., 1995). Although the closed loop architecture supporting functionally defined cerebellar output pathways is well documented, little is known regarding the synaptic targets of PCs feeding into these two efferent pathways. Our data demonstrate that PCs are organized in parallel pathways that differentially target PPN and NO efferent projection neurons, with only a small proportion of retrogradely infected neurons collateralizing to innervate both efferent pathways. Collectively, these data define important neural substrates through which integrated activity between PPN and NO efferent pathways is achieved.

Our data are largely consistent with two prior ultrastructural studies examining the percentage of PCs that collateralize to synapse upon the two morphologically distinct and

projection specific populations of DCN neurons, but the interpretation of the data in those studies differs from the conclusions we have drawn from our analysis. DeZeeuw and Berrebi provided important foundational data addressing this issue in a TEM study in which they used dual immunocytochemical localizations to quantify the number of PC terminals that synapse upon large unlabeled neurons, GABA neurons, and glycine neurons in the deep cerebellar and vestibular nuclei (De Zeeuw and Berrebi, 1995a, b). Their analysis demonstrated that approximately 3% of PC terminals synapse upon unlabeled large neurons (presumably projection neurons) and GABAergic neurons, with the number increasing to 9% in material subjected to serial analysis of the same terminals. However, in interpreting these findings, they were careful to note that the GABAergic population in the deep nuclei could consist of either nucleo-olivary projection neurons or local interneurons. Teune and colleagues followed with a very influential paper in which they used immunocytochemistry combined with tract tracing to generate triple labeled material that allowed them to identify PC terminals, NOPNs, and large neurons projecting to the red nucleus at the TEM level (Teune et al., 1998). They reported that 9 of 367 PC terminals – approximately 2.5% –contacted both classes of projection neurons. Remarkably, data from our experiments employing the same experimental paradigm employed by Teune and colleagues demonstrated that separate injection of isogenic strains of PRV recombinants into red nucleus and inferior olive produced dual infection of 2.4% of PCs following retrograde transneuronal passage of virus through the interpositus nucleus. In considering their findings in concert with the extent of arborization of PC axons revealed in Golgi investigations (Chan-Palay, 1973b, c) and biocytin labeling (De Zeeuw et al., 1994; Sugihara et al., 2009), Tuene and colleagues concluded that individual PCs have "a fair chance" of collateralizing to contact both nucleo-rubral and nucleo-olivary neurons. They therefore concluded that the data favored the

possibility that all PC axons collateralize to contact both classes of projection neurons. However, they also noted that it was not possible to exclude the possibility that only a subset of PC axons made collateralized contacts. Our data bring further insight to this question from a neural network perspective in which populations of PCs are labeled by retrograde transneuronal transport of virus through the DCN circuitry innervating both the IO and red nucleus. In contrast, the ultrastructural studies provide only a limited sampling of a very small portion of the neural network within the interpositus. Thus, the network perspective afforded by the transport of virus through the full circuit builds productively upon the ultrastructural findings to support the conclusion that PCs are organized in parallel pathways that differentially target projection-specific populations of DCN neurons, and that the small group of PCs that collateralize to both DCN efferent pathways provide additional regulatory capacity to the circuit.

The degree to which PPNs and NOPNs retrogradely infected by transport of PRV recombinants from the red nucleus and IO overlap within the IP is another important consideration in evaluating our findings. Two issues – the terminal arbors of PC axons and the dendritic fields of PPNs and NOPNs – are particularly important in evaluating our data. An extensive literature based on microinjections of anterograde tracers into the cerebellar cortex has revealed restricted terminal arbors of PC axons within the DCN (e.g., (Sugihara et al., 2009)). These data suggest that infected nucleo-rubral and nucleo-olivary neurons should also be coextensive within a restricted zone within the IP that is innervated by topographically defined projections of PCs. Although we did observe overlap of infected PPNs and NOPNs in our study, the degree of overlap varied among cases. Nevertheless, all cases produced overlapping infection in select cortical areas that were consistent with the topography demonstrated in prior analyses of the topography of PC projections to the DCN. This suggests that the projection

targets of neighboring PCs can be quite different from one another such that a patch of PCs innervates PPNs in, for example, the lateral anterior interpositus and NOPNs in the ventral parvocellular interpositus. Careful consideration of the data defining the terminal arbors of PCs within the DCN supports this conclusion. For example, Sugihara and colleagues demonstrated that neighboring PCs project to spatially disparate regions of the DCN, and their terminal projection fields can span several hundred micrometers within the DCN, allowing for the coordination of DCN neurons across large distances (Sugihara et al., 2009). These results are consistent with Golgi impregnation data published by Matsushita and Iwahori, who reported that single PC axons "arborize in a wide area of the nucleus" with terminal branches in both the dorsal and ventral portion of the nucleus (Matsushida and Iwahori, 1971). While these data do not establish evidence of dispersed synaptic contacts upon the lengths of the axons within IP, they do raise the possibility that coextensive PPNs and NPONs are not necessary to generate the segregated projection patterns documented in our viral tracing study. This is particularly true when one considers the extent of dendritic arbors of both cell types. Published Golgi studies (Beitz and Chan-Palay, 1979b; Chan-Palay, 1973a, b, c; Matsushida and Iwahori, 1971) and the impregnations included in this report clearly demonstrate that the dendritic fields of PPNs in the IP are extensive. In each case, PPNs were shown to give rise to extensive dendritic arbors that extend well beyond the topographical relations defined by PC axon arborizations. Such configurations beg an obvious question: what is the relationship between function and topography/location of projection neurons in the DCN and emphasize the importance of defining the microcircuitry through which the DCN integrate afferent projections. In order to satisfactorily address this question, paired recordings of PPNs and NOPNs are needed to compare the correspondence of synaptic inputs to these two types of projection neurons.

The remarkable segregation of PC inputs to functionally defined DCN projection neurons was unexpected. However it helps to explain several convergent lines of research on PC-DCN synaptology. Due to the inhibitory phenotype of PCs (Ito et al., 1964), it has been long hypothesized that they should pause their firing during a movement in order to disinhibit DCN projection neurons and drive movement (Albus, 1971; Ito, 1984; Marr, 1969). However, Person and Raman recently demonstrated in slice preparations that PPNs in the deep nuclei respond vigorously to synchronous PC bursts (Person and Raman, 2012a, b), similar to the synchronous bursts documented *in vivo* (Heck et al., 2007). Conversely, NOPNs are strongly depressed by Purkinje cell spike trains and fire maximally when Purkinje cell output is suppressed (Najac and Raman, 2015). Since PPNs have been extensively shown to be active during movement execution (Heiney et al., 2014b; Sanchez-Campusano et al., 2011), and it is presumed that NOPNs are also active during movement execution (Hesslow and Ivarsson, 1996; Sears and Steinmetz, 1991), it stands to reason that each must receive the appropriate input from their presynaptic PCs in order to be active during this period. Our data reveal a dynamic regulatory circuitry in which the cerebellar cortex can independently modulate PPN and NO channels through segregated PC synaptic input. We also demonstrate a small contingent of collateralized PC synaptic projections analogous to those documented in ultrastructural investigations (De Zeeuw and Berrebi, 1995a, b; Teune et al., 1998) that can modulate both efferent pathways.

The preponderance of PCs differentially infected by transport of virus from the red nucleus and IO through the interpositus nucleus suggests that this functional segregation is a common feature of PC synaptology throughout the DCN, but this remains to be established. As noted above, the presence of dual labeled PCs is likely due, at least in part, to collateralization of PC axons to innervate PPN and NOPNs. However, the diversity of cellular phenotypes and

connections that have been revealed in the DCN raise other possibilities. For example, the presence of dual infected PPNs in our material raises the possibility that these neurons issue a collateral that is synaptically linked to NOPNs. This is supported by ultrastructural analysis either alone (Hámori and Mezey, 1977) or in combination with Golgi impregnations (Chan-Palay, 1973a, b, c) showing recurrent collaterals of large projection neurons synapsing upon large and small neurons in the DCN, and the demonstration that inhibition of the IO can be elicited by stimulation of nucleo-rubral fibers, presumably via antidromic excitation of PPNs (Svensson et al., 2006). It is also possible that collateralized PCs innervate DCN interneurons that are presynaptic to both PPNs and NOPNs. Candidates include small glycinergic neurons of the DCN, which receive PC innervation and are presynaptic to PPNs (Chan-Palay, 1973c; De Zeeuw and Berrebi, 1995a, b; Gonzalez-Joekes and Schreurs, 2012; Husson et al., 2014). This synaptic relationship could serve to coordinate firing patterns between PPNs and NOPNs within the same module and/or inhibit PPN and NOPNs pairs in neighboring modules, thereby sharpening the DCN representation of cortical firing patterns. Additional local circuits (*e.g.*, via GABAergic and glutamatergic interneurons) likely exist to efficiently integrate PC input with that of other afferents. These data are consistent with the local circuits postulated in the viral tracing study of Gonzalez-Joekes and Schreurs (Gonzalez-Joekes and Schreurs, 2012) and our own data demonstrating retrograde transneuronal infection of neurons in the DCN that do not accumulate CTβ and therefore cannot be first order projection neurons. Further investigation of the routes of viral transport within the DCN is necessary to define the synaptic organization of these local neural networks. In this regard, the future use of pseudorabies virus recombinants expressing conditional reporters (Card et al., 2011a; Card et al., 2011b) and strains of rabies virus that only have the capacity to cross one synapse (Callaway, 2008; Ghanem and

Conzelmann, 2015; Schwarz et al., 2015; Wickersham et al., 2007) may be particularly informative.

In addition to convergent local circuits of the DCN hypothesized to produce dual infection of PCs, double-labeled PCs may also result from recurrent collaterals that PCs issue onto neighboring PCs (Bernard and Axelrad, 1993; Bishop, 1982; Chan-Palay, 1971; de Solages et al., 2008; Hawkes and Leclerc, 1989; Orduz and Llano, 2007; Ramón y Cajal, 1995; Sugihara et al., 2009). It is likely that these short-range collaterals serve as conduits for spread of virus to adjacent PCs within a module. Evidence for this possibility is apparent in the distribution of dual labeled PCs. Double-labeled profiles were most commonly found in areas of cortex that contained the densest infection of the PC layer. In these regions, the occasional double-labeled PC was flanked by groups of PCs expressing only one of the fluorescent reporters. Isolated double-labeled PCs were almost never found (1 profile across all cases). This pattern supports the interpretation that double labeled PCs may have become infected through the convergence of local recurrent circuits.

In conclusion, our data provide further insight into the means through which PCs regulate the activity of functionally distinct efferent projections from the DCN. Central to our findings is the demonstration of parallel pathways from the cerebellar cortex through the DCN to the red nucleus and IO, as well as individual PCs synaptically linked to both of these efferent pathways. The existence of this dynamic regulatory circuitry comports with recent findings regarding the differential influences of PCs upon neural activity within the DCN (Heck et al., 2007; Najac and Raman, 2015; Person and Raman, 2012a, b) and provides further insight into the complex synaptology resident within the DCN. The data challenge the presumed collateralization of Purkinje cell inputs to deep cerebellar nuclei projection neurons, and open new avenues for

investigating how cortical firing patterns are integrated in the DCN to control both its effector and recurrent feedback pathways.

3.0 CLOSED LOOP OLIVO-CEREBELLAR CIRCUITS REVEALED WITH COMBINED MONOSYNAPTIC AND VIRAL TRACING TECHNIQUES

3.1 INTRODUCTION

The uniform cytoarchitecture of the cerebellar cortex has led to a widely held belief that functional heterogeneity arises from a mosaic of afferent connectivity (Apps and Hawkes, 2009; Ito, 2006). A major part of the mosaic arises from the highly topographic projections from the inferior olive (IO) to the cerebellar cortex and deep cerebellar nuclei (DCN). Individual IO neurons issue an axon that targets the cerebellar cortex, but also has collateral projections that target the DCN. In the cortex, their terminal endings are seen as climbing fibers, which innervate the proximal dendrites of Purkinje cells (PC). Each PC receives one and only one climbing fiber axon (Sugihara et al., 1999), which forms enough excitatory contacts onto the PC such that if the climbing fiber issues an action potential, the PC necessarily follows suit (Eccles et al., 1964, 1966). This strong action potential has been shown to be a major driver of synaptic plasticity, and stimulating climbing fibers can be used to drive associative learning (Mauk et al., 1986). Although there is debate as to the exact type of information conveyed by climbing fibers, it is currently thought that climbing fibers may convey either an error signal (Ito, 2013) or timing signal to the cortex (Llinás, 2011).

The climbing fiber projection system is organized perpendicular to the lobular folding of the cortex, forming a series of parasagittal zones, called modules, throughout the cortex (Ruigrok, 2011; Sugihara, 2011; Sugihara and Shinoda, 2004, 2007; Sugihara et al., 1999; Voogd et al., 2013). PCs issue axons that target a number of different cells in the DCN, including both projection neurons and interneurons (De Zeeuw and Berrebi, 1995a, b). One of these cell types is the nucleo-olivary projection neuron (NOPN; (Teune et al., 1998)). NOPNs are GABAergic neurons that project exclusively to the IO (Fredette and Mugnaini, 1991). This feedback projection to the IO has been recently shown to modulate the electrotonic coupling of IO neurons and the temporal dynamics of IO responsiveness to somatosensory inputs (Hogri et al., 2014; Lefler et al., 2014; Llinás, 2013). Considerable evidence supports the conclusion that the NOPN pathway is part of a closed loop circuit. This entails that IO climbing fibers innervate the same Purkinje cells from which they receive recurrent polysynaptic feedback through the DCN (Ruigrok, 2011). However, the multisynaptic character of this olivo-cortico-nucleo-olivary (OCNO) circuit and the limitations of classical tracing technology have prevented a definitive anatomical confirmation of the closed loop architecture of the circuitry. Viral transneuronal tracers give us the tools to study long range, multisynaptic circuits using a single injection site (Card and Enquist, 1994, 2014; Strick and Card, 1992, 2011). Viral transneuronal tracers have been used to identify functionally distinct subdomains of the cerebellar cortex and deep nuclei that are linked to the basal ganglia (Bostan et al., 2010, 2013; Bostan and Strick, 2010; Hoshi et al., 2005), cerebral cortex (Dum and Strick, 2003; Kelly and Strick, 2003; Middleton and Strick, 2001), and facial motor neurons that innervate the orbicularis oculi muscle (Gonzalez-Joekes and Schreurs, 2012; Morcuende et al., 2002; Sun, 2012). We employed a similar approach to study the closed versus open loop topography of the OCNO circuit.

The goal of this study was to test the hypothesis that IO climbing fibers innervate Purkinje cells that in turn provide feedback to the same IO cells through the DCN, forming closed OCNO loops. We tested this hypothesis by combining injection of a classical tracer (the beta subunit of cholera toxin; CTβ) that does not cross synapses but is transported bidirectionally within neurons (Angelucci et al., 1996; Lanciego and Wouterlood, 2011), with a well characterized recombinant of the viral transneuronal tracer pseudorabies virus (PRV), which spreads selectively in the retrograde direction through neural circuits (Card and Enquist, 2014). Combining these two tracers into a single IO injection allowed us to visualize the topography of the entire OCNO circuit. The results confirmed our hypothesis, providing strong evidence for the existence of a closed loop architecture of OCNO circuits throughout the olivo-cerebellar system.

3.2 MATERIALS AND METHODS

Animals and Regulatory Issues.

The University of Pittsburgh Institutional Animal Care and Use Committee, Recombinant DNA Committee, and the Division of Environmental Health and Safety approved all experiments. Adult male Sprague-Dawley rats (225-375 grams) were acclimated to a Biosafety Level 2+ facility for a minimum of one day prior to the onset of experiments and lived in the facility throughout the experiment. The light/dark cycle in the facility was 12 hours of light and 12 hours of dark (lights on at 0700). The room temperature was held constant between 22 and 25°C and access to food and water was provided *ad libitum*. A total of 11 rats were used in the study. Only five cases are included in quantitative analyses due to either missed injection sites or inadequate spread of the two tracers in non-quantified cases.

Experimental Design.

In order to assess the degree to which OCNO circuits are closed loops, we made single injections of a cocktail of PRV and CTβ. This combination allowed us to map the distribution of both anterogradely filled climbing fibers originating from the IO injection site and Purkinje cells retrogradely infected with PRV by virtue of their synaptic connections to NOPNs innervating the IO injection site (Figure 7).

Viral and Classical Tracers.

Retrograde transneuronal tracing was accomplished using a well-characterized recombinant of the Bartha strain of PRV for this experiment. PRV-Bartha is an attenuated vaccine strain of virus that invades neurons and generates infectious progeny that travel exclusively in the retrograde direction through neural circuitry (Card and Enquist, 2014; Pickard et al., 2002). Swine are the natural host of PRV but the virus has a broad host range, with the capacity to infect essentially all mammals except higher primates. The genome of the virus has been sequenced (Klupp et al., 2004) and the genetic basis for virulence and directional spread of the virus through the nervous system has been defined (Pomeranz et al., 2005). The PRV Bartha recombinant used in this study was PRV-152 which expresses EGFP. Reporter expression is under the control of the cytomegalovirus immediate early gene promoter (Billig et al., 2000; Smith et al., 2000). The titer of PRV-152 was 1.24×10^9 plaque forming units per milliliter (pfu/ml). Climbing fibers and NOPNs were labeled using the monosynaptic tracer CTβ (Angelucci et al., 1996; Lanciego and Wouterlood, 2011). CTβ is a bidirectional tracer that was used to anterogradely fill climbing fibers projecting to the cerebellar cortex and deep nuclei and to retrogradely fill NOPNs in the DCN.

Stereotaxic Injections.

The PRV recombinants were injected as a cocktail with a 1% solution of CTβ in a 7:1 ratio (virus:CTβ) according to the approach developed by O'Donnell and colleagues (O'Donnell et al., 1997). Anteroposterior and mediolateral coordinates for injection of the inferior olive were calculated from Bregma and dorsoventral coordinates were calculated from the dorsal surface of the brain using the stereotaxic atlas of Swanson (Swanson, 2004). The AP (-12.7 mm) and DV (-9.7 mm) coordinates for injection of the IO were the same for each animal, but the ML coordinate varied (0.2-0.6 mm) in order to involve different IO subdivisions. The general procedures used for stereotaxic surgery in our laboratory have been published (Card and Enquist, 2014), but details specific to this study follow. All injections were made through beveled pulled glass pipettes with an internal tip diameter of ~40 μm. After drilling a hole in the cranium at the desired coordinates, the pipette was lowered into the brain and the tissue was allowed to decompress for 1 minute prior to pressure injection of 40-80 nanoliters of virus using a Picopump (World Precision Instruments, Inc., Sarasota, FL). The pipette was left *in situ* for ten minutes following each injection to allow for uptake of the two tracers and then slowly removed. The craniotomies were filled with bone wax, the incision was closed with surgical staples, and a subcutaneous injection of the analgesic Ketofen (2 mg/kg) was administered. Animals were kept on a heating pad until they recovered consciousness and then returned to their home cage. The animals lived within the BSL2+ facility for the balance of the experiment and received a daily injection of Ketofen during that period.

Tissue preparation.

Animals were deeply anesthetized by intraperitoneal injection of Fatal Plus (Vortech Pharmaceuticals, Dearborn, Michigan; 390 mg/ml sodium pentobarbital) and perfused

transcardially with saline followed by 4% paraformaldehyde-lysine-periodate (PLP) fixative (McLean and Nakane, 1974) 48 hours following virus injection. The details of this procedure as applied in our laboratory have been published (Card and Enquist, 2014). Retrograde spread of the PRV-152 through cerebellar circuits was visualized with immunocytochemical localizations of PRV, either alone or in combination with CTβ and phenotypic markers. Antibodies used for immunocytochemical localization included rabbit anti-PRV (1:10k, (Card et al., 1990)), rabbit anti-Zebrin II (Abcam, 1:100; (Li et al., 2013)) and mouse anti-ED1 (Millipore; 1:100; (Dijkstra et al., 1985; Rassnick et al., 1998)). Secondary antibodies conjugated to fluorophors (Alexafluor 488, Cy3; Jackson ImmunoReseach Laboratories) were used for immunofluorescence localizations. Biotinylated secondary antibodies (Jackson ImmunoReseach Laboratories) and Vectastain Elite reagents (Vector Laboratories) were used for immunoperoxidase localizations. Sections at a minimum frequency of 210 μm were processed and analyzed for each immunocytochemical marker, either alone or in combination. Tissue processed for dual (CTβ and PRV) immunoperoxidase localizations was first incubated in the appropriate antibodies against CTβ, immersed in 100ml of a nickel-intensified diaminobenzidine solution and the reaction catalyzed with 10 μl of H_2O_2 for 10-15 minutes to stain CTβ+ neurons blue-black. Sections were then incubated with the appropriate antibodies against PRV, immersed in 100ml of a saturated diaminobenzidine solution and the reaction catalyzed with 35 μl of H_2O_2 for 3.5-5 minutes to stain infected neurons brown.

Localization of Injection Sites.

Defining the primary injection site was essential for each of the experimental paradigms. Toward this end we analyzed multiple bins of tissue with sections at a minimum frequency of 210 μm processed for one or more phenotypic marker. We initially processed one bin of tissue

for dual immunoperoxidase localization of viral antigens (brown) and CTβ (black) (Figure 7 A1-8). These localizations defined the full extent of viral spread through the nervous system and also allowed an initial assessment of the localization of injection sites. Figure 7 A1 through A8 illustrate the spread of virus (brown) and CTβ (black) through the rostrocaudal extent of the IO at a frequency of 210 μm. To precisely determine the subfield of the IO that was the primary site of injection we also processed an adjacent bin of tissue for triple immunofluorescence localization of viral antigens, CTβ, and ED1 (B1). Figures 7 B2-B4 illustrate the immunofluorescence signal of each of these antigens visualized in the individual channels that illuminate their fluorophors. ED1 identifies a cytoplasmic antigen expressed by cells of phagocytic cells of monocytic lineage (Dijkstra et al., 1985), which we have previously demonstrated to be a reliable marker of immune cells trafficking to areas of damage (*e.g.*, cannula tracks) and viral infection (Rassnick et al., 1998; Rinaman et al., 1993). Consistent with these prior studies we established objective criteria to precisely define the primary site of injection and map the extent of virus and CTβ spread from that site. The primary site of injection was determined by following the cannula tract to its termination within the IO. This assessment was aided by the accumulation of ED1+ immune cells along the track and dense aggregates of these cells within the region surrounding the tip where viral replication was most advanced (B4). Injection sites were photographed in optical stacks spanning the depth of the tissue (35 μm) using a confocal microscope at 10x magnification at 1 μm intervals. The primary site of viral uptake was defined as the region most densely labeled with all three markers. Within this region PRV and CTβ uptake from the extracellular space produces retrograde infection and CTβ labeling of first order neurons. Thus, there is a temporal advantage in the spread of infection from this region that is reflected in the distribution of viral antigens within

infected neurons (i.e., early replication is characterized by restriction of viral antigens to the cell soma and proximal dendrites, whereas advanced replication is characterized by presence of viral antigens throughout the somatodendritic compartment). Areas outside of the primary injection site were marked by neurons at earlier stages of infection (see following section) and more diffuse accumulation of CTβ, consistent with a prior investigation that established this approach (O'Donnell et al., 1997).

Data analysis.

The initial analysis of each case involved immunoperoxidase localization of PRV, either alone or in combination with nickel intensified CTβ, to precisely define the spread of infection in relation to retrograde and anterograde transport of CTβ and to determine the location of injection sites. These localizations, which involved sections at a frequency of 210 μm through the rostrocaudal extent of the neuraxis, also served as templates for directing fluorescence analyses. Localization of reporters of viral infection in combination with immunofluorescence localization of CTβ and the immune marker ED1 was used to precisely define the primary sites of injection in the IO that generated first order uptake of virus and infection.

OCNO loop quantification.

In order to determine the extent to which OCNO loops are closed circuits, we quantified labeled climbing fiber and infected Purkinje cell (PC) distribution in five cases. Three animals received a single 40 nl injection of the CTβ-PRV cocktail into the inferior olive. The remaining two cases were animals that received dual 80 nl cocktail injections into the IO and the red nucleus (from the first study in Chapter 2). The latter cases lacked any detectable retrograde spread of virus from the red nucleus to PCs in the cerebellar cortex, as confirmed by epifluorescence analysis of the entire cerebellar cortex in an adjacent series of sections. These

cases are thereby taken to be quantitatively equivalent to cases involving injections only into the inferior olive. All animals for this analysis survived for 48hrs post-inoculation.

In each case, we analyzed ten sections per animal that were standardized between cases and aligned with the closest corresponding Swanson Atlas plate (Swanson, 2004). Within each section the cerebellar cortex was divided into regions belonging to one of two categories: 1) cortical areas previously demonstrated to receive climbing fiber innervation from the primary site of viral injection (Sugihara and Shinoda, 2004, 2007) and 2) all other cortical areas. Tissue was processed for dual immunoperoxidase localization of viral antigens (brown) and climbing fibers (nickel-intensified black). Infected neurons were mapped using StereoInvestigator image analysis software. Within category 1 areas, the tissue was systematically scanned and mapped at 40x magnification in order to ensure counting of all labeled neurons and fibers. The objective criterion for virally infected neurons was the clear presence of brown viral antigen staining within somata and dendrites; the objective criterion for CTβ filled climbing fibers was the presence of blue-black puncta that could be distinguished from PC dendrites in the molecular layer of cerebellar cortex. PCs were counted as either single labeled (PRV+) or dual labeled (CTβ+/PRV+) and were graded for the stage of viral infection. A PC was taken to be dual labeled if it met the criterion for viral infection and its overlying dendrites were co-extensive with a CTβ labeled climbing fiber. The percentage of dual labeled PCs in the cortical lobule known to receive climbing fiber input from the injected IO subfield was calculated. Group data were calculated as this percentage plus or minus the standard error of the mean.

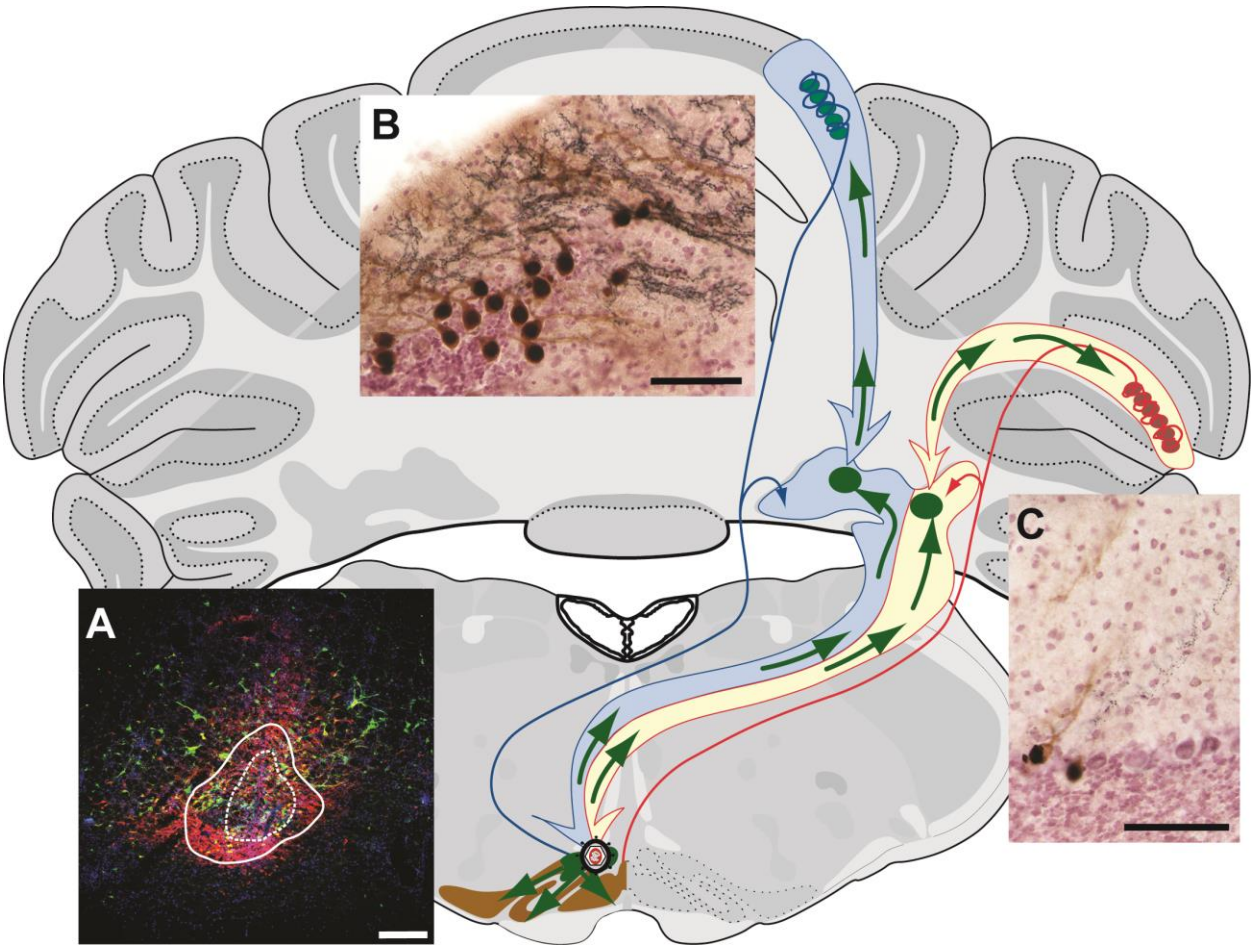

Figure 7. *Spread of virus and CTβ through olivo-cerebellar circuits.*

Overall schematic of quantification design. In panel (A) is a typical injection site immunofluorescently labeled for PRV (green), CTβ (red) and ED1 (blue). The primary uptake zone, as defined by the densest accumulation of ED1, is outlined in a dotted line and secondary spread of the tracers is outlined in a solid line. Neurons infected via the primary injection site (blue route in schematic) display dense viral immunoreactivity and heavy labeling of climbing fibers (B). These dense infected cortical regions were predicted by known topography of climbing fibers (Sugihara and Shinoda, 2004) and were the only regions quantified as they represent the most directly route through which both tracers spread. Cortical regions synaptically linked to the secondary injection sites are infected at later time points, due to secondary spread of PRV through the IO. CTβ spread to these regions is also more limited due to the more diffuse spread of tracer in the secondary zones compared to primary zones. The lack of late infected PCs and dense CTβ in secondary cortical regions can be seen in (C). Marker bars = 100 μm.

3.3 RESULTS

Closed Loop Architecture of OCNO Circuits.

A considerable literature supports the conclusion that neurons in the IO that collateralize to the deep nuclei and cortex are components of a closed polysynaptic loop in which olivary neurons projecting into the cortex and DCN are recipient of a polysynaptic projection from their target PCs though the deep nuclei. However, direct confirmation of the closed loop architecture of this circuitry has been limited by the inability of classical tracers to cross synapses. To determine if OCNO circuits are indeed closed loops, we combined injection of a cocktail of the beta subunit of CTβ and PRV-152 or PRV-614 into the IO. The capacity of CTβ to be transported in both the retrograde and anterograde directions after co-injection with α-herpesvirus recombinants (Voogd and Ruigrok, 2004) allowed us to visualize the distribution of climbing fiber cerebellar afferents in relation to neurons infected by retrograde transneuronal spread of PRV from the IO to the DCN and cerebellar cortex. Importantly, this approach allows for the assessment of closed vs. open loops associated with a single injection site. Thus we are not constrained by the need to align multiple injection sites of classical tracers within the circuit and we can perform a quantitative analysis of the divergence and convergence of OCNO loops.

IO Injection sites.

As noted above, the zone of primary viral uptake is also the primary zone of uptake for CTβ, which has a larger radius of diffusion compared to PRV (Figure 7B red channel) (O'Donnell et al., 1997). This increased area of CTβ uptake will label climbing fibers emanating from IO regions outside the zone of primary viral uptake, thereby highlighting climbing fibers outside of the circuit infected with PRV. Similarly, PRV will replicate and spread locally within the IO, leading to a second temporally delated wave of retrograde spread of virus through the

DCN to infect PCs in the cerebellar cortex. A typical injection site is shown in Figure 8B, a triple immunofluorescence localization of PRV-152, CTβ, and ED1. The dotted line indicates the zone of primary uptake of both PRV and CTβ, while the solid line outlines the extended region of CTβ primary uptake and the regions into which PRV spreads through the IO via gap junctions(Card et al., 2014). For a full list of primary injection site locations for quantified cases see Figure 10.

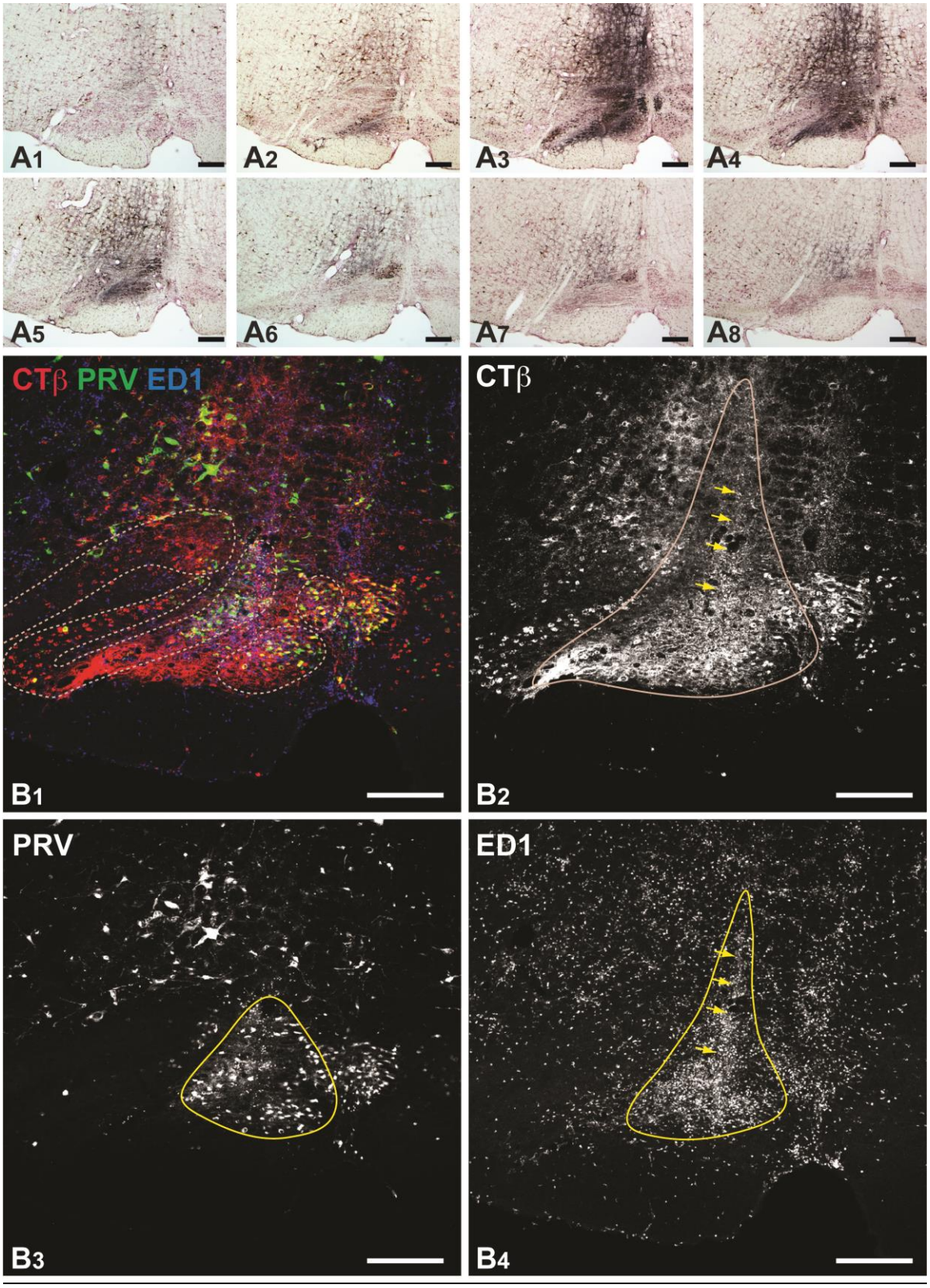
A1
A2
A3
A4
A5
A6
A7
A8
CTβ PRV ED1
B1
CTβ
B2
PRV
B3
ED1
B4

Figure 8. *Localization of injection sites.*

Defining the primary injection site was essential for each of the experimental paradigms. Toward this end we analyzed multiple bins of tissue with sections at a minimum frequency of 210 μm processed for one or more phenotypic marker. We initially processed one bin of tissue for dual immunoperoxidase localization of viral antigens (brown) and CTβ (black) (A1– A8). These localizations allowed an initial assessment of the localization of injection sites. Panels (A1 – A8) illustrate the spread of virus (brown) and CTβ (black) through the rostrocaudal extent of the IO at a frequency of 210 μm in a representative case. To precisely determine the subfield of the IO that was the primary site of injection we also processed an adjacent bin of tissue for triple immunofluorescence localization of viral antigens, CTβ, and ED1 (B1). Panels (B2 – B4) illustrate the immunofluorescence signal of each of these antigens visualized in the individual channels that illuminate their fluorophors. ED1 identifies a cytoplasmic antigen expressed by cells of phagocytic cells of monocytic lineage (Dijkstra et al., 1985) and we have previously demonstrated that it is a reliable marker of immune cells trafficking to areas of damage (*e.g.*, cannula tracks) and viral infection (Card et al., 1993; Rinaman et al., 1993). Consistent with these prior studies we established objective criteria to precisely define the primary site of injection and map the extent of virus and CTβ spread from that site. The primary site of injection was determined by following the cannula tract to its termination within the IO. This assessment was aided by the accumulation of ED1+ immune cells along the track and dense aggregates of these cells within the region surrounding the tip where rival replication was most advanced (B4). Injection sites were photographed in optical stacks spanning the depth of the tissue (35 μm) using a confocal microscope at 10x magnification at 1 μm intervals. The primary site of viral uptake was defined as the region most densely labeled with all three markers. Within this region PRV and CTβ uptake from the extracellular space produces retrograde infection and CTβ labeling of first order neurons. Thus, there is a temporal advantage in the spread of infection from this region that is reflected in the distribution of viral antigens within infected neurons. Areas outside of the primary injection site were marked by neurons at earlier stages of infection (see following section) and, consistent with a prior investigation that established this approach (O'Donnell et al., 1997), diffuse spread of CTβ (B2). Marker bars = 250 μm.

Overall Spread of the Two Tracers.

Fluorescence analysis demonstrated that first-order NOPNs colocalizing retrogradely transported CTβ and reporters of viral infection were found throughout the IP and dentate nuclei, but were differentially concentrated within the ventral parvocellular region of the interpositus nucleus (pcIP). We also observed retrograde transneuronal infection of PCs in the cerebellar cortex with a distribution that would be predicted on the basis of the previously documented topography of PC projections to the DCN (Voogd and Ruigrok, 2004). However, there are two important considerations to evaluating the distribution of labeled climbing fibers and infected neurons in the DCN and cortex in our study. First, it has been previously demonstrated that the diffusion of CTβ from the injection site exceeds that of virions following intracerebral injection (O'Donnell et al., 1997). Thus, the expectation is that labeled climbing fibers would be observed in areas of the cortex that do not contain infected neurons. This result was confirmed in our experimental material (Figure 7). Second, we have recently established that PRV is able to move through gap junctions within the IO (Card et al., 2014). Thus, infection of neurons at the primary site of injection would ultimately lead to secondary infection of IO neurons in adjacent subfields, followed by temporally delayed retrograde spread of infection of neurons to the DCN and cortex. Consequently, defining the primary site of recombinant injection within the IO was crucial to the experimental goals. Toward this end we employed triple staining techniques involving immune cell antigens that allow unambiguous identification of primary sites of injection (Rinaman et al., 1993) (Figure 8B).

The distribution of viral antigens within infected neurons also provided important insights into the temporal kinetics of viral infection that informed our analysis of the closed loop architecture of OCNO loops arising from the primary site of injection. In this regard, it is firmly

established that the distribution of viral antigens in neurons early in viral replication is more restricted (*e.g.*, concentrated in the cell nucleus and soma) than observed in neurons advanced in replication (*e.g.*, present throughout the somatodendritic compartment). The utility of these features in defining the temporal kinetics of viral replication and routes of viral transport through neural networks have been reported (Cano et al., 2001; Card and Enquist, 2014). Briefly, having defined the sites of primary infection and secondary spread of virus in the IO we used prior literature that mapped the topography of climbing fiber projections to cortex to predict the lobules of cortex that should be in advanced (primary injection site) and early (secondary spread of infection) stages of viral replication (Figure 7). That analysis consistently revealed PCs in advanced stages of viral replication in regions of cortex known to receive climbing fiber input from the primary site of injection. Importantly, these neurons were coextensive with labeled climbing fibers. Similarly, areas known to receive climbing fiber projections from areas of secondary spread in the IO exhibited early stages of viral replication, with viral antigens largely limited to cell nuclei and somata (Figure 7C). This pattern of labeling is consistent with the delayed temporal kinetics required for virus to spread through the IO prior to retrograde transneuronal spread to the cortex through the DCN.

PRV and CTβ labeling within the DCN.

The bidirectional transport of CTβ allowed us to define the distribution of climbing fiber collaterals emanating from the IO, in relation to retrograde spread of PRV recombinants from the IO (Figures 9A-D). In agreement with the reported topography of olivo-nuclear and nucleo-olivary projection (Ruigrok and Voogd, 2000; Sugihara and Shinoda, 2004, 2007; Sugihara et al., 2001; Voogd et al., 2013), and consistent with a closed loop architecture, CTβ+ axonal varicosities were coextensive with dual labeled NOPNs (CTβ + PRV) following injection of a

cocktail of virus and CTβ into the IO (Figure 9C and D; CTβ channel). CTβ-labeled climbing fiber collaterals were never located in regions of the DCN that did not contain retrogradely labeled NOPNs. Though we cannot firmly establish that the CF collaterals observed here make synaptic contact onto retrogradely filled NOPNs, we take this as preliminary support for closed OCNO loops at the level of the DCN.

Regions that contained coextensive climbing fiber collaterals and retrogradely labeled NOPNs also contained putative PPNs expressing markers of viral infection (Figure 9C, D). Putative PPNs were defined by their large multipolar morphology in addition to the absence of CTβ. Putative PPNs were not located in regions of the DCN that did not contain retrogradely infected NOPNs. Infected putative PPNs were always located within 100-300 μm of infected NOPNs, which we interpret as evidence supporting the existence of a short recurrent collateral from PPNs onto NOPNs. This result strengthens evidence for this same connection observed in Chapter 2.

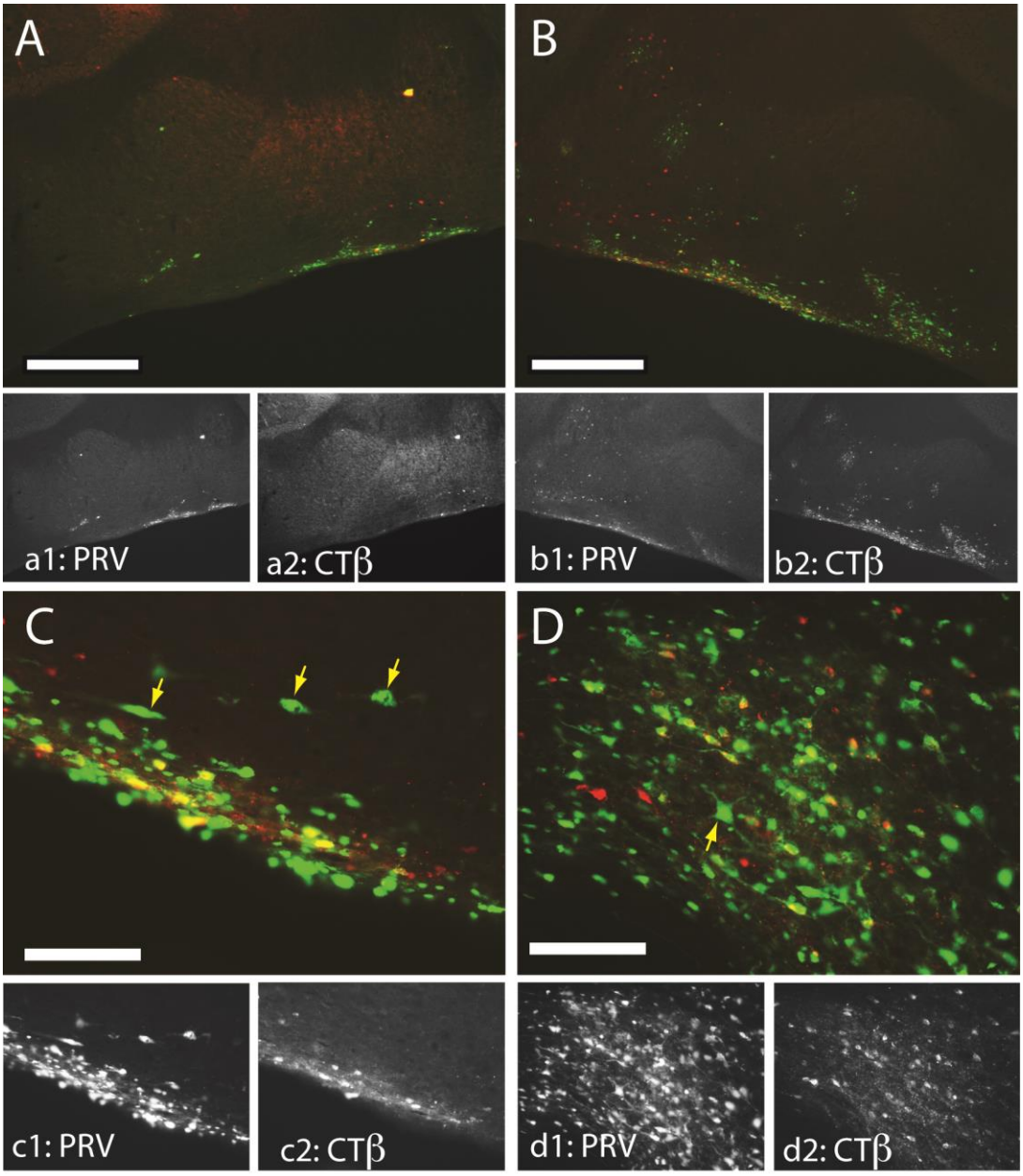

Figure 9. *Spread of virus and CTβ in the DCN.*

Panels (A) and (B) show the distribution of virus (green) and CTβ (red) containing neurons in the DCN. Panel (A) is ipsilateral to the IO injection site and (B) is contralateral to the injection site. This particular case (OCNO 2) had a dense infection of the pcIP from the injection site which included the principal IO and the rMAO. In (A) note the viral infection in the corresponding region of the DCN on the opposite side, commonly observed whenever infection was located in the pcIP. Panel (C) depicts a higher magnification of (B). Many NOPNs containing both CTβ and virus are seen in the center of the viral labeling. Cells not containing CTβ (i.e. infected transneuronallyare located in the immediate vicinity of dual labeled neurons. Many of these were large multipolar neurons reminiscent of PPNs. Panel (D) depicts labeling more rostrally in the same case in the ventral dentate nucleus. Again both dual labeled (NOPNs) and single labeled can be observed. Many of the single labeled neurons appear to be PPN morphologically. Individual channels for virus or CTβ are displayed in (a1-2), (b1-2) (c1-2) and (d1-2). Scale bars in (A) and (B) = 500 μm; in (C) and (D) = 100 μm.

PRV and CTβ labeling within the Cerebellar Cortex.

Quantitative morphometric analysis of virus and CTβ spread from the primary site of injection in five cases demonstrated a near one-to-one correspondence between retrograde transneuronal spread of virus to PCs and climbing fibers emanating from the primary site of injection in the IO (Figure 10). This analysis revealed a 78.4 ± 2.7% correspondence between PRV+ Purkinje cells and CTβ+ climbing fibers, with nearly every infected PC in cortices associated with the primary injection site had an overlying CTβ+ climbing fiber (Figure 10). Cortices associated with secondary spread of either CTβ or virus through the olive contained a mix of either only CTβ+ climbing fibers or PRV+ PCs, depending upon the degree to which spread of CTβ and PRV from the primary injection site overlapped. For example when in case OCNO 2, the primary injection site was in the principal olive and also included parts of the rMAO. Correspondingly, PCs with the most advanced infection were located in crus II and in the paraflocculus. PCs in these areas had detectable levels of viral antigen throughout their somata and dendritic trees, indicating that they had been replicating virus for some time. Infected granule cells were occasionally present in these regions, indicating that virus had been replicating long enough in PCs to be transported retrogradely to their presynaptic granule cell inputs. In this case (OCNO 2), the secondary injection site was located primarily in the DAO. As such, a few infected PCs were present in vermis lobule V, but these cells stained very lightly for viral antigen, often only staining the nucleus. Likewise, scattered climbing fibers were labeled in these regions, but neither viral labeling nor climbing fiber labeling ever approached the density of labeling located in areas of cortex innervated by the primary injection site, and infected granule cells were never located in secondary regions. These results strongly argue for the closed loop architecture of the OCNO circuit, as previously hypothesized.

Given the demonstration of the divergent of PC input to DCN projection neurons in Chapter 2, one important question is whether CFs contact all classes of PCs, or only PCs synapsing upon NO neurons. To address this issue we conducted fluorescence localizations of reporters of viral infection from dual injection studies (experiment 1 above) and CTβ. We observed that climbing fibers contact all classes of PCs*; e.g.*, PCs expressing only one reporter of infection and dual infected cells expressing both reporters. This result re-affirms the long-established finding that each PC is innervated by one and only one climbing fiber (Sugihara et al., 1999).

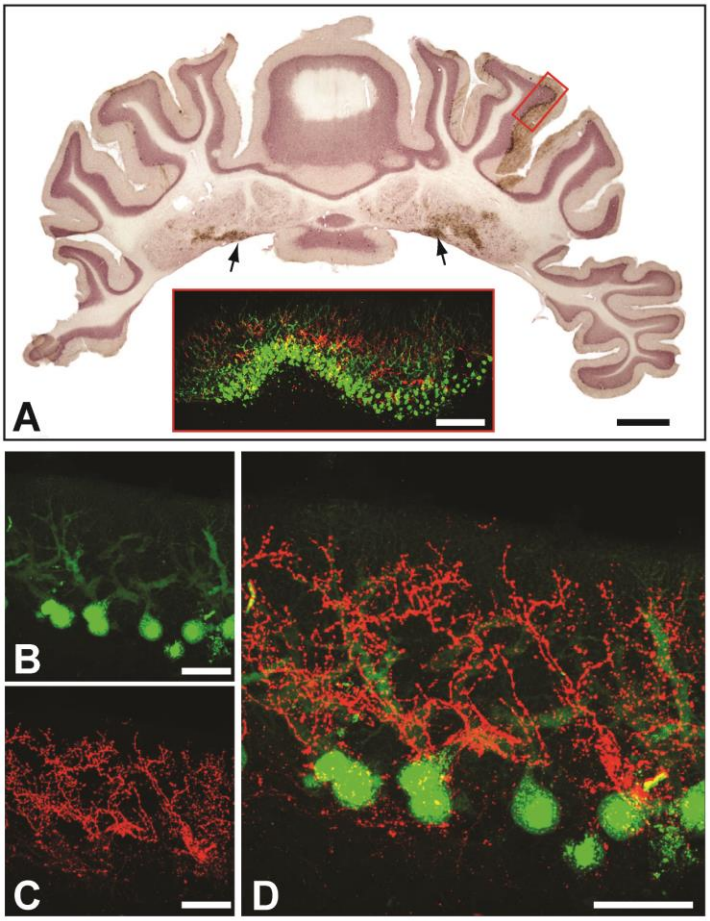

Case	IO Target	Total # PCs	PRV+/CTβ-	PRV+/CTβ+
OCNO 1	DM	794	26.6%	73.4%
OCNO 2	PO/rMAO	1,287	17.0%	83.0%
OCNO 3	vf-DAO	134	12.7%	87.3%
OCNO 4	vl-PO	1,135	26.3%	73.7%
OCNO 5	PO	2,112	19.7%	80.3%
Weighted Average:			**78.73 ± 2.7%**	

Figure 10. *Olivo-cortico-nucleo-olivary circuits are closed loop networks.*

Data supporting the closed loop architecture of OCNO loops are illustrated. Injection of the PRV/CTβ cocktail into the inferior olive resulted in retrograde spread of both tracers to the deep cerebellar nuclei and transneuronal infection of synaptically linked PCs in the cerebellar cortex (A). Anterograde transport of CTβ also labeled climbing fiber afferents to topographically defined populations of neurons in both the DCN and cortex. (A) illustrates the pattern of infection typical of that resulting from localized injection of PRV into IO subfields. Note the circumscribed patterns of infection in the DCN, with a particular concentration of infected neurons in the pcIP bilaterally (arrows) and overlying cortex. The coextensive distribution of disynaptically infected PCs (green) and labeled climbing fibers (red) was revealed in adjacent sections processed for immunofluorescence localization of infected PCs and climbing fibers. The images in (B-D) are taken from high magnification confocal stacks and demonstrate the overlapping distribution of infected PCs and climbing fibers. Coextensive distribution of the labeled profiles was confirmed in quantitative analysis (Table). Marker bars = 1 mm; 200 μm in inset; 50 μm in (B-D).

3.4 DISCUSSION

Contemporary literature has firmly established that the function of the cerebellum extends far beyond the control of movement. This is evident from the topographically organized, multisynaptic loops the cerebellum forms with both motor and non-motor targets (Strick et al., 2009), as well as the presence of non-motor deficits displayed by patients with cerebellar abnormalities (D'Mello and Stoodley, 2015; Schmahmann, 2004; Schmahmann et al., 2007; Stoodley, 2014). The cerebello-cerebro-cerebellar loops that orchestrate these diverse functions arise solely from the principal projection neurons in the DCN, which target the red nucleus and the thalamus (Dum and Strick, 2003; Kelly and Strick, 2003; Middleton and Strick, 2001; Ruigrok and Teune, 2014). Intermixed among PPNs in the DCN are nucleo-olivary projection neurons, which give rise to the inhibitory feedback circuit between the cerebellum and the inferior olive: the OCNO loop (Ruigrok and Teune, 2014; Teune et al., 1995). Although the closed loop architecture supporting functionally defined cerebellar output pathways is well documented, definitive anatomical evidence has been unavailable.

The presence of closed OCNO circuits has been widely accepted in cerebellar research since its theoretical inception in the 1980s (Ito, 1984). Closed OCNO networks have since come to define the proposed functional unit of the cerebellum: *i.e.*, the cerebellar module (Ruigrok, 2011). In the present study, combination of both viral transneuronal and classical monosynaptic tracers permitted direct assessment of whether small inferior olivary subfields are reciprocally connected with the cerebellum via closed loop circuits. In all subfields investigated the date support the hypothesis that OCNO circuits are closed loops, such that Purkinje cells disynaptically feed back to the olivary neurons from which they receive direct climbing fiber input. Thus, each small patch of cerebellar cortex gates its own sensory input from the olive by

innervating NOPNs that innervate IO neurons that provide the source of the PC's climbing fiber input. This arrangement permits discrete cerebellar modules to either learn or execute behaviors without affecting neighboring, functionally distinct modules. The utility of this architecture is illustrated in the recent demonstration of the ability to train rabbits to respond independently to two conditioned stimuli, one driving a hind limb flexion, and the other driving an eyeblink (Mojtahedian et al., 2007). This acquisition of distinct learned behaviors is possible due to the segregated modules that differentially incorporate neurons in the medial anterior IP involved in hind limb flexion and those in the lateral anterior IP essential for eyeblink (C1 and C3 zones, respectively; (Voogd et al., 2003)). Similarly, in a phenomenon known as "Kamin" blocking (Kamin, 1968; Kim et al., 1998), suppression of the olive by the cerebellum during eyeblink conditioning blocks the acquisition of two different conditioned stimuli (e.g., a light and a tone) to the same unconditioned stimulus (e.g., airpuff to the cornea). Thus, the cerebellar module mediating eyeblink conditioning suppresses its own olivary input as learning progresses, regardless of the conditioned stimulus. If OCNO loops were open, then Kamin blocking would occur across different cerebellar modules, and multiple cue learning for multiple behaviors would be impossible. Collectively, these data are consistent with a large body of functional literature demonstrating that nucleo-olivary neurons inhibit only functionally related subfields of the olive i.e., OCNO modules are closed loop circuits (for review see (Ruigrok, 2011; Witter and De Zeeuw, 2015)).

The dense concentration of nucleo-olivary neurons in the ventral parvocellular interpositus revealed in the present study raises many questions regarding the role of this subfield of the DCN compared to other magnocellular subfields of the DCN. The relative absence of PPNs and preponderance of NOPNs within this subfield suggests that it may be specialized for dynamic

regulatory control of the inferior olive. This is supported by the consistent viral labeling found in this region from injections into several different olivary subfields (*e.g.* DM, DAO, rMAO, PO, DMCC). A possible explanation for this is that the pcIP could be involved in specific flexible behaviors that require strong modulation of olivary networks. Determining the exact function of the pcIP, or why it is so densely connected to the IO, is beyond the scope of the studies here. However, the preponderance of NOPNs, paucity of PPNs, and its consistent infection in viral tracing experiments suggest that this subfield operates uniquely compared to the better understood magnocellular divisions of the DCN.

The results presented here uphold the existence of topographically closed OCNO loops and reveals new features of a cytoarchitectonically, and connectionally unique DCN subfield: the parvocellular interpositus nucleus.

4.0 NUCLEO-CORTICAL NEURONS OF THE PARVOCELLULAR INTERPOSITUS TARGET THE PURKINJE CELL LAYER OF THE PARAFLOCCULUS

4.1 INTRODUCTION

One of the main goals of cerebellar research has been to understand the firing patterns of Purkinje cells (PC), and in turn how those signals are related to behavior. The focus of this pursuit has been on the convergence of incoming mossy fiber and climbing fiber afferents onto PC dendrites, where these afferent systems modulate the synaptic weights of excitatory and inhibitory synapses (D'Angelo and De Zeeuw, 2009; Dobson and Bellamy, 2015; Hirano et al., 2016; Mapelli et al., 2015; Rinaldo and Hansel, 2013; Schonewille et al., 2011). Although a considerable amount of progress has been made studying these two afferent systems, one aspect of cerebellar cortical processing has received less scientific attention: feedback projections from the DCN (Houck and Person, 2014). There is growing consensus that the DCN are not simple relays of PC activity, but rather have extensive computational capacities, imparted by a rich diversity of neuronal phenotypes and afferent input (Uusisaari and De Schutter, 2011). This local circuitry allows the DCN to serve as the essential memory trace of learned associative behaviors (e.g., conditioned eyeblinks) and even to function without an intact cortex (Lavond and Steinmetz, 1989; Lavond et al., 1987; Luque et al., 2014). Given the DCN's functional

prominence within the cerebellar circuit, it is imperative that we work to define its local and efferent connections so that we may better understand the DCN's role in both healthy and disease states.

Recently there has been a revival of interest in the nucleo-cortical (NC) projections stemming from the deep nuclei to innervate the cerebellar cortex. The majority of the NC projection is excitatory (eNC) and targets the granular layer where NC fibers contact both granule and Golgi cells, similar to mossy fibers (Houck and Person, 2014). Many, if not all, of these mossy fibers are the collaterals of principal projection neurons (PPNs) that primarily target the red nucleus and thalamus (Houck and Person, 2015). NC fibers mainly target areas of cortex from which they receive Purkinje cell afferents, thus preserving the "closed-loop" functional architecture of the cerebellum (Umetani, 1990). This excitatory nucleo-cortical projection is morphologically distinct from pontine mossy fibers and is thought to function as an efference copy of outgoing deep nuclear processing to amplify signal processing in the cortex (Gao et al., 2016).

In addition to the eNC projection, an inhibitory nucleo-cortical (iNC) pathway has recently been described originating from glycinergic neurons of the DCN (Uusisaari and Knöpfel, 2010; Uusisaari and Knöpfel, 2012). This pathway originates from large, silent cells that are dedicated nucleo-cortical neurons (*i.e.,* they do not project outside of the cerebellum). The terminal endings of these axons do not resemble mossy fibers, but instead resemble traditional synaptic boutons that branch extensively throughout the granular layer (Ankri et al., 2015). It was further shown by Ankri and colleagues that this projection may serve to recruit cerebellar cortical processing by disinhibiting granule cells. Hámori and Tackács described another iNC pathway that terminates as mossy fiber rosettes, similar to the eNC fibers, but

instead contains GABA as a neurotransmitter (Hámori and Takács, 1989). These inhibitory mossy fibers were demonstrated with combined retrograde tracing and immunocytochemistry to originate from the all subdivisions of the DCN (Batini et al., 1989; Batini et al., 1992), placing them in a powerful position to alter the inhibitory tone of the cerebellar cortex. Given the existence of functionally distinct classes of NC projections, it is clear that the DCN are not passive receivers of cortical afferent input, but can have a significant impact on cortical processing. Thus it is imperative to fully characterize the identity, phenotype and projection patterns of NC neurons in order to fully understand the range of nuclear influences of cortical processing.

Here we report the discovery of a novel excitatory nucleo-cortical projection that primarily targets the Purkinje cell layer in the paraflocculus (Purkinje cell layer targeting; PLT). PLT fibers were labeled after injecting the anterograde tracer biotinylated dextran amine into the parvocellular region of the interpositus (pcIP). Ultrastructural analysis revealed this projection to be morphologically excitatory (lucent, spherical vesicles). The data presented here advance our understanding of the numerous and diverse classes of nucleo-cortical fibers, and provide new opportunities for the functional manipulation of nucleo-cortical circuits in order to assess how the deep nuclei and cortex work in tandem to control the smooth execution of behaviors.

4.2 MATERIALS AND METHODS

Animals and Regulatory Issues.

The University of Pittsburgh Institutional Animal Care and Use Committee, and the Division of Environmental Health and Safety approved all experiments. Adult male Sprague-Dawley rats (225-510 grams) were individually housed in a controlled environment: the light/dark cycle in the facility was 12 hours of light and 12 hours of dark (lights on at 0700) and the room temperature was held constant between 22 and 25°C. Animals had *ad libitum* access to food and water. A total of 20 rats were used in the study. 16 animals were used for tracing experiments with light microscopic analyses. Of these, 11 animals received a BDA infusion into the DCN (with 3 having injection sites contained within the pcIP), 2 animals received an infusion of a cocktail of BDA and FG into the pcIP, and 3 animals received an infusion of a cocktail of BDA and FG into the paraflocculus. Four further animals received an infusion of BDA alone into the DCN (only 1 of which was contained in the pcIP) for ultrastructural analysis.

Experimental Design.

To study the projections from the deep cerebellar nuclei to the cerebellar cortex, we made iontophoretic infusions of the anterograde tracer biotinylated dextran amine (BDA; (Reiner et al., 2000)) into the DCN and examined labeled fibers in the cortex (n=11). Injection sites that were within the parvocellular interpositus (pcIP; n=3) produced clear labeling of the novel PLT-fiber projection described above, and so additional injections were targeted to this region of the DCN. Since PLT fibers have not been previously described, we first analyzed their overall topography within the paraflocculus. Since previous nucleo-cortical projections have been observed to be

reciprocally connected with the patches of cortex that they innervate, BDA and the retrograde tracer Fluorogold (FG) were con-infused into the pcIP in 2 animals. This permitted analysis of the distribution of retrogradely filled PCs and anterogradely filled PLT fibers. To further confirm the reciprocal topography of NC fibers, BDA and FG were co-infused into the parafloccular region found to be recipient of PLT fibers in three animals, and the distribution of retrogradely labeled nucleo-cortical cells in the pcIP and anterogradely labeled PC axons was assessed. After the overall topography of PLT fibers was investigated, the synaptic targets of PLT fibers and their neurotransmitter content was assessed at the light microscopic level. To do this we processed tissue for immunofluorescent localization of different neuronal phenotypic markers and analyzed this tissue using a confocal microscope. Relationships between PLT boutons and phenotypically labeled neurons and the neurotransmitter content of PLT fibers were assessed in both optical stacks and in single optical planes. Finally, to better understand the exact synaptic contacts of PLT fibers, tissue from one animal with a pressure injection of BDA into the pcIP at the ultrastructural level was analyzed.

Stereotaxic Infusions.

Rats were iontophoretically infused with either biotinylated dextran amine (BDA; 5% solution; MW 10,000; Invitrogen, Carlsbad, CA) alone or with BDA mixed together with Fluorogold (FG; Fluorochrome, Denver, CO). Equal volumes of 10% BDA and 2% FG were thoroughly mixed to yield a 5% BDA - 1% FG solution. Animals used for ultrastructural analysis received an 80nl pressure injection of 5% BDA using a Picopump (World Precision Instruments, Inc., Sarasota, FL). Anteroposterior and mediolateral coordinates for injection of the pcIP and cerebellar cortex were calculated from Bregma and dorsoventral coordinates were calculated from the dorsal surface of the brain using the stereotaxic atlas of Swanson (Swanson,

2004). The coordinates for injection of the pcIP were anteroposterior (AP): -11.6 mm, mediolateral (ML): 2.6 mm, dorsoventral (DV): -5.9 mm in relation to Bregma with the incisor bar at -3.3 mm. Coordinates for the paraflocculus were AP: -10.8 mm, ML: 7.0 mm, DV: -8.3 mm. The general procedures used for stereotaxic surgery in our laboratory have been published (Card and Enquist, 2014), but details specific to this study follow. All infusions were made through beveled pulled glass pipettes with an internal tip diameter of ~41-43 μm. After drilling a hole in the cranium at the desired coordinates, the pipette was lowered into the brain and the tissue was allowed to relax for 1 minute prior to infusion. The solution was inotophoresed using a 7 second on/7 second off pulsed current of 5 μA for 10 minutes (current source: Stoelting, Wood Dale, IL). The pipette was left *in situ* for ten minutes to allow for adequate absorption of tracer(s). After this period a -1.5 μA retaining current was applied to minimize tracer leakage while the pipette was removed. The craniotomies were filled with bone wax, the incision was closed with surgical staples and a subcutaneous injection of the analgesic Ketofen (2 mg/kg) was administered. Animals were kept on a heating pad until they recovered consciousness and then returned to their home cage. The animals lived within the experimental facility for the balance of the experiment and received a daily injection of Ketofen during that period.

Tissue Preparation for Light Microscopy.

Animals were deeply anesthetized by intraperitoneal injection of Fatal Plus (Vortech Pharmaceuticals, Dearborn, Michigan; 390 mg/mL sodium pentobarbital) and perfused transcardially with saline followed by 4% paraformaldehyde-lysine-periodate (PLP) fixative 3-7 days following tracer infusion. The details of this procedure as applied in our laboratory have been published (Card and Enquist, 2014). Brains were submerged in 20% and 30% sucrose solutions overnight and then sectioned in the coronal planed using a freezing microtome (Leica

SM2000R). Tissue was sectioned at 35 μm into a 1-in-6 series, yielding a sampling frequency of 210 μm. Analysis of tracer spread was achieved by localization of BDA alone or in combination with FG and/or phenotypic markers. Free floating sections were pretreated with a 1% sodium borohydride solution and a 0.5% H_2O_2 solution to reduce background staining. Tissue processed for dual (BDA and FG) immunoperoxidase localizations was first incubated in avidin biotinylated horseradish peroxidase macromolecular complex (ABC; Vector Laboratories), immersed in 100mL of a nickel-intensified diaminobenzidine solution and the reaction catalyzed with 10 μl of H_2O_2 for 10-15 minutes to stain BDA+ fibers blue-black. Sections were then incubated with biotinylated antibodies against FG (rabbit anti-FG, 1:30,000; Fluorochrome, LLC; (Schmued and Fallon, 1986)), immersed in 100mL of a saturated diaminobenzidine solution and the reaction catalyzed with 35 μL of H_2O_2 for 3.5-5 minutes to stain FG+ neurons brown. Bright field images of this tissue were taken with an Olympus BX51 microscope.

Tissue processed for fluorescent analysis was pretreated identically to tissue above and then incubated in streptavidin-horseradish peroxidase for 2 hours. Sections were then incubated in 2mL of a 0.25% of Tyramide Signal Amplification Plus-Cy3 solution for 10 minutes; after which 20 μL of 0.3% H_2O_2 was added and shaken vigorously for 15 minutes. Sections were then incubated in the appropriate antibodies for visualization of L7 (pcp2; stains all Purkinje cells; rabbit anti-L7; 1:500; Aviva Systems Biology), calbindin (Cb; alternate stain for all Purkinje cells; mouse anti-Cb; 1:1,000; Swant, Bellinzona, Switzerland; (Airaksinen et al., 1997)), Glutamic acid decarboxylaxse 67 (GAD67; stains GABAergic neurons; mouse anti-GAD67; 1:1,000; Millipore; (Varea et al., 2005)), choline acetyltransferase (ChAT; stains cholinergic neurons; goat anti-ChAT; 1:50; Millipore; (Heinze et al., 2007)), tyrosine hydroxylase (TH; stains catecholaminergic neurons; mouse anti-TH; 1:1,000; Millipore; (Sanchez-Gonzalez et al.,

2005), and/or NeuN (mouse anti-NeuN; 1:1,000; Millipore, (Rubio et al., 2000)). All studies cited after antibody descriptions have previously established the specificity of primary anti-sera. Secondary antibodies conjugated to fluorophors (Alexafluor 488, Cy3, Cy5; Jackson ImmunoReseach Laboratories) were used for immunofluorescence localizations.

The overall distribution of BDA labeled PLT fibers was assessed using an epifluorescence Olympus BX51microscope. For analysis of potential synaptic targets of PLT fibers, single optical plane images were taken using a 63x oil immersion objection and a LeicaTCS SP5 II confocal microscope (Leica Microscystems, Buffalo Grove, IL). Confocal projection stacks were created by merging single optical planes taken every 1 μm throughout the thickness of the section (~35 μm).

Tissue Preparation for Ultrastructural Analysis.

To assess the synaptic targets of nucleo-cortical fibers four animals were injected for ultrastructural analysis. One of these animals had an injection confined to the pcIP. This animal received a pressure injection of BDA into the ventral parvocellular interpositus nucleus that was seen in previous experiments to project to the paraflocculus. This animals was deeply anesthetized by intraperitoneal injection of Fatal Plus (Vortech Pharmaceuticals, Dearborn, Michigan; 390 mg/mL sodium pentobarbital) and perfused transcardially with 250 mL of phosphate buffered saline followed by 500 mL of 2% paraformaldehyde – 0.5% glutaraldehyde fixative 6 days following tracer infusion. The brain was allowed to further fix in this solution overnight. The entire floccular complex (including the flocculus and paraflocculus) was then removed and sectioned into two bins using a vibratome at 50 μm. Free floating sections were first pretreated with 1% sodium borohydride and 1% H_2O_2 solutions. Sections were then acclimated to cryoprotectant, and then placed in a -80°C freezer for 20 minutes. After thawing

and diluting cryoprotectant with a graded series of PBS and TBS, sections were pretreated for 30 minutes in blocking solution (TBS containing 1% bovine serum albumin, 3% normal donkey serum and 0.4% Triton-X). Sections were then incubated for 90 minutes in avidin-biotin complex reagents (ABC; Vector Laboratories) and then immersed in 100mL of a saturated diaminobenzidine solution and the reaction catalyzed with 35 μL of H_2O_2 for 3.5-5 minutes. After washing the tissue, sections were post-fixed in 1% osmium tetroxide in 0.1M phosphate buffer for 1 hour and dehydrated in a graded ethanol series. The sections were then passed through two changes of acetone followed by increasing concentrations of Epon-Araldite plastic resin diluted in acetone (1:1 overnight; 3:1 for 4 hours; pure resin for 4 hours). Sections were then flat-embedded between acrylic sheets and the resin polymerized overnight at 60°C. Once sections were flat embedded they were photographed using a Sections from the remainder of the brain were processed for immunoperoxidase localization as described in the previous section to confirm the location of the injection site in the DCN with light microscopy.

Flat embedded sections were first photographed at the light microscopic level to direct analysis at the electron microscopic level (Olympus SZX10 Research Stereomicroscope). Sections were trimmed into a trapezoid and then sectioned using a Leica Ultracut R ultramicrotome. We followed the approach used previously in this lab (Agassandian et al., 2012). Two thick sections (1 μm) were cut and one was stained with toluidine blue to aid cytoarchitectural localization of the different cerebellar cortical layers. One section was left unstained in order to visualize the distribution of labeled PLT fibers. Immediately after these thick sections a series of thin (70nm) serial sections were collected onto formvar-coated slot grids (2x1mm). These were kept in serial registration in order to allow for analysis to the same labeled profiles in multiple adjacent sections. Thin sections were analyzed with a transmission

electron microscope (Morgani, FEI, Hillsboro, OR) equipped with a CCD camera (Advanced Microscopy Techniques, Danvers, MA). Insertion of objective apertures into the path of the electron beam provided the necessary contrast in order to visualize anatomical landmarks (e.g. blood vessel, somata) observed in thick sections. The tissue was then scanned systematically at 5,600x magnification and all observed immunoperoxidase positive profiles were photographed at several magnifications. Profiles that could be identified in multiple serial sections were photographed in order to obtain a 3 dimensional perspective of putative synaptic contacts of PLT fibers.

4.3 RESULTS

General Findings.

In all cases (n=5) involving an infusion of BDA into the parvocellular interpositus nucleus (pcIP) nucleo-cortical fibers that target the Purkinje cell layer of the paraflocculus were observed. This is a novel nucleo-cortical projection system, given that the morphology of PLT fibers from pcIP infusions does not match any previous descriptions of nucleo-cortical fibers (Ankri et al., 2015; Gao et al., 2016). Cases in which tracer infusion missed the pcIP (n=12) and was instead contained within magnocellular divisions of the IP did not label PLT fibers, but did stain other nucleo-cortical fibers which ended as mossy fiber like terminals as has been previously described (for review see (Houck and Person, 2014)). In all cases, nucleo-cortical fibers were only found in regions of cortex previously known to target the region of DCN in

which the tracer was infused. This confirms the reciprocal topography observed in descriptions of other nucleo-cortical projection systems (Houck and Person, 2015; Umetani, 1990).

Description of PLT Nucleo-Cortical Fibers.

PLT fibers were observed primarily when infusions of tracer were located in the ventral parvocellular interpositus nucleus (two representative injection sites shown in Figure 11A, B). These cases all displayed a very large plexus of PLT fibers that targeted the paraflocculus. These fibers were morphologically distinct from previously documented nucleo-cortical fibers. Cases with injection into other subdivisions of the DCN revealed few to no PLT fibers. It is important to note that although scattered PLT fibers were found with tracer infusions into the magnocellular DCN, these PLT projections never approached the density of connections seen in pcIP infusion cases. These magnocellular cases labeled other nucleo-cortical fiber classes, primarily ending as mossy-like fibers in the granular layer, while cases with infusions into the pcIP very prominently labeled PLT fibers in the paraflocculus that appear to form the majority of nucleo-cortical projections arising from the pcIP. PLT fibers emanating from the pcIP predominantly targeted the paraflocculus (Figure 11C), but a small number of PLT fibers were found within crus II as well (Figure 11D). Within the paraflocculus PLT fibers ascended through the granular layer and upon reaching the innermost Purkinje cell layer arborized to elaborate putative synaptic boutons (Figure 11E). The bulk of labeled boutons were always found immediately underneath the PC layer, representing its primary target. On their course to the PC layer, PLT fibers were also observed issuing occasional synaptic swellings within the granular layer (Figure 11F). Finally scattered PLT fibers were found ascending into the molecular layer where the formed putative synaptic boutons, typically in close apposition to molecular layer interneurons (Figure 11F). Contacts in the granule and molecular layers made up a minority of the total boutons; the majority were found either in or directly beneath the PC layer.

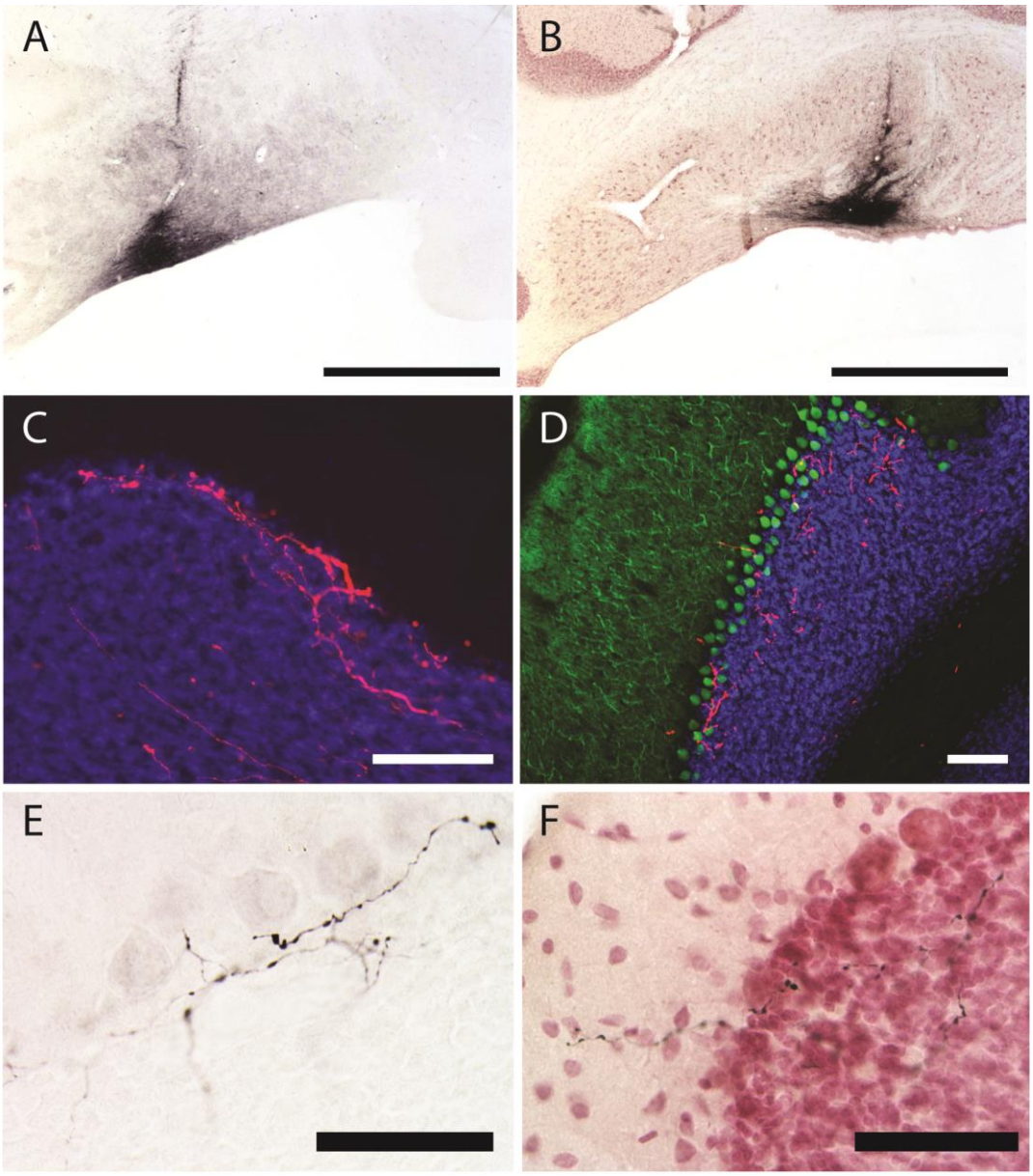

Figure 11. *General description of PLT fibers.*

Representative injection sites into the caudolateral pcIP and the rostromedial pcIP are shown in panels (A) and (B), respectively. In panel (C) PLT fibers (red) can be seen in the paraflocculus coursing along the PC layer and issuing synaptic boutons that are concentrated in the outermost granule cell layer (NeuN: blue) and PC layer. In crus II (D) PLT fibers can also be found. Notice in panel (C) individual PLT fibers can be seen coursing along the space occupied by several PC's in a sagittal plane, but in a coronal plane (D) individual PLT fibers can only be observed innervating a very focal patch of cortex. In panel (E) PLT fibers (black) are seen at higher magnification in relationship to the PC layer. In panel (F) PLT fibers are observed issuing synaptic boutons in both the granule and molecular layers. Marker bars in (A) and (B) = 1 mm; in (C) and (D) = 100 μm; in (E) and (F) = 50 μm.

Orientation and Topography of PLT Fibers.

Similar to other afferent and intrinsic fiber systems of the cerebellum, PLT fibers were observed to follow a strict planar alignment. Individual PLT fibers were consistently seen coursing parallel to the orientation of Purkinje cell dendritic trees (i.e., perpendicular to the orientation of parallel fibers; Figure 12A; Figure 13). Although whole brains were cut coronally, due the complex lobular folding of the cerebellar cortex the floccular complex is actually sectioned sagittally while the rest of the cortex (hemispheres and vermis) ends up being sectioned coronally or tangentially. This allowed us to analyze the distribution of PLT fibers in two different planes of view, depending on which parts of the cortex were being examined. When observed in the sagittal plane (i.e., in the floccular complex), individual PLT fibers were observed issuing putative synaptic swellings at or immediately below the PC layer along the space occupied by 3-5 neighboring PCs (Figure 11E). Observed in the coronal plane (i.e., in crus II of the hemisphere), PLT fibers innervated a focal patch of the PC layer approximately 1-3 neighboring PC in length (Figure 11D). These patches were observed in corresponding regions of neighboring sections. The parasagittal orientation of PLT fibers is reminiscent of that reported of climbing fibers stemming from the inferior olive (Sugihara and Shinoda, 2004; Sugihara et al., 1999).

As mentioned above, we found that PLT fibers, in addition to other nucleo-cortical fibers, respected a largely reciprocal relationship with regions of cortex to which they projected. This relationship was determined in cases that received an infusion of a cocktail of BDA and FG. When BDA and FG were co-infused into the pcIP, PLT fibers were located only in regions of the paraflocculus that also contained retrogradely labeled PCs (Figure 12B). To confirm the reciprocal nature of PLT fibers BDA and FG were co-infused into the paraflocculus and

observed FG+ neurons in the pcIP along with BDA+ PC axon terminals (Figure 12C). These neurons were large and multipolar, which suggest that PLT fibers may arise from the resident PPN population in the pcIP. These two results together indicate that PLT fibers target the same patches of cortex from which they receive cortical input.

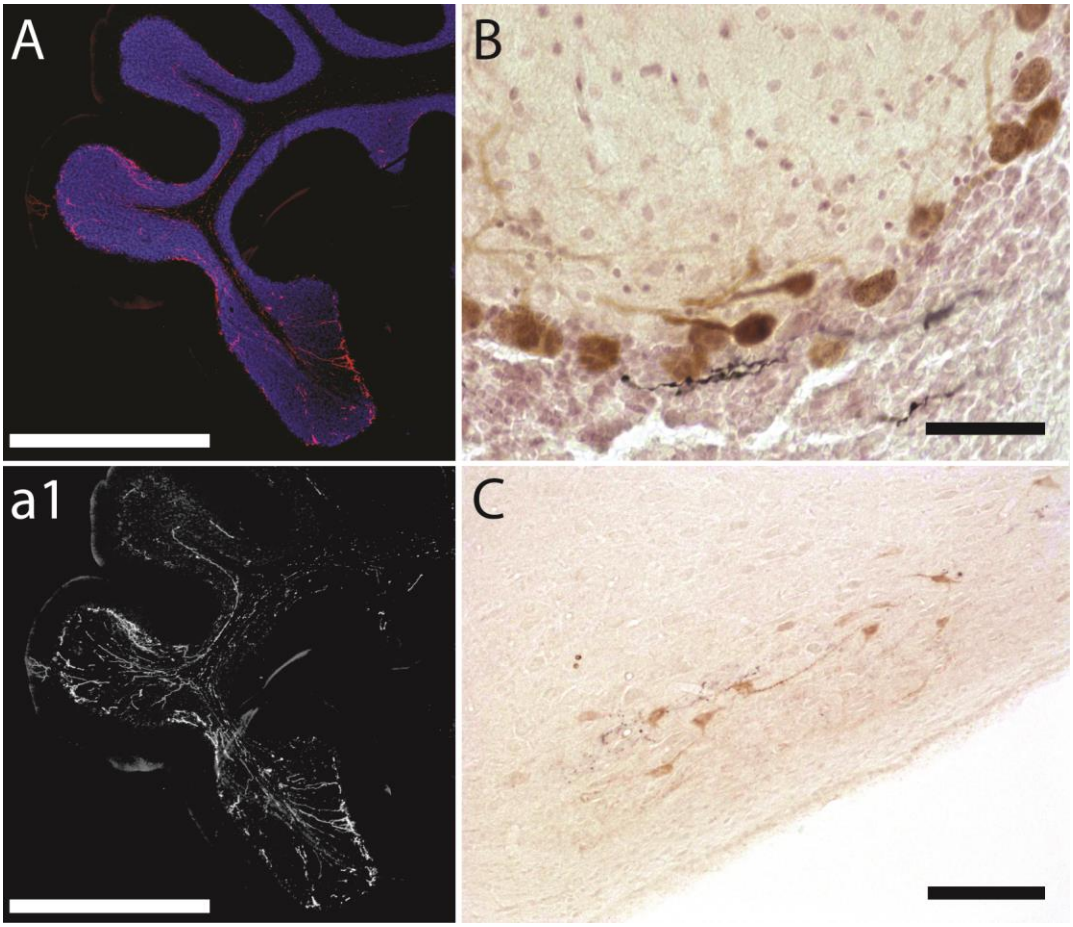

Figure 12. *Orientation and Topography of PLT fibers.*

In panel (A) PLT fibers are observed in a sagittal cut of the paraflocculus (BDA: red; NeuN: blue). Panel (B) depicts the same as (A) without the NeuN signal to highlight the parasagittal innervation pattern of PLT fibers. Panels (C) and (D) demonstrate the reciprocal projections of PLT fibers and PC axons. In panel (C), retrogradely labeled PCs (FG; brown) are in the immediate vicinity of anterogradely labeled PLT fibers (BDA; black) from an injection site in the pcIP. Conversely, panel (D) depicts a case in which FG and BDA were infused into the paraflocculus, retrogradely labeling NC neurons in the pcIP (FG; brown) and anterogradely labeled PC axons (BDA; black). Note the relatively large size of NC neurons in the pcIP and their multipolar dendritic morphology. Marker bars = 1 mm in (A); 50 μm in (B); 100 μm in (C).

Confocal Analysis of Putative Synaptic Swellings.

In order to better ascertain possible synaptic targets we performed confocal analysis of tissue fluorescently labeled for phenotypic markers of different cerebellar cortical neurons. Tissue labeled with NeuN (granule cells and MLIs), L7 (PCs) and BDA revealed putative synaptic swellings concentrated in the Purkinje cell layer (Figure 13A). Single optical plane analysis revealed that boutons were in close apposition to PC somata (Figure 13B), axon collaterals of PCs that target neighboring PCs (arrow in Figure 13B) and descending PC axons in the granular layer (arrow in Figure 13C). Other boutons were observed in the granular layer that were not associated with PC axons, but determining a putative target at this level of analysis was not possible (see ultrastructural results below). Tissue stained with GAD67 (GABAergic neurons) revealed many putative synaptic boutons associated with GAD67+ profiles. The most prominent was the pinceau formation, which is a collection of axons of MLIs ensconcing the initial axon segment of PCs (arrows in Figure 14B; (Bobik et al., 2004; Iwakura et al., 2012)).

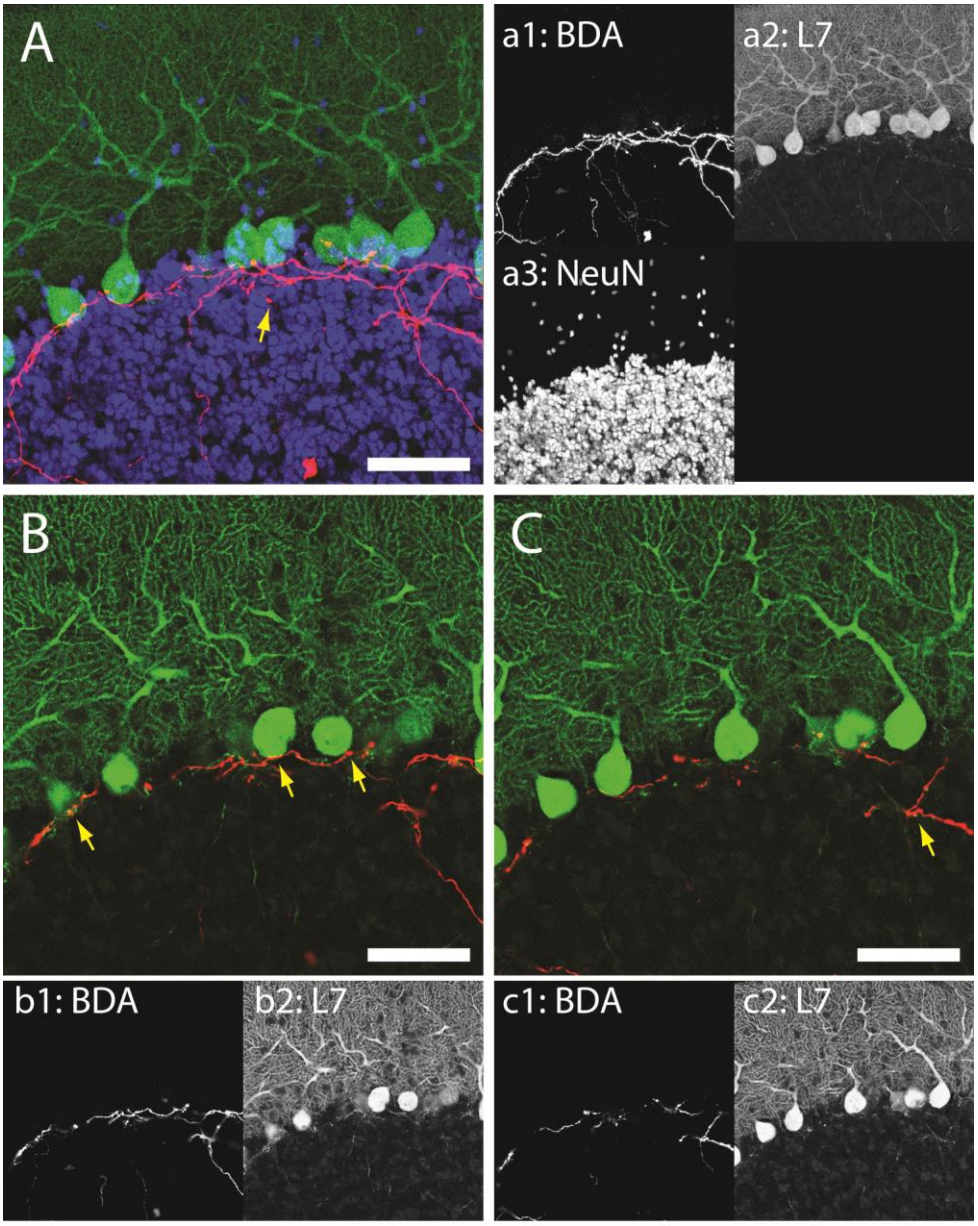

Figure 13. *Confocal analysis of synaptic targets of PLT fibers.*

Panel (A) is a confocal stack of tissue immunofluorescently labeled for BDA (red), NeuN (blue) and L7 (green). Signals from each channel are separated in the 3 images in (A1-3). Panels (B) and (C) are single optical planes of the image in (A) with the NeuN channel removed for clarity. The planes in panels (B) and (C) are separated by 4 μm. Individual channels for BDA and L7 of panels (B) and (C) are shown in (B1-2) and (C1-2), respectively. Putative synaptic contacts are indicated with arrow (see full text for complete description). Marker bars = 50μm.

Neurotransmitter Content of PLT Fibers.

To determine the neurotransmitter content of PLT fibers, BDA+ fibers were co-localized with known markers of different neuronal and neurotransmitter phenotypes using fluorescent immunohistochemistry. These analyses confirmed that PLT fibers are not PC recurrent collaterals by localizing BDA, L7 and calbindin (L7 and calbindin are phenotypic markers of all PCs which can be observed throughout the soma, dendrites and axons of PCs; Figure 13; (Nordquist et al., 1988; Oberdick et al., 1988)). As can be seen in single optical planes in Figure 13, L7+ PC axons and BDA+ PLT fibers do not overlap, though they are often in very close apposition. Tissue processed for immunofluorescence localization of GAD67 and BDA yielded no dual labeled profiles, indicating that PLT fibers are likely non-GABAergic (Figure 14A, B). This result is in line with ultrastructural analysis of PLT fibers (see below). Tissue processed for BDA, tyrosine hydroxylase (a marker for catecholamine neurons) and choline acetyltransferase (a marker for cholinergic neurons) also yielded no double labeled fibers (Figure 14B). This indicates that PLT fibers are not neuromodulatory fibers that are known to innervate large swathes of the cerebellum (Cicero et al., 1972; Ikeda et al., 1991; Jaarsma et al., 1997; Libster and Yarom, 2013; Nelson et al., 1997; Woolf and Butcher, 1989). Interestingly, cholinergic fibers were consistently found in close apposition with PLT fibers, often forming putative synaptic boutons along the length of the PLT fiber (arrow in Figure 14D).

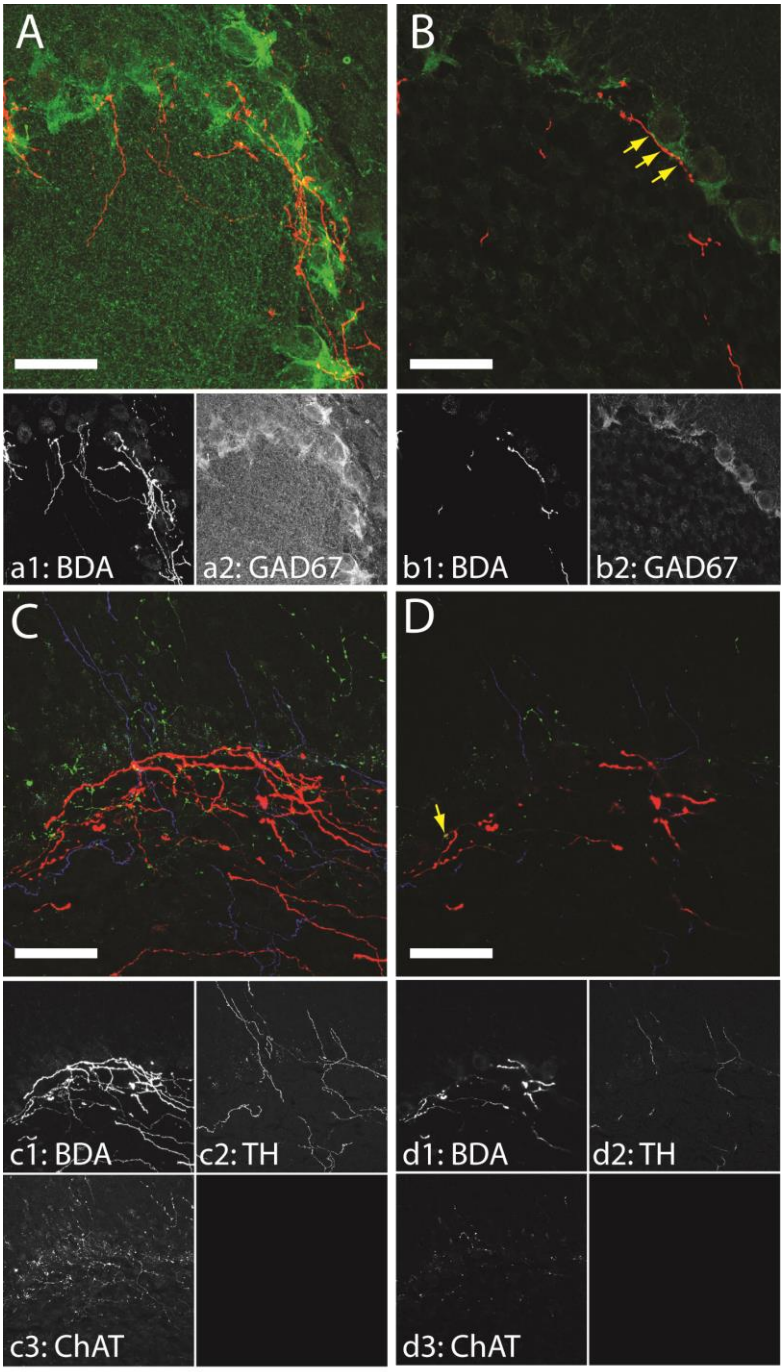

Figure 14. *Neurotransmitter content of PLT fibers.*

Panel (A) is a confocal stack of tissue immunofluorescently labeled for BDA (red) and GAD67 (green). Signals from each channel are separated in the 2 images in (A1-2). A single optical plane from panel (A) is shown in (B) to highlight the lack of GAD67 co-localization with BDA fibers and the close appositions PLT fibers form with the pinceau formation (arrow). Signals from each channel are separated in the 2 images in (B1-2). (C) Confocal stack of tissue immunofluorescently labeled for BDA (red), TH (blue) and ChAT (green). Signals from each channel are separated in the 3 images in (C1-3). A single optical plane from (C) is shown in (D) to highlight the lack of co-localization of PLT fibers with either TH or ChAT. Signals from each channel are separated in the 2 images in (D1-2). Note the close apposition of ChAT fibers to PLT fibers (arrow in D). Marker bars = 50μm.

Ultrastructural Analysis.

To further probe the synaptic targets of PLT fibers we inspected tissue processed for immunoperoxidase localization of BDA at the ultrastructural level. In a case with an injection site localized within the pcIP (Figure 15A) we first confirmed the presence of PLT fibers photographed at the light microscopic level in plastic embedded sections (Figure 15B). Thick (1μm) sections stained with toluidine blue (Figure 15C) provided anatomical landmarks for systematic analysis of the ultrathin (70nm) sections at the electron microscopic level. BDA labeled fibers contained lucent, spherical vesicles approximately 40nm in diameter, which would indicate that PLT fibers are likely excitatory (Figure 15D). Terminal swellings in the granular layer (Figure 15D-F) were found in apposition to small dendritic profiles (Figure 15D, E), and somata of small neurons (granule cells, Figure 15E, F). One terminal in the granular layer was also found to receive an excitatory axo-axonic synapse from a fiber of unknown origin (arrow in Figure 15F). Directly underneath the Purkinje cell layer (outermost granule cell layer, Figure 15G-I) we observed PLT terminals directly apposed to small dendritic profiles (Figure 15H), myelinated and unmyelinated axons (Figure 15I). In the molecular layer we observed PLT fibers nearby but not directly touching PC profiles (Figure 15J, K). Interestingly some of these profiles were still myelinated (Figure 15K), suggesting that PLT fiber demyelinate immediately prior to their synaptic targets. Unmyelinated segments of PLT fibers in the molecular layer were found in direct relation to very small profiles (possible parallel fibers or distal dendrites). We were not able to confirm synapses formed by PLT fibers onto the profiles described above at this time, however further analysis of serial sections (insets in Figure 15) and examining tissue processed for phenotypic markers of different cortical neuronal phenotypes will be necessary to determine the synaptic targets of PLT fibers.

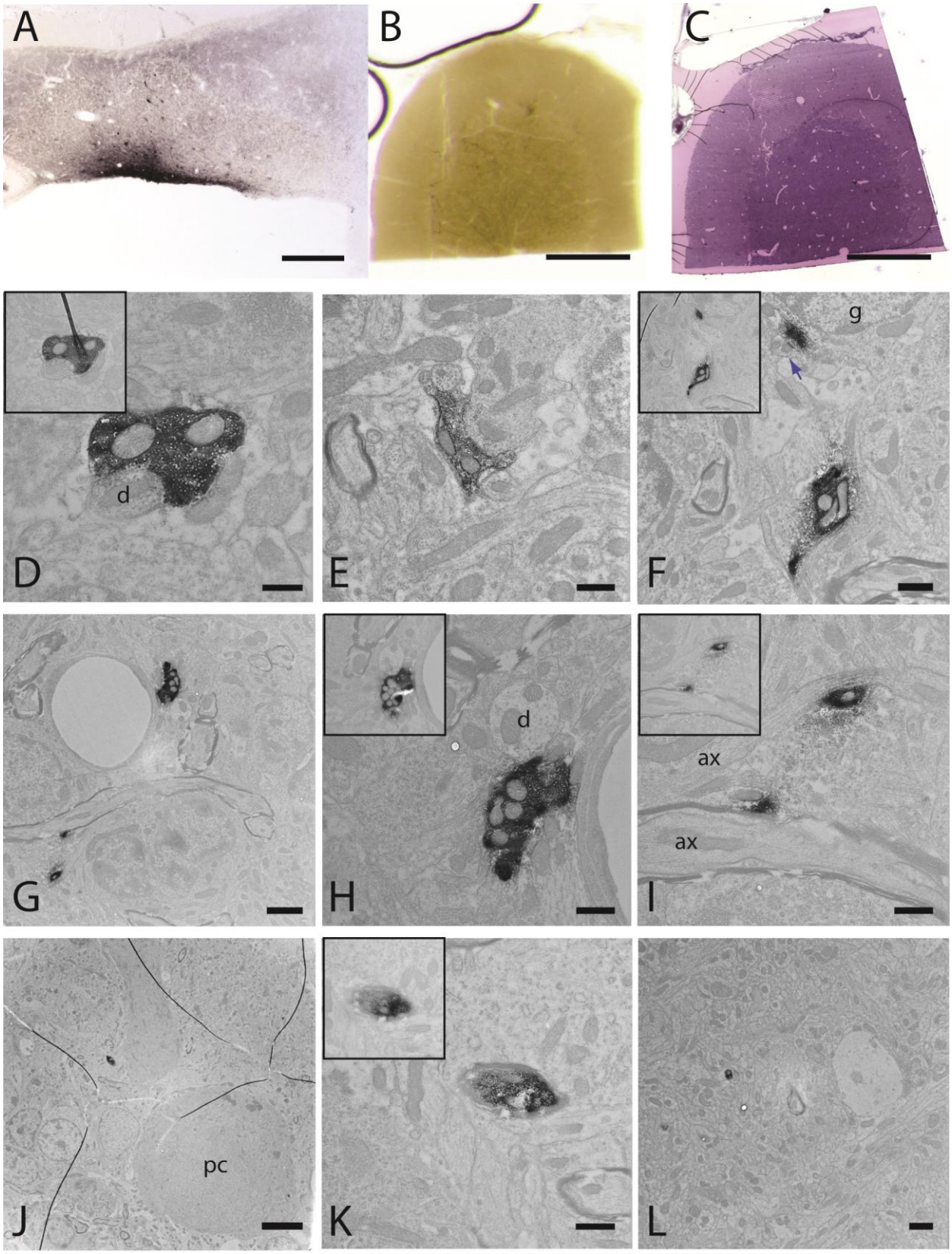
A
B
C
d
D
E
g
F
G
d
H
ax
ax
I
pc
J
K
L

Figure 15. *Ultrastructural Analysis of PLT fibers.*

Panel (A) depicts the injection site of BDA into the pcIP. Panel (B) depicts a flat embedded section of the paraflocculus processed for immunoperoxidase localization of BDA. BDA labeled fibers can be seen in the boxed region. Panel (C) shows a thick (1 μm) section of the same tissue shown in (B). Stained thick sections were used to guide ultrastructural analyses, so that we could be confident of the location of labeling found at the ultrastructural level. Panels (D-F) depict labeled fibers found in the granular layer. Panel (D) depicts a large synaptic terminal making contact onto an unlabeled small dendrite. Lucent spherical vesicles can be seen in this terminal indicating the PLT fibers are most likely excitatory. Panel (E) shows a PLT terminal targeting two distal dendritic processes and an unlabeled soma. The arrow in (E) points to an excitatory axon that is synapsing directly onto a labeled PLT fiber. Panel (F) shows an intervaricose segment (lower profile) and a synaptic terminal contacting a granule cell soma (upper profile). Panels (G-I) depict labeled PLT fibers found immediately below the PC layer. Panel (G) is a low mag image of three profiles seen in (H) and (I). In panel (H) there is a synaptic terminal making contact onto a very small dendritic process and also a larger dendrite, lucent spherical vesicles can be seen here as well. Panel (I) depicts labeled PLT fibers in close relation to a myelinated (lower profile) and unmyelinated (upper profile) axons. Panels (J-L) depict labeled profiles in the molecular layer. In panel (J) a labeled PLT fiber can be seen close to the proximal dendrite of a PC. Panel (K) is a higher magnification of the process in (J). A myelin sheath can be seen surrounding this profile. Panel (L) depicts an unmyelinated PLT fiber that contacts but does not synapse onto several small profiles in the molecular layer. All insets depict the same profiles seen in their corresponding picture but in an adjacent serial section at the same magnification. Abbreviations: d = dendrite; ax = axon; g = granule cell somata; pc = Purkinje cell. Marker bars in (A) = 500 μm; in (B) and (C) = 250 μm; in (D) = 400 nm; in (E) = 500 nm; in (F) and (L) = 1 μm; in (G) = 2 μm; in (J) = 6 μm; in (K), (H) and (I) = 600 nm.

4.4 DISCUSSION

Though the existence of nucleo-cortical fibers was first discovered by two independent groups in the mid-1970s (Gould and Graybiel, 1976; Tolbert et al., 1976), investigators are still hammering out the details of the exact sources and targets of this projection system. Evidence is provided in this report demonstrating a novel excitatory nucleo-cortical projection that targets the PC layer, but also issues occasional synaptic boutons in the granule and molecular layers.

The Parvocellular Interpositus Subnucleus

While scattered PLT fibers were found in other regions of cortex (i.e. crus II, Figure 1D), the vast majority were found to exclusively target the paraflocculus and originate from the parvocellular interpositus (pcIP). Their abundance within the paraflocculus a relative absence elsewhere suggests that they are specialized to support the behavior(s) performed by the paraflocculus and its deep nuclear recipient, the pcIP. The pcIP is a densely packed subregion of the posterior interpositus that is primarily composed of small cells that lie just dorsal to the fourth ventricle (Card et al., 2013). A recent report described the pcIP as the primary target of a new afferent fiber system originating from the caudal raphe interpositus area (CRI). This unique afferent system generally does not project to the cortex, as the majority of its synaptic targets are within the pcIP (Luo and Sugihara, 2014). The few collaterals of this projection that do ascend to the cortex arborize in a similar manner as PLT fibers (i.e. targeting the PC layer), hinting that these two projections (PLT fibers and CRI axons) and the pcIP may be part of a cerebellar module that has unique anatomical characteristics which set it apart from other modules. Work in monkeys and cats indicate that the paraflocculus is heavily involved in eye movements

(Lisberger, 2009, 2010; Medina and Lisberger, 2008). Given its reciprocal connections with the paraflocculus, the pcIP may be specialized for the control of eye movements. However, more research is needed to test this idea and to probe what behavior(s) are supported by this cerebellar module and why it would require such unique circuitry.

Impact on the Activity of Purkinje Cells.

Previously described NC fibers primarily target the granular layer, providing a means of altering the tone of mossy fiber input to the parallel fiber system (Ankri et al., 2015; Houck and Person, 2014). Conversely, PLT fibers primarily target the Purkinje cell layer and thus have the possibility to strongly alter the firing patterns of their target PCs. Although at the light microscopic level PLT fibers were observed in apposition to PC somata, the present ultrastructural data do not support a direct synaptic contact onto PCs. However, to date, only a small fraction of the available material from ultrastructural analyses has been analyzed, so it may be seen in later analyses that PLT fibers do directly contact PCs. A lack of synapses directly upon PCs though, would be similar to both the inhibitory and excitatory nucleo-cortical projections described previously (Ankri et al., 2015; Gao et al., 2016). Putative synaptic contacts were observed onto small dendritic profiles and granule cell somata in the granular layer, supporting this idea. If synapses onto granule cells are confirmed then it is likely that PLT fibers amplify granule cell activity directly and PC activity indirectly. Excitatory axo-axonic synapses onto PLT fibers contacting granule cell somata further implies that PLT fibers may serve to increase the gain of granule cell firing rates. Although we could not establish synapses in the molecular layer, PLT fibers were observed directly touching putative parallel fibers, which would provide another excitatory drive to granule cell processing. If these synaptic contacts are confirmed in further analyses they would be reminiscent of the granule cell signal amplification

observed by both the excitatory mossy-like fibers (Gao et al., 2016) and the inhibitory glycinergic nucleo-cortical fibers (Ankri et al., 2015).

The morphology of retrogradely labeled NC cells in the pcIP (large, multipolar) suggests that they may be the resident PPNs of the pcIP. If this is the case, then the PLT fiber projection could be merely a different innervation pattern of PPNs to the cortex than has been observed elsewhere. Collaterals of PPNs projecting to the hemispheres or vermis appear as mossy-like fibers and target the glomeruli of the granular layer (Gao et al., 2016; Houck and Person, 2015). Occasionally, mossy-like ending in the paraflocculus cortex were observed, but the NC projection to the paraflocculus is dominated by the PLT fibers. This may suggest that NC neurons in the pcIP, while still exciting the granular layer, do so in a manner that is distinct from other excitatory NC projections. This could be directly assessed by injecting a lentiviral vector which encodes for channelrhodopsin into the pcIP and optogenetically exciting these fibers in slice while recording from nearby granule cells (Gao et al., 2016).

Interestingly, however, the light microscopic data argue strongly for synaptic swellings in relation to processes of molecular layer interneurons. This included swellings nearby the somata of MLIs and their axon processes ensconcing PC axons as the pinceau formation. The pinceau formation is a fascinating structure which is the accumulation of the axons of several MLIs which then form a tight sheath around the PC axon initial segment. This puts the GABAergic MLIs in position to powerfully inhibit the production of action potentials in the PCs they target. Interestingly though, the pinceau formation is largely devoid of chemical synapses (Iwakura et al., 2012). Instead, the pinceau axons ephaptically inhibit the PC axon by depolarizing the extracellular space around the PC axon initial segment (Blot and Barbour, 2014). This ephaptic transmission is instantaneous, providing an extremely quick means of inhibiting PCs without the

need for chemical signal transduction (Blot and Barbour, 2014). These two contacts together would then serve to amplify MLI processing, which in turn inhibits PC firing. Given the strong inhibitory control MLIs have over PCs (Heiney et al., 2014a), PLT fiber activation could have a significant depressing effect on PC firing rates. This may be particularly true if PLT nucleo-cortical neurons in the pcIP are indeed PPNS, which are known to have a high tonic level of activity (Uusisaari and Knöpfel, 2011; Uusisaari et al., 2007; Uusisaari and Knöpfel, 2012). If both contacts onto granule cell and MLI processes are confirmed then it is likely that PLT fibers have a complex effect on the overall activity of PCs. The observations in this report predict that PLT fibers initially hyperpolarize PCs by virtue of activation of MLI pinceaus and fast ephaptic inhibition of the axon initial segment, followed by depolarization of PCs by inputs of stimulated granule cells onto distal PC dendrites. Of course this prediction remains to be tested *in vivo*, but the anatomical results presented here offer at least a theoretical framework for assessing the electrophysiological effects of PLT fibers on PC firing rates.

5.0 GENERAL DISCUSSION

5.1 SUMMARY AND INTERPRETATION OF EXPERIMENTAL FINDINGS

The deep cerebellar nuclei represent the nexus of all major inputs to the cerebellum. They are the target of mossy fiber collaterals, climbing fiber collaterals, neuromodulatory inputs and importantly, the DCN are the primary target of Purkinje cells (PC). All of these afferent inputs are integrated by the DCN to shape the activity of its projection neurons. These projection neurons are then the predominant means by which the cerebellum affects a wide array of behaviors ranging from motor control to cognition. The activity of projection neurons has commonly been conceptualized as the reverse of PC activity, due to the inhibitory nature of the PC projection. However, it has become increasingly clear that a diversity of neuronal phenotypes within the DCN may actively shape DCN output beyond a simple sign reversal of PC activity. In order to fully characterize how afferent activity shapes cerebellar output a detailed wiring diagram of the local DCN network and its afferents is needed. The studies in this dissertation were designed to re-examine the role of the deep cerebellar nuclei (DCN) within the canonical cerebellar circuit. We aimed to fill some of the gaps in our knowledge of how the DCN integrate cortical and extracerebellar inputs and in turn project back to these same input structures.

The primary afferents of the DCN are PCs in the cerebellar cortex (Chan-Palay, 1973c). Although the DCN also receive input from local neurons and the collaterals of afferent climbing and mossy fibers, the PC projection accounts for upwards of 80% of synapses on somata and 50% of synapses on the dendrites of large neurons (Chan-Palay, 1973c). Thus many researchers have rightly focused on this projection in order to probe DCN function. As a first step to understanding how cortical activity influences DCN activity, it is vital to map the exact cellular targets of PCs and how this projection is integrated within the DCN. At the ultrastructural level, PCs have been shown to collateralize onto both principal projection neurons (PPN) and nucleo-olivary projection neurons (NOPN; (Teune et al., 1998)). However the question of PC collateralization has not been addressed at the circuit level. The first study aimed to test the generalizability of the findings of Teune and colleagues at the circuit level using transneuronal viral tracing. To accomplish this we, for the first time, used dual retrograde transneuronal tracing with isogenic recombinants of PRV that each express a unique fluorescent reporter injected into the red nucleus and the inferior olive. This study revealed that PCs antecedent to projection neurons in the DCN selectively innervate either PPNs or NOPNs and rarely both. We interpret this as evidence for an extra layer of dynamic control the cortex has over projection neurons. With this segregated projection, the cortex is theoretically able to modulate the electrotonic coupling of IO neurons and the control of behavior independently. Furthermore this finding may help to reconcile data reported by Raman and colleagues demonstrating highly divergent responses of PPNs and NOPNs neurons to PC inputs (Najac and Raman, 2015; Person and Raman, 2012a). PPNs were shown to respond vigorously to PC input whenever that input was synchronized. When PC input was de-synchronized, it produced general depression of PPN spiking, but synchronizing PC input allowed PPNs to issue a rebound action potential in between

synchronized PC depression. This was supported by the quick time decay constant (2.4±0.2 ms) of GABA receptors on PPNs that allow them to quickly rebound from PC inhibition (Person and Raman, 2012a). This contrasts with a subsequent report demonstrating a 10 fold slower decay rate for GABA receptors on NOPNs. This increased time decay caused NOPNs to summate PC inhibition such that high frequency PC inputs greatly depressed NOPN spiking (Najac and Raman, 2015). The segregated projection here may be best suited to controlling two classes of cells that respond in opposite manners to similar inputs. Our study further demonstrated that that PPNs and NOPNs are synaptically linked via recurrent collaterals of PPNs onto NOPNs. Given their segregated PC inputs, this link could serve to coordinate between cerebellar output to the IO and red nucleus. This in addition to the numerous unidentified interneurons found to be antecedent to projection neurons points to the DCN as dynamic recipients of cortical and extracerebellar afferents that actively transform these inputs into coherent outputs to the numerous targets of the cerebellum.

The second study tested the long standing hypothesis that the cerebellum and inferior olive form a series of topographically closed loop circuits. We injected a cocktail of a bidirectional monosynaptic tracer, CTβ, and a retrograde viral transneuronal tracer PRV into the IO. This study revealed that climbing fibers emanating from the IO target the same PCs in the cortex and NOPNs in the DCN that feedback to IO neurons in the injection site. Although many studies have aimed to address the issue of closed versus open OCNO loops, the study presented here is the first to map the entire OCNO circuit using a single injection site. This is important as previous studies have relied upon multiple injection sites, which inherently limits the interpretation of closed versus open loops to the level of *regions* in the cerebellum and IO as opposed to single cells. Because PRV spreads exclusively along synaptic connections, we know

that each cell within the loop is synaptically linked and the use of a single injection site gives us the strongest evidence available for closed OCNO loops.

From these first two studies it became increasingly clear that the anatomical organization of the parvocellular interpositus (pcIP) is remarkably different from other subdivisions of the DCN. This region lies directly dorsal to the roof of the fourth ventricle and is seen in Nissl stains as composed primarily of small pale staining neurons. We consistently found that this region became densely labeled whenever it was infected via retrograde spread of virus from the inferior olive and that viral spread in this region was always along its mediolateral axis, compared to radial viral spread seen in magnocellular divisions of the DCN. Although results from chapter 2 confirm that neurons in the pcIP conform to the closed OCNO loop architecture, we aimed to test whether or not this projection displays any unique characteristics in its efferent projections. It has been demonstrated that all subdivisions of the DCN issue feedback projections to the cortex (Batini et al., 1989; Batini et al., 1992; Gould and Graybiel, 1976; Houck and Person, 2015; Tolbert et al., 1976; Trott et al., 1998a, b), so we aimed to characterize nucleo-cortical projections from the pcIP and how they may differ from nucleo-cortical fibers from magnocellular DCN subdivisions.

The third study aimed to test whether the parvocellular interpositus nucleus (pcIP) displays the same nucleo-cortical connectivity seen arising from other DCN subdivisions. We therefore injected a monosynaptic anterograde tracer, BDA, into the pcIP and analyzed the morphology, phenotype, and cellular targets of the pcIP nucleo-cortical projection. We found that the pcIP issues a previously undocumented NC projection that targets the Purkinje cell layer in the paraflocculus. In addition to the interneuron network discovered in the first study this NC projection into the PC layer gives the DCN, and specifically the pcIP, another means to shape the

activity of projection neurons influence by PCs in the cortex. This projection is quite unique as no other NC projection is known to target the PC layer. This could mean that the pcIP is more actively involved in the way the cortex processes cerebellar inputs, which could be related to a specific type of behavior, but this remains to be tested using functional manipulations of the circuit (see below).

5.2 REVISITING CANONICAL CEREBELLAR CIRCUITS WITH VIRAL TRANSNEURONAL TRACERS

Viral transneuronal tracing has begun to open up a world of possibilities for exploring functional output and input channels of the cerebellum. Until relatively recently, the cerebellum was thought to be involved only in motor control. Accordingly, transneuronal viruses were first employed to assess cerebellar inputs to motor regions of the neocortex such as M1 in monkeys (Hoover and Strick, 1999). Unlike studies employing monosynaptic tracers, that study allowed the researchers to visualize the entire polysynaptic network that links the cerebellum to M1 via the thalamus, and to map functional domains within the cortex that are specifically involved in motor control. This approach was expanded to reveal that the cerebellum, specifically the ventral dentate nucleus in monkey, is reciprocally connected via a polysynaptic circuit with non-motor regions of the prefrontal cortex, such as areas 46 and 9L (Kelly and Strick, 2003; Middleton and Strick, 1998, 2001). Both of these patches of cortex are known to be involved in cognitive processing, a domain not previously attributed to the cerebellum. Importantly, the anatomical connectivity to non-motor regions of neocortex solidified the idea that the cerebellum is not relegated to motor control alone, but may influence many aspects of behavior.

These reciprocal connections to different regions of the neocortex led to the idea that the cerebellum and neocortex form a series of closed-loop circuits that can be delineated not only by their topography but also by their putative functions (i.e., cognitive versus motor domains; (Middleton and Strick, 2000)). The idea of closed loop circuits was further expanded to include cerebellar projections to and from the basal ganglia (Bostan et al., 2010; Bostan and Strick, 2010; Hoshi et al., 2005). These studies together defined functional domains within the DCN and cerebellar cortex that confirm that, although the entire cerebellar cortex is almost cytoarchitecturally identical, different regions of the cortex are involved in different domains of behavior by virtue of their connectivity with the rest of the brain.

Projections to either the neocortex or the basal ganglia originate from PPNs in the DCN (Ichinohe et al., 2000; Ruigrok and Teune, 2014). In Chapter 3 we employed transneuronal viral tracing to study a similar putatively closed loop the cerebellum makes with the IO stemming from NOPNs: the OCNO loop. Recapitulating the closed loops found by the Strick group, we demonstrated that regardless of the IO/DCN/cerebellar cortical subdivision involved, OCNO loops remain closed circuits down to the cellular level. These data together reveal that both projection systems of the cerebellum (PPN and NOPN) are organized into a series of parallel closed loop circuits with their efferent targets. Such loops help to bridge disparate brain regions that are all involved in a single behavior.

Although the macrocircuitry of OCNO loops seems to be preserved across the cerebellum, viral spread through the DCN did not appear to be identical across different DCN subdivisions. For example, viral labeling helped to delineate the pcIP by virtue of the dense mediolateral spread of virus through this region. This dense spread suggests that the pcIP is densely interconnected with itself. Other regions of the DCN may also form local connections

that delineate one subdivision from the next. Although the anterior interpositus is not typically subdivided into anatomically distinct subunits, functional dissociations between its medial and lateral portions suggest that the entire IP does not function as a whole (Mojtahedian et al., 2007). Likewise, the dentate nucleus has been shown by the Strick group to contain both motor and non-motor domains (Dum et al., 2002). Viral tracing can be used to analyze the local connectivity of different DCN subdivisions by assessing the rate and extent of viral spread within a putative subnucleus. With this approach researchers could begin to understand if and how differences in local circuit arrangement allow different DCN subdivisions be involved in different behaviors.

The use of viruses to trace cerebellar circuits has greatly expanded our understanding of the diverse functional domains the cerebellum supports. However, the entirety of the cortex has yet to be mapped, both anatomically and functionally. The approach employed here and by the Strick group, if expanded, holds the promise of parceling out regions of the DCN and cortex that are involved in different aspects of associative learning, cognitive control, affective control, visceral control and skeletomotor control.

5.3 THE ROLE OF THE DCN IN CEREBELLAR CIRCUITS

The DCN were long held to be relays of cortical processing, but in recent years have received considerable more experimental and theoretical attention. The pioneering work of Richard Thompson to delineate the eyeblink conditioning circuit greatly helped to direct attention to the integral role the DCN play in associative learning (Thompson and Steinmetz, 2009). The essential eyeblink circuitry was initially localized to the cerebellum with decerebrate

rabbits, demonstrating that the cerebellum and its input structures in the brainstem were sufficient to support conditioning (McCormick et al., 1981; Oakley and Russell, 1972). Additional lesion and reversible inactivation manipulations narrowed the eyeblink region down to the lateral cerebellum (McCormick et al., 1982), then further localized it to lobule HVI in the cortex (Lavond and Steinmetz, 1989; Lavond et al., 1987; Yeo et al., 1985a, b) and the anterior interpositus in the DCN (Clark et al., 1984). These anatomical localizations led to recording studies to demonstrate which neurons in the lateral anterior interpositus increase their firing rates immediately prior to a conditioned eyeblink response (Heiney et al., 2014b; McCormick and Thompson, 1984; Thompson and Krupa, 1994). Conditioned responses were also shown to develop concomitantly with the maturation of IP activity across development (Freeman and Nicholson, 2000). Lesioning the IP, either permanently or transiently, completely abolishes previously learned conditioned responses and further prevents the learning of new conditioned eyeblinks (Freeman et al., 2005). Although results vary from study to study, it has been demonstrated that the IP without cortical input from lobule HVI is sufficient to support expression of previously learned conditioned eyeblinks (Lavond et al., 1987). Lesions of HVI before conditionings do not block learning, but animals acquire conditioned responses at a slower rate (Lavond and Steinmetz, 1989). Finally, lesions of the anterior lobe of the cerebellum have been shown to affect the timing and magnitude of conditioned responses, such that they are no longer adaptive; however conditioned responses still develop (Perrett et al., 1993). These cumulative findings led Thompson to the conclusion that the essential memory trace for eyeblink conditioning is stored in the interpositus nucleus, and that the cortex helps to support optimal condition but is not entirely necessary for conditioning in general (Thompson, 2013).

Now that it has been recognized that the DCN can store learned associations, the question is: how is this learning supported by the neuronal elements within the DCN?

Characterization of the resident neurons within the DCN began in the early 1970s with a series of Golgi impregnation studies which classified resident neurons into six categories, at least 2 of which were local interneurons (Chan-Palay, 1973b; Matsushida and Iwahori, 1971). In her analysis of the dentate nucleus, Chan-Palay highlighted that many of the neurons (both large and small) issue synaptic boutons that contact other resident DCN cells and that DCN neurons are also contacted by the collaterals of both mossy and climbing fibers along their dendrites. These collaterals provide the DCN access to extracerebellar afferents that appear to be sufficient to drive behavior in eyeblink conditioning experiments. The lack of known phenotypic markers in the DCN hindered further classification of DCN neurons until more advanced techniques were available (Aizenman et al., 2003; Czubayko et al., 2001). In the mid-2000s, using a combination of genetic and electrophysiological techniques, at least six unique neuronal phenotypes were again confirmed to be distributed in the DCN (Bagnall et al., 2009; Uusisaari and Knöpfel, 2011). Interestingly, two of these neuronal phenotypes were differentially distributed. Glycinergic projection neurons were found by Bagnall and colleagues to reside in the ventral fastigial nucleus. These neurons target the ipsilateral vestibular nuclei, while glutamatergic in the same region target the contralateral vestibular nuclei (Bagnall et al., 2009). A class of glycinergic neurons in the dentate nucleus, however, was found to exclusively target the cortex (Ankri et al., 2015; Uusisaari and Knöpfel, 2010). Additionally, at least two classes of interneurons (one GABA/glycinergic; one putatively glutamatergic) have been identified based on their intrinsic firing properties (Uusisaari and Knöpfel, 2008, 2011; Uusisaari et al., 2007; Uusisaari and Knöpfel, 2012). Interestingly, these studies also demonstrated that unlike in the

neocortex, GABAergic interneurons were characterized by slow action potentials with a low maximal firing rate while glutamatergic interneurons displayed the opposite qualities. An early ultrastructural analysis of the synaptic inputs onto GABAergic, glycinergic and unlabeled (putatively glutamatergic) neurons revealed that large unlabeled neurons (likely PPNs) received glycinergic input (De Zeeuw and Berrebi, 1995a, b). This result was bolstered by viral transneuronal tracing from the orbicularis oculi muscle which provided evidence for local glycinergic interneuron input onto PPNs projecting to the red nucleus (Gonzalez-Joekes and Schreurs, 2012). This connection was validated in slice using a combination of retrograde tracing and genetic markers to show that glycinergic interneurons directly inhibit PPNs in the DCN (Husson et al., 2014). The diversity of neuronal elements within the DCN, and the fact that many display unique intrinsic electrophysiological characteristics strongly implies that the role of the DCN is not merely a sign reversal of PC activity. Instead, such a collection of neuronal elements likely actively shapes the way in which DCN neurons respond to PC and extracerebellar inputs.

The studies in this dissertation have demonstrated additional internal circuit elements of the DCN: PC axons rarely collateralize onto both PPNs and NOPNs, and PPNs issue a short collateral directly onto NOPNs. These two findings help to explain several other observations noted in the literature. First, remarkable differences are seen in the innervation patterns of PPNs and NOPNs by PCs. Since Chan-Palay's seminal studies it has been known that PCs form a series of perisomatic contacts onto PPNs, such that the almost the entire PPN is ensconced by the axons of several PCs (Chan-Palay, 1973c; Matsushida and Iwahori, 1971). This contrasts with the sparser perisomatic input onto NOPNs, and the preferential targeting of their dendritic processes (Chan-Palay, 1973c). This result was further recapitulated in the vestibular nuclei,

which are also targets of the cortex and are often conceptualized as analogous to the DCN (Shin et al., 2011). The presence of at least two classes of PCs (PPN targeting; NOPN targeting) could help to explain how the differences in innervation patterns and responses to PC input are resolved in order to produce the appropriate activity of each projection neuron during behavior.

With segregated PC inputs, the question arises of how the activity patterns of NOPNs and PPNs are coordinated. One of the earliest local synaptic contacts described was from the recurrent collaterals of large projection neurons onto small neurons (Chan-Palay, 1973a, c; Matsushida and Iwahori, 1971). It was later established that inhibition of the IO could be elicited by antidromic stimulation of PPNs (Svensson et al., 2006). These findings point to a direct collateral from PPNs onto NOPNs. This is in fact what we observed in both chapters 2 and 3. Whenever virus spread through the DCN via an IO injection site, we observed transneuronal infection of PPNs in the immediate vicinity of NOPNs. This finding confirms that NOPNs are innervated by the recurrent collaterals of PPNs. Such a projection gives NOPNs access to the rate code of PPN firing and would serve to ensure that the two projection systems remain in registration with one another despite their differential inputs from the cortex. Furthermore, since PPNs and NOPNs are known to be contacted by both climbing fibers and mossy fibers, a local connection between the two neurons ensures that even when the cortex is absent, the two projection systems coordinated enough to support expression of previously conditioned eyeblinks (Lavond et al., 1987).

The identity and targets of interneurons in the DCN have not been well established (Uusisaari and De Schutter, 2011). Glycinergic interneurons were recently functional demonstrated to innervate PPNs, confirming previous anatomical reports (De Zeeuw and Berrebi, 1995a; De Zeeuw et al., 1995; Gonzalez-Joekes and Schreurs, 2012; Husson et al.,

2014). Here we confirm that there exists an interneuron network that is synaptically linked to PPNs, but were unable to directly assess their identity. However, the extensive local viral transport observed from cases with IO injections was particularly interesting. One explanation for this is the short collateral of PPNs discussed above that gives virus access to both PPNs and their antecedent network. Not all cells observed infected transneuronally via NOPNs were large putative PPNs though; there was a substantial network of small cells that became infected as well. There are two possible arrangements that would produce this pattern: 1) NOPNs, similar to PPNs, have at least one interneuron class which synapses onto them or 2) NOPNs are locally linked with each other directly. It is important to state that these two options are not mutually exclusive. Preliminary evidence from our own ultrastructural analysis of the organization of the pcIP (where the densest IO infection was found) indicated that neurons in that region may be linked to one another via a glomerular organization (unpublished observations). If these aggregates of dendrites arise from NOPNs or interneurons antecedent to NOPNs, then it would provide a quick route of infection for a retrogradely transported viral tracer such as PRV. Regardless of the exact route of infection, it is clear from our data that there is some local neural network that synapses upon NOPNs. Determining the identity of these neurons, whether interneurons or other NOPNs, will be crucial for understanding how NOPNs spike during behavior, a matter that has not been directly assessed to date.

In addition to the rich local circuit plexus linking resident DCN neurons, we report in this dissertation the discovery of a novel nucleo-cortical projection that targets the Purkinje cell layer. This was found to arise predominantly from the parvocellular interpositus nucleus to target the paraflocculus. To date, there is little data available in rats as to the function of the paraflocculus or the pcIP. In monkeys, however, it has been demonstrated that the ventral paraflocculus and

flocculus are heavily involved in eye movements, particularly for smooth pursuit movements (Lisberger, 2009). In monkeys, Purkinje cells in these areas have been shown to encode the direction of eye movements and are actively involved in the learning of smooth pursuit tasks (Medina and Lisberger, 2008). The neural network that links the paraflocculus to eye muscles was confirmed in rats using viral tracing from the rectus muscles (Billig and Balaban, 2004). Projections from the pcIP to the superior colliculus (unpublished data from chapter 4) also support the idea that the pcIP and paraflocculus are involved in the control of eye muscles. Eye movements are some of the most precisely controlled behaviors performed by the body and as such require neural activity to be equally as precise. The pcIP neurons that target the PC layer described in chapter 4 may help to further coordinate the activity of PCs in the cortex with their PPN and NOPN counterparts in the DCN. The fact that this projection had not been demonstrated elsewhere in the cortex points to a potentially unique relationship between the pcIP and the cortex. This could open up future opportunities to test how differences in connectivity change the way in which pcIP neurons respond to cortical input versus how, for example, the eyeblink region of the DCN (anterolateral IP) responds to a similar pattern of cortical input. This also emphasizes the point that the DCN are not homogenous, and if we are to understand how the cerebellum supports such a vast array of behaviors, we need understand how differences across the DCN may be specialized to support those disparate functions.

5.4 FUTURE DIRECTIONS

The experiments in chapter 2 highlighted the interconnectivity of the projection neurons in the DCN. The next critical step is to determine how the activity of each cell type affects the

activity of its neighbors. For example, Husson and colleagues (2014) used a combination of retrograde tracing and genetic markers to isolate glycinergic interneurons in a slice preparation (Husson et al., 2014). They then identified nearby PPNs onto which those glycinergic interneurons synapsed and assessed how glycinergic interneuron activation affected PPN electrical activity. This approach can be adapted to study the electrophysiological characteristics of the PPN to NOPN collateral. By retrogradely labeling PPNs and NOPNs with monosynaptic tracers they could be identified in slice preparations. Neighboring PPNs and NOPNs could be then recorded and stimulated to test the effects of the activity of one onto the other. The functional strength of this collateral projection will help to determine how closely the firing patterns of each neuron may mirror the other *in vivo*. This is a first approach to understanding DCN local connectivity, but as there are at least six identified neuronal phenotypes a considerable amount of work is needed to parcel out the effects each phenotype on its synaptic pattern. Importantly, this work needs to be done in a DCN subdivision specific manner so that we may ascertain how different patterns of local connectivity affect the integration of cortical and extracerebellar afferents. In addition to determining the properties of local DCN circuits, electrophysiological interrogation of PPN or NOPN projecting PCs is also possible with currently available methods. A number of groups have used transneuronal tracing with PRV152 to record labeled neurons in slices in the suprachiasmatic nucleus (Smith et al., 2000), the nucleus tractus solitarius (Glatzer et al., 2003) and the spinal cord (Derbenev et al., 2010). This approach can be taken to determine if PPN and NOPN projecting PCs display different electrophysiological properties that may make them better suited for control of one projection neuron class over the other.

Now that we have established that OCNO loops are closed circuits, a number of interesting experimental questions can be assessed. The first question is the extent to which neurons within an OCNO loop function as a single unit. It has been proposed that cerebellar modules represent the functional unit of the cerebellum but it is unclear if the entire module, which can span several lobules, functions as a whole or if it can be further subdivided. Reports in the literature localizing function within the cortex often find "microzones" within a module that are directly related to behavior (Joseph et al., 1978; Shambes et al., 1978). Microzones are typically on the order of hundreds of micrometers in diameter, far small than the entirety of an olivo-cerebellar module (Heiney et al., 2014a). This would imply that the entirety of an OCNO module is not functioning together but rather is composed of many microzones that all share similar olivary input. A recent review suggests that the cerebellum may initially allow widespread olivary input to reach the cortex and deep nuclei, and that this widespread input is honed down to a single (or multiple) microzones by means of nucleo-olivary inhibition (Schweighofer et al., 2013). This could be tested *in vivo* along OCNO loop circuits during eyeblink conditioning. For example, by placing an electrode within the eyeblink microzone delineated by Heiney and colleagues (2014) and a second electrode elsewhere within the same zebrin II band (i.e. same OCNO module) one could record the activity of climbing fiber responses and determine if IO input is indeed honed down to a single microzone (Heiney et al., 2014a). This would be observed as both regions showing strong IO input early in conditioning, but gradually as learning progresses, climbing fiber responses are lost outside of the eyeblink microzone, but persist throughout training within the eyeblink microzone. If this were to be established then it would be worthwhile to ask the question: what exactly defines the functional role of the OCNO module? A possibility is that the OCNO module is defined by the modality of

its sensory inputs, such that all regions within an OCNO loop receive the same sensory input. It has been demonstrated that different subregions within the IO respond to different sensory modalities such as tactile versus visual stimuli (Barmack and Hess, 1980; Sears and Steinmetz, 1991). We could then test this by comparing the location of the eyeblink microzone using an airpuff for the US versus a bright light as the US. If the microzone remains in the exact same position, then we must assume that microzones are strictly dependent on somatotopy such that conditioned eyeblinks using any modality of US will always be in the same spot. If the microzone moves but is still within the same OCNO module, i.e., directly rostral or caudal to the airpuff zone, then we could interpret this as OCNO modules being responsible for conditioning in a single bodily region. This entails that individual regions within the module process different sensory modalities for that one bodily region. A third interesting possibility is if the eyeblink conditioning microzone using a bright light US is located outside of the OCNO module for airpuffs as a US. This could be seen as the microzone being positioned laterally or medially outside of the zebrin band the airpuff zone is in. If this were the case then researchers should be able to find multiple regions within the cerebellum that all support eyeblink conditioning but each is responsible for conditioning with only a single sensory modality for the US. This result could help to explain the fractured somatotopy seen across the cerebellar hemispheres (Gonzalez et al., 1993; Joseph et al., 1978; Shambes et al., 1978) and the numerous regions synaptically linked to the orbicularis oculi muscle (Gonzalez-Joekes and Schreurs, 2012; Morcuende et al., 2002; Sun, 2012). Thus having multiple representations of each bodily region would allow for each to be impacted by US inputs of only one sensory modality. Regardless of the result, it is essential that we answer this question to begin to ascertain the common characteristics that link OCNO loops into such distinct closed circuits.

The presence of a novel nucleo-cortical projection that targets the Purkinje cell layer in the paraflocculus opens up a number of intriguing experimental questions. First, what are the direct electrophysiological effects of these fibers on PCs and indirectly on the activity of PPNs? These considerations were outlined in detail in the discussion section of chapter 4. To this end however, it is essential to define both the neurotransmitter content of PLT fibers and their *exact* synaptic targets in the cortex. Light microscopic analysis revealed that PLT fibers do not stain for GAD67, ChAT, or TH, indicating they most likely do not contain GABA, acetylcholine or catecholamines, respectively. Ultrastructural analysis further revealed that the synaptic vesicles within PLT fibers are spherical and lucent. These results together would suggest that PLT fibers are excitatory and possibly glutamatergic. Determining the cellular origin of PLT fibers will help in this pursuit. Retrograde tracing labeled larger neurons in the pcIP, but due to the fact that anterograde tracing experiments in chapter 4 also labeled mossy-like nucleo-cortical fibers (Houck and Person, 2014) and the injection sites for retrograde tracing included both the granular and molecular layers, we cannot fully determine if all or only a subset of these cells give rise to the PLT fibers specifically. Injecting a bidirectional tracer, such as CTβ used in chapter 3, into the superior colliculus or the IO could help to determine if PLT fibers arise from projection neurons of the pcIP or if they arise from a local DCN neuron similar to the glycinergic dedicated nucleo-cortical neurons (Houck and Person, 2015; Uusisaari and Knöpfel, 2010). Our light microscopic results revealed a number of putative synaptic boutons that are concentrated in the PC layer, but also are observed both in the granule and molecular layers. Appositions were found in relation to Purkinje cell somata, PC axons in the granular layer, the pinceau formation and molecular layer interneurons (MLIs). Given the predominance of inhibitory transmission in the cerebellum, the exact targets of PLTs fibers could drastically alter their function in the

circuit. The most important consideration is the appositions to PC somata seen in light microscopic analyses. If PLT fibers do synapse directly onto PCs, then they could serve to drive PC activity (direct excitatory) and presumably inhibit DCN activity. However, if PLT fibers instead synapse on the axon terminals of MLIs targeting PC somata or on their unique pinceau formation around the PC axon initial segment (Blot and Barbour, 2014; Iwakura et al., 2012), then PLT fibers could suppress PC activity (indirect inhibition) and drive DCN activity. Additional putative synaptic contacts were observed at the ultrastructural level on processes in the molecular layer (possible parallel fibers, MLI dendrites, or Golgi cell dendrites) and in the granular layer (possible granule cell dendrites and somata, mossy fiber terminals). Both the nucleo-cortical projections from PPNs (Gao et al., 2016) and glycinergic neurons (Ankri et al., 2015) serve to amplify granule cell activity, so it is likely that PLT fibers serve a similar purpose, but this highly dependent upon which cells they contact. Further ultrastructural analyses using immunoperoxidase localization of the tracer combined with immunogold labeling of markers for Purkinje cells (calbindin; (Nordquist et al., 1988)), Golgi cells (glycine; (Ottersen et al., 1988)), MLIs (nNOS; (Tsuda et al., 2013)) or granule cells (vGluT1; (Fremeau et al., 2001; Hioki et al., 2003)) will reveal which of the cortical cell types are contacted by PLT fibers and will help to inform how these fibers affect on-going cortical processing.

5.5 FINAL REMARKS

The studies presented in this dissertation help to answer key questions regarding the synaptic organization of the deep cerebellar nuclei. We have presented evidence for a local circuit network linking PPNs and NOPNs which each receive segregated PC inputs, closed

OCNO loop circuits, and a novel nucleo-cortical projection stemming from the parvocellular interpositus nucleus. Together the data strongly argue that the DCN possess the neuronal circuitry necessary to meaningfully impact cerebellar output and open new avenues for exploring the dynamic contributions of the DCN to the myriad of behaviors under the cerebellum's influence.

BIBLIOGRAPHY

Adler, E.S., Hollis, J.H., Clarke, I.J., Grattan, D.R., and Oldfield, B.J. (2012). Neurochemical characterization and sexual dimorphism of projections from the brain to abdominal and subcutaneous white adipose tissue in the rat. The Journal of neuroscience : the official journal of the Society for Neuroscience *32*, 15913-15921.

Agassandian, K., Shan, Z., Raizada, M., Sved, A.F., and Card, J.P. (2012). C1 catecholamine neurons form local circuit synaptic connections within the rostroventrolateral medulla of rat. Neuroscience *227*, 247-259.

Ahn, A.H., Dziennis, S., Hawkes, R., and Herrup, K. (1994). The cloning of zebrin II reveals its identity with aldolase C. Development *120*, 10.

Airaksinen, M.S., Eilers, J., Garaschuk, O., Thoenen, H., Konnerth, A., and Meyer, M. (1997). Ataxia and altered dendritic calcium signaling in mice carrying a targeted null mutation of the calbindin D28k gene. Proceedings of the National Academy of Sciences of the United States of America *94*, 6.

Aizenman, C., Huang, E., and Linden, D.J. (2003). Morphological Correlates of Intrinsic Electrical Excitability in Neurons of the Deep Cerebellar Nuclei. Journal of Neurophysiology *89*, 10.

Albus, J.S. (1971). A Theory of Cerebellar Function. Mathematical Biosciences *10*, 37.

Angelucci, A., Clascá, F., and Sur, M. (1996). Anterograde axonal tracing with the subunit B of cholera toxin: a highly sensitive immunohistochemical protocol for revealing fine axonal morphology in adult and neonatal brains. Journal of neuroscience methods *65*, 12.

Angulo, A., Fernández, E., Merchán, J.A., and Molina, M. (1996). A reliable method for Golgi staining of retina and brain slices. Journal of neuroscience methods *66*, 5.

Ankri, L., Husson, Z., Pietrajtis, K., Proville, R., Léna, C., Yarom, Y., Dieudonne, S., and Uusisaari, M. (2015). A novel inhibitory nucleo-cortical circuit controls cerebellar Golgi cell activity. eLife, 26.

Apps, R., and Hawkes, R. (2009). Cerebellar cortical organization: a one-map hypothesis. Nature reviews Neuroscience *10*, 670-681.

Armstrong, C.L., Chung, S.H., Armstrong, J.N., Hochgeschwender, U., Jeong, Y.G., and Hawkes, R. (2009). A novel somatostatin-immunoreactive mossy fiber pathway associated with HSP25-immunoreactive purkinje cell stripes in the mouse cerebellum. The Journal of comparative neurology *517*, 524-538.

Armstrong, C.L., Krueger-Naug, A.R., Currie, R.W., and Hawkes, R. (2001). Expression of Heat-Shock Protein Hsp25 in Mouse Purkinje Cells During Development Reveals Novel Features of Cerebellar Complartmentalization. The Journal of comparative neurology *429*, 15.

Asante, C.O., and Martin, J.H. (2013). Differential joint-specific corticospinal tract projections within the cervical enlargement. PLoS One *8*, e74454.

Bagnall, M.W., Zingg, B., Sakatos, A., Moghadam, S.H., Zeilhofer, H.U., and du Lac, S. (2009). Glycinergic projection neurons of the cerebellum. The Journal of neuroscience : the official journal of the Society for Neuroscience *29*, 10104-10110.

Banfield, B.W., Kaufman, J.D., Randall, J.A., and Pickard, G.E. (2003). Development of Pseudorabies Virus Strains Expressing Red Fluorescent Proteins: New Tools for Multisynaptic Labeling Applications. Journal of virology *77*, 10106-10112.

Barmack, N.H., and Hess, D.T. (1980). Multiple-Unit Activity Evoked in Dorsal Cap of Inferior Olive of the Rabbit by Visual Stimulation. Journal of Neurophysiology *43*, 14.

Batini, C., Buisseret-Delmas, C., Compoint, C., and Daniel, H. (1989). The GABAergic neurones of the cerebellar nuclei in the rat: projections to the cerebellar cortex. Neuroscience Letters *99*, 7.

Batini, C., Compoint, C., Buisseret-Delmas, C., Daniel, H., and Guegan, M. (1992). Cerebellar Nuclei and the Nucleocortical Projections in the Rat: Retrograde Tracing Coupled to GABA and Glutamate Immunohistochemistry. The Journal of comparative neurology *315*, 11.

Beitz, A., and Chan-Palay, V. (1979a). A Golgi Analysis of Neuronal Organization in the Medial Cerebellar Nucleus of the Rat. Neuroscience *4*, 17.

Beitz, A., and Chan-Palay, V. (1979b). The Medial Cerebellar Nucleus in the Rat: Nuclear Volume, Cell Number, Density and Orientation. Neuroscience *4*, 15.

Bernard, C., and Axelrad, H. (1993). Effects of recurrent collateral inhibition on Purkinje cell activity in the immature rat cerebellar cortex--an in vivo electrophysiological study. Brain research *626*, 25.

Billig, I., and Balaban, C.D. (2004). Zonal organization of the vestibulo-cerebellum in the control of horizontal extraocular muscles using pseudorabies virus: I. Flocculus/ventral paraflocculus. Neuroscience *125*, 507-520.

Billig, I., Foris, J.M., Enquist, L.W., Card, J.P., and Yates, B.J. (2000). Definition of Neuronal Circuitry Controlling the Activity of Phrenic and Abdominal Motoneurons in the Ferret Using Recombinant Strains of Pseudorabies Virus. The Journal of neuroscience : the official journal of the Society for Neuroscience *20*, 9.

Bishop, G. (1982). The pattern of distribution of the local axonal collaterals of Purkinje cells in the intermediate cortex of the anterior lobe and paramedian lobule of the cat cerebellum. The Journal of comparative neurology *210*, 9.

Blot, A., and Barbour, B. (2014). Ultra-rapid axon-axon ephaptic inhibition of cerebellar Purkinje cells by the pinceau. Nature neuroscience *17*, 289-295.

Bobik, M., Ellisman, M.H., Rudy, B., and Martone, M.E. (2004). Potassium channel subunit Kv3.2 and the water channel aquaporin-4 are selectively localized to cerebellar pinceau. Brain research *1026*, 168-178.

Boele, H.J., Koekkoek, S.K., and De Zeeuw, C.I. (2010). Cerebellar and extracerebellar involvement in mouse eyeblink conditioning: the ACDC model. Frontiers in cellular neuroscience *3*, 19.

Boldogkoi, Z., Reichart, A., Tóth, I.E., Sik, A., Erdélyi, F., Medveczky, I., Llorens, C., C., Palkovits, M., and Lenkei, Z. (2002). Construction of recombinant pseudorabies viruses optimized for labeling and neurochemical characterization of neural circuitry. Molecular Brain Research *109*, 14.

Bostan, A.C., Dum, R.P., and Strick, P.L. (2010). The basal ganglia communicate with the cerebellum. Proceedings of the National Academy of Sciences of the United States of America *107*, 8452-8456.

Bostan, A.C., Dum, R.P., and Strick, P.L. (2013). Cerebellar networks with the cerebral cortex and basal ganglia. Trends in cognitive sciences *17*, 241-254.

Bostan, A.C., and Strick, P.L. (2010). The cerebellum and basal ganglia are interconnected. Neuropsychology review *20*, 261-270.

Boyden, E.S., Katoh, A., and Raymond, J.L. (2004). Cerebellum-dependent learning: the role of multiple plasticity mechanisms. Annual review of neuroscience *27*, 581-609.

Brochu, G., Maler, L., and Hawkes, R. (1990). Zebrin II: a polypeptide antigen expressed selectively by Purkinje cells reveals compartments in rat and fish cerebellum. The Journal of comparative neurology *291*, 15.

Callaway, E.M. (2008). Transneuronal circuit tracing with neurotropic viruses. Current opinion in neurobiology *18*, 617-623.

Campolattaro, M.M., and Freeman, J.H. (2008). Eyeblink conditioning in 12-day-old rats using pontine stimulation as the conditioned stimulus. Proceedings of the National Academy of Sciences of the United States of America *105*, 8120-8123.

Cano, G., Card, J.P., and Sved, A.F. (2004). Dual viral transneuronal tracing of central autonomic circuits involved in the innervation of the two kidneys in rat. The Journal of comparative neurology *471*, 462-481.

Cano, G., Sved, A.F., Rinaman, L., Rabin, B.S., and Card, J.P. (2001). Characterization of the Central Nervous System Innervation of the Rat Spleen Using Viral Transneuronal Tracing. The Journal of comparative neurology *439*, 18.

Card, J.P., and Enquist, L.W. (1994). The use of neurotropic herpesviruses for defining synaptically linked populations of neurons in the central nervous system. . In Methods In Molecular Genetics, Molecular Virology Techniques Part A, K.W. Adolph, ed. (San Diego: Academic Press), pp. 363-382.

Card, J.P., and Enquist, L.W. (2014). Transneuronal circuit analysis with pseudorabies viruses. Current protocols in neuroscience / editorial board, Jacqueline N Crawley [et al] *68*, 1 5 1-39.

Card, J.P., Kobiler, O., Ludmir, E.B., Desai, V., Sved, A.F., and Enquist, L.W. (2011a). A dual infection pseudorabies virus conditional reporter approach to identify projections to collateralized neurons in complex neural circuits. PLoS One *6*, e21141.

Card, J.P., Kobiler, O., McCambridge, J., Ebdlahad, S., Shan, Z., Raizada, M.K., Sved, A.F., and Enquist, L.W. (2011b). Microdissection of neural networks by conditional reporter expression from a Brainbow herpesvirus. Proceedings of the National Academy of Sciences of the United States of America *108*, 3377-3382.

Card, J.P., Richard, M., Enquist, L.W., and Wojaczynski, G.J. (2014). Evidence for Transneuronal Passage of Pseudorabies Virus Through Gap Junctions (Presented as a poster for the *Society for Neuroscience* annual conference).

Card, J.P., Rinaman, L., Lynn, R.B., Lee, B.H., Meade, R.P., Miselis, R.R., and Enquist, L.W. (1993). Pseudorabies Virus Infection of the Rat Central Nervous System: Ultrastructural Characterization of Viral Replication, Transport, and Pathogenesis. The Journal of neuroscience : the official journal of the Society for Neuroscience *13*, 25.

Card, J.P., Schwaber, J.S., Miselis, R.R., Whealy, M.E., Robbins, A.K., and Enquist, L.W. (1990). Neurotropic Properties of Pseudorabies Virus: Uptake and Transneuronal Passage in the Rat Central Nervous System. The Journal of neuroscience : the official journal of the Society for Neuroscience *10*, 21.

Card, J.P., Sved, J.C., Craig, B., Raizada, M., Vazquez, J., and Sved, A.F. (2006). Efferent projections of rat rostroventrolateral medulla C1 catecholamine neurons: Implications for the central control of cardiovascular regulation. The Journal of comparative neurology *499*, 840-859.

Card, J.P., Volk, D.W., Sengupta, E.J., Steren, K.E., Khan, N.Z., and Wojaczynski, G.J. (2013). The Cytoarchitecture and Neurochemical Profile of the Rat Deep Cerebellar Nuclei with a Focus upon Nucleus Interpositus. (Presented as a poster for the *Society for Neuroscience* annual conference).

Carrel, A.J., Zbarska, S., Zenitsky, G.D., and Bracha, V. (2012). A trigeminal conditioned stimulus yields fast acquisition of cerebellum-dependent conditioned eyeblinks. Behavioural brain research *226*, 189-196.

Cerminara, N.L., Aoki, H., Loft, M., Sugihara, I., and Apps, R. (2013). Structural basis of cerebellar microcircuits in the rat. The Journal of neuroscience : the official journal of the Society for Neuroscience *33*, 16427-16442.

Chan-Palay, V. (1971). The recurrent collaterals of Purkinje cell axons: a correlated study of the rat's cerebellar cortex with electron microscopy and the Golgi method. Zeitschrift für Anatomie und Entwicklungsgeschichte *134*, 35.

Chan-Palay, V. (1973a). Axon Terminals of the Intrinsic Neurons in the Nucleus Lateralis of the Cerebellum: An Electron Microscope Study. Zeitschrift für Anatomie und Entwicklungsgeschichte *142*, 20.

Chan-Palay, V. (1973b). Cytology and Organization in the Nucleus Lateralis of the Cerebellum: The Projection of Neurons and Their Processes into Afferent Axon Bundles. Zeitschrift für Anatomie und Entwicklungsgeschichte *141*, 9.

Chan-Palay, V. (1973c). Neuronal Circuitry in the Nucleus Lateralis of the Cerebellum. Zeitschrift für Anatomie und Entwicklungsgeschichte *142*, 7.

Chan-Palay, V. (1973d). On the Identification of the Afferent Axon Terminals in the Nucleus Lateralis of the Cerebellum: An Electron Microscope Study. Zeitschrift für Anatomie und Entwicklungsgeschichte *142*, 38.

Chen, F.P., and Evinger, C. (2006). Cerebellar modulation of trigeminal reflex blinks: interpositus neurons. The Journal of neuroscience : the official journal of the Society for Neuroscience *26*, 10569-10576.

Christian, K.M., and Thompson, R.F. (2003). Neural substrates of eyeblink conditioning: acquisition and retention. Learning & memory *10*, 30.

Cicero, T.J., Sharpe, L.G., Robins, E., and Grote, S.S. (1972). Regional distribution of tyrosine hydroxylase in rat brain. Journal of Neurochemistry *19*, 3.

Clark, G., McCormick, D., Lavond, D., and Thompson, R.F. (1984). Effects of lesions of cerebellar nuclei on conditioned behavioral and hippocampal neuronal responses. Brain research *291*, 12.

Collazos-Castro, J.E., Soto, V.M., Gutiérrez-Dávila, M., and Nieto-Sampedro, M. (2005). Motoneuron Loss Associated with Chronic Locomotion Impairments after Spinal Cord Contusion in the Rat. Journal of Neurotrauma *22*, 15.

Czubayko, U., Sultan, F., Thier, P., and Schwarz, C. (2001). Two Types of Neurons in the Rat Cerebellar Nuclei as Distinguished by Membrane Potentials and Intracellular Fillings. Journal of Neurophysiology, 13.

D'Angelo, E., and De Zeeuw, C.I. (2009). Timing and plasticity in the cerebellum: focus on the granular layer. Trends in neurosciences *32*, 30-40.

D'Mello, A.M., and Stoodley, C.J. (2015). Cerebro-cerebellar circuits in autism spectrum disorder. Frontiers in neuroscience *9*, 408.

Daniel, H., Billard, J.M., Angaut, P., and Batini, C. (1987). The interposito-rubrospinal system. Anatomical tracing of a motor control pathway in the rat. Neuroscience research *5*, 26.

de Solages, C., Szapiro, G., Brunel, N., Hakim, V., Isope, P., Buisseret, P., Rousseau, C., Barbour, B., and Lena, C. (2008). High-frequency organization and synchrony of activity in the purkinje cell layer of the cerebellum. Neuron *58*, 775-788.

De Zeeuw, C.I., and Berrebi, A. (1995a). Individual Purkinje Cell Axons Terminate on Both Inhibitory and Excitatory Neurons in the Cerebellar and Vestibular Nuclei. Annals of the New York Academy of Sciences *781*, 4.

De Zeeuw, C.I., and Berrebi, A. (1995b). Postsynaptic Targets of Purkinje Cell Terminals in the Cerebellar and Vestibular Nulcei of the Rat. The European journal of neuroscience *7*, 12.

De Zeeuw, C.I., Digiorgi, P., and Simpson, J. (1994). Projections of individual Purkinje cells of identified zones in the flocculus to the vestibular and cerebellar nuclei in the rabbit. The Journal of comparative neurology *349*, 20.

De Zeeuw, C.I., Hertzberg, E.L., and Mugnaini, E. (1995). The Dendritic Lamellar Body: A New Neuronal Organelle Putatively Associated with Dendrodendritic Gap Junctions. The Journal of neuroscience : the official journal of the Society for Neuroscience *15*, 18.

De Zeeuw, C.I., Hostege, J.C., Ruigrok, T.J., and Voogd, J. (1989). Ultrastructural Study of the GABAergic, Cerebellar, and Mesodiencephalic Innervation of the Cat Medial Accessory Olive: Anterograde Tracing Combined with Immunocytochemistry. The Journal of comparative neurology *284*, 24.

De Zeeuw, C.I., Simpson, J., Hoogenraad, C., Galjart, N., Koekkoek, S.K., and Ruigrok, T.J. (1998). Microcircuitry and function of the inferior olive. Trends in neurosciences *21*, 10.

De Zeeuw, C.I., Van Alphen, A.M., Hawkins, R.K., and Ruigrok, T.J. (1997). Climbing Fibre Collaterals Contact Neurons in the Cerebellar Nuclei that Provide a GABAergic Feedback to the Inferior Olive. Neuroscience *80*, 6.

Derbenev, A.V., Duale, H., Rabchevsky, A.G., and Smith, B.N. (2010). Electrophysiological characteristics of identified kidney-related neurons in adult rat spinal cord slices. Neurosci Lett *474*, 168-172.

Desmond, J.E., and Fiez, J.A. (1998). Neuroimaging studies of the cerebellum: language, learning and memory. Trends in cognitive sciences *2*, 8.

Dietrichs, E., and Haines, D. (1989). Interconnections between hypothalamus and cerebellum. Anatomy and Embryology *179*, 14.

Dijkstra, C.D., Döpp, E.A., Joling, P., and Kraal, G. (1985). The heterogeneity of mononuclear phagocytes in lymphoid organs: distinct macrophage subpopulations in the rat recognized by monoclonal antibodies ED1, ED2 and ED3. Immunology *54*, 11.

Dix, R.D., Baringer, J.R., Panitch, H.S., Rosenberg, S.H., Hagedorn, J., and Whaley, J. (1983a). Recurrent herpes simplex encephalitis: recovery of virus after Ara-A treatment. Ann Neurol *13*, 5.

Dix, R.D., McKendall, R.R., and Baringer, J.R. (1983b). Comparative Neruovirulence of Herpes Simplex Virus Type 1 Strains After Peripheral or Intracerebral Inoculation of BALB/c Mice. Infection and Immunity *40*, 10.

Dobson, K.L., and Bellamy, T.C. (2015). Localization of Presynaptic Plasticity Mechanisms Enables Functional Independence of Synaptic and Ectopic Transmission in the Cerebellum. Neural plasticity *2015*, 602356.

Dolan, R. (1998). A cognitive affective role for the cerebellum. Brain: A Journal of Neurology *121*, 2.

Dum, R.P., Li, C., and Strick, P.L. (2002). Motor and Nonmotor Domains in the Monkey Dentate. Ann NY Acad Sci *978*, 12.

Dum, R.P., and Strick, P.L. (2003). An unfolded map of the cerebellar dentate nucleus and its projections to the cerebral cortex. J Neurophysiol *89*, 634-639.

Eccles, J.C., Llinas, R.R., and Sasaki, K. (1964). Excitation of Cerebellar Purkinje Cells by the Climbing Fibres. Nature *203*, 2.

Eccles, J.C., Llinas, R.R., and Sasaki, K. (1966). The Excitatory Synaptic Action of Climbing Fibres on the Purkinje Cells of the Cerebellum. Journal of Physiology *182*, 29.

Flaten, M., and Blumenthal, T. (1998). A parametric study of the separate contributions of the tactile and acoustic components of airpuffs to the blink reflex. Biological Psychology *48*, 8.

Fredette, B.J., and Mugnaini, E. (1991). The GABAergic cerebello-olivary projection in the rat. Anatomy and Embryology *184*, 19.

Freeman, J.H., Jr., Halverson, H.E., and Poremba, A. (2005). Differential effects of cerebellar inactivation on eyeblink conditioned excitation and inhibition. The Journal of neuroscience : the official journal of the Society for Neuroscience *25*, 889-895.

Freeman, J.H., and Steinmetz, A.B. (2011). Neural circuitry and plasticity mechanisms underlying delay eyeblink conditioning. Learning & memory *18*, 12.

Freeman, J.H.J., and Nicholson, D.A. (2000). Developmental changes in eye-blink conditioning and neuronal activity in the cerebellar interpositus nucleus. Journal of neuroscience methods *20*, 7.

Fremeau, R.T., Troyer, M.D., Pahner, I., Nygaard, G.O., Tran, C.H., Reimer, R.J., Bellocchio, E.E., and Edwards, R.H. (2001). The Expression of Vesicular Glutamate Transporters Defines Two Classes of Excitatory Syanpse. Neuron *31*, 14.

Gao, Z., Proietti-Onori, M., Lin, Z., Ten Brinke, M.M., Boele, H.J., Potters, J.W., Ruigrok, T.J., Hoebeek, F.E., and De Zeeuw, C.I. (2016). Excitatory Cerebellar Nucleocortical Circuit Provides Internal Amplification during Associative Conditioning. Neuron *89*, 645-657.

Garcia, K., and Mauk, M.D. (1998). Pharmacological analysis of cerebellar contributions to the timing and expression of conditioned eyelid responses. Neuropharmacology *37*, 10.

Ghanem, A., and Conzelmann, K.K. (2015). G gene-deficient single-round rabies viruses for neuronal circuit analysis. Virus research.

Giaquinta, G., Casabona, A., Smecca, G., Bosco, G., and Perciavalle, V. (1999). Cortical control of cerebellar dentato-rubral and dentato-olivary neurons. NeuroReport *10*, 5.

Giuditta, M., Ruggiero, D.A., and Del Bo, A. (2009). Anatomical Basis for the Fastigial Pressor Response. Blood Pressure *12*, 175-180.

Glatzer, N.R., Hasney, C.P., Bhaskaran, M.D., and Smith, B.N. (2003). Synaptic and morphologic properties in vitro of premotor rat nucleus tractus solitarius neurons labeled transneuronally from the stomach. The Journal of comparative neurology *464*, 525-539.

Gonzalez-Joekes, J., and Schreurs, B.G. (2012). Anatomical characterization of a rabbit cerebellar eyeblink premotor pathway using pseudorabies and identification of a local modulatory network in anterior interpositus. The Journal of neuroscience : the official journal of the Society for Neuroscience *32*, 12472-12487.

Gonzalez, L., Shumway, C., Morissette, J., and Bower, J.M. (1993). Developmental plasticity in cerebellar tactile maps: fractured maps retain a fractured organization. The Journal of comparative neurology *332*, 12.

Gould, B.B., and Graybiel, A.M. (1976). Afferents to the cerebellar cortex in the cat: evidence for an intrinsic pathway leading from the deep nuclei to the cortex. Brain research *110*, 11.

Graham, D.J., and Wylie, D.R. (2012). Zebrin-immunopositive and -immunonegative stripe pairs represent functional units in the pigeon vestibulocerebellum. The Journal of neuroscience : the official journal of the Society for Neuroscience *32*, 12769-12779.

Haines, D., and Dietrichs, E. (1989). Nonsomatic Cerebellar Circuits: A Broader View of Cerebellar Involvement in Locomotion. Journal of Motor Behavior *21*, 8.

Halverson, H.E., and Freeman, J.H. (2010a). Medial auditory thalamic input to the lateral pontine nuclei is necessary for auditory eyeblink conditioning. Neurobiology of learning and memory *93*, 92-98.

Halverson, H.E., and Freeman, J.H. (2010b). Ventral lateral geniculate input to the medial pons is necessary for visual eyeblink conditioning in rats. Learning & memory *17*, 80-85.

Hámori, J., and Mezey, É. (1977). Serial and Triadic Synapses in the Cerebellar Nuclei of the Cat. Experimental brain research *30*, 15.

Hámori, J., and Takács, J. (1989). Two types of GABA-containing axon terminals in cerebellar glomeruli of cat: an immunogold-EM study. Experimental brain research *74*, 9.

Hámori, J., Takács, J., and Petrusz, P. (1990). Immunogold Electron Microscopic Demonstration of Glutamate and GABA in Normal and Deafferented Cerebellar Cortex: Correlation Between Transmitter Content and Syaptic Vescicle Size. The Journal of Histochemistry and Cytochemistry *38*, 11.

Hawkes, R., and Leclerc, N. (1989). Purkinje cell axon collateral distributions reflect the chemical compartmentation of the rat cerebellar cortex. Brain research *476*, 12.

Heck, D.H., Thach, W.T., and Keating, J.G. (2007). On-beam synchrony in the cerebellum as the mechanism for the timing and coordination of movement. Proceedings of the National Academy of Sciences of the United States of America *104*, 7658-7663.

Heiney, S.A., Kim, J., Augustine, G.J., and Medina, J.F. (2014a). Precise control of movement kinematics by optogenetic inhibition of Purkinje cell activity. The Journal of neuroscience : the official journal of the Society for Neuroscience *34*, 2321-2330.

Heiney, S.A., Wohl, M.P., Chettih, S.N., Ruffolo, L.I., and Medina, J.F. (2014b). Cerebellar-dependent expression of motor learning during eyeblink conditioning in head-fixed mice. The Journal of neuroscience : the official journal of the Society for Neuroscience *34*, 14845-14853.

Heinze, L., Harvey, R.J., Haverkamp, S., and Wassle, H. (2007). Diversity of glycine receptors in the mouse retina: localization of the alpha4 subunit. The Journal of comparative neurology *500*, 693-707.

Hesslow, G., and Ivarsson, M. (1996). Inhibition of the inferior olive during conditioned responses in the decerebrate ferret. Experimental brain research *110*, 11.

Hettigoda, N.S., Fong, A.Y., Badoer, E., McKinley, M.J., Oldfield, B.J., and Allen, A.M. (2015). Identification of CNS neurons with polysynaptic connections to both the sympathetic and parasympathetic innervation of the submandibular gland. Brain structure & function *220*, 2103-2120.

Hioki, H., Fujiyama, F., Taki, K., Tomioka, R., Furuta, T., Tamamaki, N., and Kaneko, T. (2003). Differential distribution of vesicular glutamate transporters in the rat cerebellar cortex. Neuroscience *117*, 1-6.

Hirano, T., Yamazaki, Y., and Nakamura, Y. (2016). LTD, RP, and Motor Learning. Cerebellum *15*, 51-53.

Hogri, R., Segalis, E., and Mintz, M. (2014). Cerebellar inhibitory output shapes the temporal dynamics of its somatosensory inferior olivary input. Cerebellum *13*, 452-461.

Hoover, J.E., and Strick, P.L. (1999). The Organization of Cerebellar and Basal Ganglia Outputs to Primary Motor Cortex as Revealed by Retrograde Transneuronal Transport of Herpes Simplex Virus Type 1. The Journal of neuroscience : the official journal of the Society for Neuroscience *19*, 18.

Horiuchi, T., and Kawahara, S. (2010). Effects of ipsilateral cerebellum ablation on acquisition and retention of classically conditioned eyeblink responses in rats. Neurosci Lett *472*, 148-152.

Hoshi, E., Tremblay, L., Feger, J., Carras, P.L., and Strick, P.L. (2005). The cerebellum communicates with the basal ganglia. Nature neuroscience *8*, 1491-1493.

Houck, B.D., and Person, A.L. (2014). Cerebellar loops: a review of the nucleocortical pathway. Cerebellum *13*, 378-385.

Houck, B.D., and Person, A.L. (2015). Cerebellar Premotor Output Neurons Collateralize to Innervate the Cerebellar Cortex. The Journal of comparative neurology *523*, 2254-2271.

Husson, Z., Rousseau, C.V., Broll, I., Zeilhofer, H.U., and Dieudonne, S. (2014). Differential GABAergic and glycinergic inputs of inhibitory interneurons and Purkinje cells to principal cells of the cerebellar nuclei. The Journal of neuroscience : the official journal of the Society for Neuroscience *34*, 9418-9431.

Ichinohe, N., Mori, F., and Shoumura, K. (2000). A di-synaptic projection from the lateral cerebellar nucleus to the laterodorsal part of the striatum via the central lateral nucleus of the thalamus in the rat. Brain research *880*, 7.

Ikeda, M., Houtani, T., Ueyama, T., and Sugimoto, T. (1991). Choline acetyltransferase immunoreactivity in the cat cerebellum. Neuroscience *45*, 20.

Ito, M. (1984). The Modifiable Neuronal Network of the Cerebellum. Japanese Journal of Physiology *34*, 12.

Ito, M. (2006). Cerebellar circuitry as a neuronal machine. Prog Neurobiol *78*, 32.

Ito, M. (2013). Error detection and representation in the olivo-cerebellar system. Frontiers in neural circuits *7*, 1.

Ito, M., and Kano, M. (1982). Long-lasting Depression of Parallel Fiber-Purkinje Cell Transmission Induced by Conjunctive Stimulation of Parallel Fibers and Climbing Fibers in the Cerebellar Cortex. Neuroscience Letters *33*, 6.

Ito, M., Yoshida, A., and Obata, K. (1964). Monosynaptic Inhibition of the Intracerebellar Nuclei Induced from the Cerebellar Cortex. Experientia *20*, 2.

Iwakura, A., Uchigashima, M., Miyazaki, T., Yamasaki, M., and Watanabe, M. (2012). Lack of molecular-anatomical evidence for GABAergic influence on axon initial segment of cerebellar Purkinje cells by the pinceau formation. The Journal of neuroscience : the official journal of the Society for Neuroscience *32*, 9438-9448.

Jaarsma, D., Ruigrok, T.J., Caffé, R., Cozzari, C., Levey, A.I., Mugnaini, E., and Voogd, J. (1997). Cholinergic innervation and receptors in the cerebellum. Progress in brain research *114*, 31.

Joseph, J.W., Shambes, G.M., Gibson, J.M., and Welker, W. (1978). Tactile projections to granule cells in caudal vermis of the rat's cerebellum. Brain Behav Evol *15*, 9.

Kamin, L.J. (1968). Attention-like processes in classical conditioning. In Miami Symposium on the Prediction of Behavior: Aversive Stimulation, M.R. Jones, ed. (Coral Gables: University of Miami Press).

Kampe, J., Tschop, M.H., Hollis, J.H., and Oldfield, B.J. (2009). An anatomic basis for the communication of hypothalamic, cortical and mesolimbic circuitry in the regulation of energy balance. The European journal of neuroscience *30*, 415-430.

Kelly, R.M., and Strick, P.L. (2003). Cerebellar Loops with Motor Cortex and Prefrontal Cortex of a Nonhuman Primate. The Journal of neuroscience : the official journal of the Society for Neuroscience *23*, 13.

Kim, J., Krupa, D., and Thompson, R.F. (1998). Inhibitory Cerebello-Olivary Projections and Blocking Effect in Classical Conditioning. Science *279*, 5.

Kim, J.S., Enquist, L.W., and Card, J.P. (1999). Circuit-specific coinfection of neurons in the rat central nervous system with two pseudorabies virus recombinants. Journal of virology *73*, 11.

Klupp, B.G., Hengartner, C.J., Mettenleiter, T.C., and Enquist, L.W. (2004). Complete, annotated sequence of the pseudorabies virus genome. Journal of virology *78*, 17.

Korneliussen, H. (1966). On the Morphology and Subdivision of the Cerebellar Nuclei of the Rat. Journal für Hirnforschung, 14.

Lanciego, J.L., and Wouterlood, F.G. (2011). A half century of experimental neuroanatomical tracing. Journal of chemical neuroanatomy *42*, 157-183.

Lavond, D., and Steinmetz, J.E. (1989). Acquisition of classical conditioning without cerebellar cortex. Behavioural brain research *33*, 52.

Lavond, D., Steinmetz, J.E., Yokaitis, M.H., and Thompson, R.F. (1987). Reacquisition of classical conditioning after removal of cerebellar cortex. Experimental brain research *67*, 25.

Lefler, Y., Yarom, Y., and Uusisaari, M.Y. (2014). Cerebellar inhibitory input to the inferior olive decreases electrical coupling and blocks subthreshold oscillations. Neuron *81*, 1389-1400.

Legendre, A., and Courville, J. (1987). Origin and Trajectory of the Cerebello-olivary Projection: An Experimental Study with Radioactive and Fluorescent Tracers in the Cat. Neuroscience *21*, 15.

Li, J., Hart, R.P., Mallimo, E.M., Swerdel, M.R., Kusnecov, A.W., and Herrup, K. (2013). EZH2-mediated H3K27 trimethylation mediates neurodegeneration in ataxia-telangiectasia. Nature neuroscience *16*, 1745-1753.

Libster, A.M., and Yarom, Y. (2013). In and out of the loop: external and internal modulation of the olivo-cerebellar loop. Frontiers in neural circuits *7*, 73.

Lisberger, S.G. (2009). Internal models of eye movement in the floccular complex of the monkey cerebellum. Neuroscience *162*, 763-776.

Lisberger, S.G. (2010). Visual guidance of smooth-pursuit eye movements: sensation, action, and what happens in between. Neuron *66*, 477-491.

Llinás, R.R. (1974). Eighteenth Bowditch Lecture: Motor Aspects of Cerebellar Control. The Physiologist *17*, 28.

Llinás, R.R. (2011). Cerebellar motor learning versus cerebellar motor timing: the climbing fibre story. Journal of Physiology *589*, 10.

Llinás, R.R. (2013). The olivo-cerebellar system: a key to understanding the functional significance of intrinsic oscillatory brain properties. Frontiers in neural circuits *7*, 96.

Loewy, A.D. (1998). Viruses as Transneuronal Tracers for Defining Neural Circuits. Neuroscience and biobehavioral reviews *22*, 6.

Luo, Y., and Sugihara, I. (2014). Cerebellar afferents originating from the medullary reticular formation that are different from mossy, climbing or monoaminergic fibers in the rat. Brain research *1566*, 31-46.

Luque, N.R., Garrido, J.A., Carrillo, R.R., D'Angelo, E., and Ros, E. (2014). Fast convergence of learning requires plasticity between inferior olive and deep cerebellar nuclei in a manipulation task: a closed-loop robotic simulation. Frontiers in computational neuroscience *8*, 97.

Mapelli, L., Pagani, M., Garrido, J.A., and D'Angelo, E. (2015). Integrated plasticity at inhibitory and excitatory synapses in the cerebellar circuit. Frontiers in cellular neuroscience *9*, 169.

Marr, D. (1969). A Theory of Cerebellar Cortex. Journal of Physiology *202*, 35.

Marzban, H., Sillitoe, R.V., Hoy, M., Chung, S.H., Rafuse, V.F., and Hawkes, R. (2004). Abnormal HNK-1 expression in the cerebellum of an N-CAM null mouse. Journal of Neurocytology *33*, 14.

Matsushida, M., and Ikeda, M. (1976). Projections from the lateral reticular nucleus to the cerebellar cortex and nuclei in the cat. Experimental brain research *24*, 19.

Matsushida, M., and Iwahori, N. (1971). Structural Organization of the Interpositus and the Dentate Nuclei. Brain research *35*, 20.

Mauk, M.D., Steinmetz, J.E., and Thompson, R.F. (1986). Classical conditioning using stimulation of the inferior olive as the unconditioned stimulus. Proceedings of the National Academy of Sciences of the United States of America *83*, 5.

McCormick, D., Clark, G., Lavond, D., and Thompson, R.F. (1982). Initial localization of the memory trace for a basic form of learning. Proceedings of the National Academy of Sciences of the United States of America *79*, 5.

McCormick, D., Lavond, D., Clark, G., Kettner, R., Rising, C., and Thompson, R.F. (1981). The engram found? Role of the cerebellum in classical conditioning of nicitating membrane and eyelide responses. Bulletin of the Psychonomic Society *18*, 3.

McCormick, D., and Thompson, R.F. (1984). Neuronal responses of the rabbit cerebellum during acquisition and performance of a classically conditioned nictitating membrane-eyelid response. The Journal of neuroscience : the official journal of the Society for Neuroscience *4*, 12.

McLean, I.W., and Nakane, P.K. (1974). Periodate-lysine-paraformaldehyde fixative. A new fixation for immunoelectron microscopy. J Histochem Cytochem *22*, 7.

Medina, J.F., and Lisberger, S.G. (2008). Links from complex spikes to local plasticity and motor learning in the cerebellum of awake-behaving monkeys. Nature neuroscience *11*, 1185-1192.

Medina, J.F., Repa, J.C., Mauk, M.D., and LeDoux, J.E. (2002). Parallels between cerebellum- and amygdala-dependent conditioning. Nature reviews Neuroscience *3*, 10.

Middleton, F.A., and Strick, P.L. (1998). Cerebellar output: motor and cognitive channels. Trends in cognitive sciences *2*, 7.

Middleton, F.A., and Strick, P.L. (2000). Basal ganglia and cerebellar loops: motor and cognitive circuits. Brain research reviews *31*, 15.

Middleton, F.A., and Strick, P.L. (2001). Cerebellar Projections to the Prefrontal Cortex of the Primate. The Journal of neuroscience : the official journal of the Society for Neuroscience *21*, 13.

Mihailoff, G.A. (1994). Identification of pontocerebellar axon collateral synaptic boutons in the rat cerebellar nuclei. Brain research *648*, 6.

Miller, L., Holdefer, R., and Houk, J. (2002). The Role of the Cerebellum in Modulating Voluntary Limb Movement Commands. Archives Italiennes de Biologie *140*, 9.

Mojtahedian, S., Kogan, D.R., Kanzawa, S.A., Thompson, R.F., and Lavond, D.G. (2007). Dissociaton of conditioned eye and limb responses in the cerebellar interpositus. Physiology & behavior *91*, 9-14.

Morcuende, S., Delgado-García, J.M., and Ugolini, G. (2002). Neuronal Premotor Networks Involved in Eyelid Responses: Retrograde Transneuronal Tracing with Rabies Virus from the Orbicularis Oculi Muscle in the Rat. The Journal of neuroscience : the official journal of the Society for Neuroscience *22*, 11.

Najac, M., and Raman, I.M. (2015). Integration of Purkinje cell inhibition by cerebellar nucleo-olivary neurons. The Journal of neuroscience : the official journal of the Society for Neuroscience *35*, 544-549.

Nelson, T.E., King, J.S., and Bishop, G. (1997). Distribution of tyrosine hydroxylase-immunoreactive afferents to the cerebellum differs between species. The Journal of comparative neurology *379*, 12.

Nordquist, D.T., Kozak, C.A., and Orr, H.T. (1988). cDNA Cloning and Characterization of Three Genes Uniquely Expressed in Cerebellum by Purkinje Neurons. The Journal of neuroscience : the official journal of the Society for Neuroscience *8*, 10.

O'Donnell, P., Lavín, A., Enquist, L.W., Grace, A.A., and Card, J.P. (1997). Interconnected Parallel Circuits between Rat Nucleus Accumbens and Thalamus Revealed by Retrograde Transsynaptic Transport of Pseudorabies Virus. The Journal of neuroscience : the official journal of the Society for Neuroscience *17*, 25.

Oakley, D.A., and Russell, I.S. (1972). Neocortical lesions and Pavlovian conditioning. Physiology & behavior *8*, 12.

Oberdick, J., Levinthal, F., and Levinthal, C. (1988). A Purkinje Cell Differentiation Marker Shows a Partial DNA Sequence Homology to the Cellular sis/PDGF2 Gene. Neuron *1*, 10.

Ohmae, S., and Medina, J.F. (2015). Climbing fibers encode a temporal-difference prediction error during cerebellar learning in mice. Nature neuroscience *18*, 1798-1803.

Oka, H., Yoshida, K., Yamamoto, T., and Samejima, A. (1985). Organization of Afferent Connections to the Lateral and Interpositus Cerebellar Nuclei from the Brainstem Relay Nuclei: a Horseradish Peroxidase Study in the Cat. Neuroscience research *2*, 13.

Orduz, D., and Llano, I. (2007). Recurrent axon collaterals underlie facilitating synapses between cerebellar Purkinje cells. Proceedings of the National Academy of Sciences of the United States of America *104*, 17831-17836.

Ottersen, O.P., Storm-Mathisen, J., and Somogyi, P. (1988). Colocalization of glycine-like and GABA-like immunoreactivities in Golgi cell terminals in the rat cerebellum: a postembedding light and electron microscopic study. Brain research *450*, 12.

Pacheco-Calderón, R., Carretero-Guillén, A., Delgado-García, J.M., and Gruart, A. (2012). Red nucleus neurons actively contribute to the acquisition of classically conditioned eyelid responses in rabbits. The Journal of neuroscience : the official journal of the Society for Neuroscience *32*, 15.

Perrett, S., Ruiz, B., and Mauk, M.D. (1993). Cerebellar Cortex Lesions Disrupt Learning-depedent Timing of Conditioned Eyelide Responses. The Journal of neuroscience : the official journal of the Society for Neuroscience *13*, 11.

Person, A.L., and Raman, I.M. (2012a). Purkinje neuron synchrony elicits time-locked spiking in the cerebellar nuclei. Nature *481*, 502-505.

Person, A.L., and Raman, I.M. (2012b). Synchrony and neural coding in cerebellar circuits. Frontiers in neural circuits *6*, 97.

Pickard, G.E., Smeraski, C.A., Tomlinson, C.C., Banfield, B.W., Kaufman, J.D., Wilcox, C.L., Enquist, L.W., and Sollars, P.J. (2002). Intravitreal injection of the attenuated pseudorabies virus PRV Bartha results in infection of the hamster suprachiasmatic nucleus only by retrograde transsynaptic transport via autonomic circuits. The Journal of neuroscience : the official journal of the Society for Neuroscience *22*, 10.

Pijpers, A., Apps, R., Pardoe, J., Voogd, J., and Ruigrok, T.J. (2006). Precise spatial relationships between mossy fibers and climbing fibers in rat cerebellar cortical zones. The Journal of neuroscience : the official journal of the Society for Neuroscience *26*, 12067-12080.

Pijpers, A., Voogd, J., and Ruigrok, T.J. (2005). Topography of olivo-cortico-nuclear modules in the intermediate cerebellum of the rat. The Journal of comparative neurology *492*, 193-213.

Pomeranz, L.E., Reynolds, A.E., and Hengartner, C.J. (2005). Molecular biology of pseudorabies virus: impact on neurovirology and veterinary medicine. Microbiology and molecular biology reviews : MMBR *69*, 462-500.

Popa, L.S., Streng, M.L., Hewitt, A.L., and Ebner, T.J. (2016). The Errors of Our Ways: Understanding Error Representations in Cerebellar-Dependent Motor Learning. Cerebellum *15*, 93-103.

Ramón y Cajal, S. (1995). Histology of the Nervous System, Vol II (New York, Oxford: Oxford University Press).

Rassnick, S., Enquist, L.W., Sved, A.F., and Card, J.P. (1998). Pseudorabies Virus-Induced Leukocyte Trafficking into the Rat Central Nervous System. Journal of virology *72*, 12.

Reeber, S.L., Otis, T.S., and Sillitoe, R.V. (2013). New roles for the cerebellum in health and disease. Frontiers in systems neuroscience *7*, 83.

Reiner, A., Veenman, C.L., Medina, L., Jiao, Y., Del Mar, N., and Honig, M. (2000). Pathway tracing using biotinylated dextran amines. Journal of neuroscience methods *103*, 15.

Rinaldo, L., and Hansel, C. (2013). Muscarinic acetylcholine receptor activation blocks long-term potentiation at cerebellar parallel fiber-Purkinje cell synapses via cannabinoid signaling. Proceedings of the National Academy of Sciences of the United States of America *110*, 11181-11186.

Rinaman, L., Card, J.P., and Enquist, L.W. (1993). Spatiotemporal Responses of Astrocytes, Ramified Microglia, and Brain Macrophages to Central Neuronal Infection with Pseudorabies Virus. The Journal of neuroscience : the official journal of the Society for Neuroscience *13*, 18.

Rinaman, L., and Schwartz, G. (2004). Anterograde transneuronal viral tracing of central viscerosensory pathways in rats. The Journal of neuroscience : the official journal of the Society for Neuroscience *24*, 2782-2786.

Rubio, F.J., Bueno, C., Villa, A., Navarro, B., and Martínez-Serrano, A. (2000). Genetically perpetuated human neural stem cells engraft and differentiate into the adult mammalian brain. Molecular and cellular neurosciences *16*, 1-13.

Ruigrok, T.J. (2011). Ins and outs of cerebellar modules. Cerebellum *10*, 464-474.

Ruigrok, T.J., and Teune, T.M. (2014). Collateralization of cerebellar output to functionally distinct brainstem areas. A retrograde, non-fluorescent tracing study in the rat. Frontiers in systems neuroscience *8*, 23.

Ruigrok, T.J., and Voogd, J. (1990). Cerebellar nucleo-olivary projections in the rat: an anterograde tracing study with Phaseolus vulgaris-leucoagglutinin (PHA-L). The Journal of comparative neurology *298*, 19.

Ruigrok, T.J., and Voogd, J. (2000). Organization of Projections from the Inferior Olive to the Cerebellar Nuclei in the Rat. The Journal of comparative neurology *426*, 20.

Sanchez-Campusano, R., Gruart, A., and Delgado-García, J.M. (2011). Dynamic changes in the cerebellar-interpositus/red-nucleus-motoneuron pathway during motor learning. Cerebellum *10*, 702-710.

Sanchez-Gonzalez, M.A., Garcia-Cabezas, M.A., Rico, B., and Cavada, C. (2005). The primate thalamus is a key target for brain dopamine. The Journal of neuroscience : the official journal of the Society for Neuroscience *25*, 6076-6083.

Schmahmann, J.D. (2004). Disorders of the Cerebellum: Ataxia, Dysmetria of Thought, and the Cerebellar Cognitive Affective Syndrome. Neuropsychiatric Practice and Opinion *16*, 12.

Schmahmann, J.D. (2010). The role of the cerebellum in cognition and emotion: personal reflections since 1982 on the dysmetria of thought hypothesis, and its historical evolution from theory to therapy. Neuropsychology review *20*, 236-260.

Schmahmann, J.D., and Schmahmann, J.C. (1998). The cerebellar cognitive affective syndrome. Brain: A Journal of Neurology *121*, 19.

Schmahmann, J.D., Weilburg, J.B., and Sherman, J.C. (2007). The neuropsychiatry of the cerebellum — insights from the clinic. The Cerebellum *6*, 254-267.

Schmued, L.C., and Fallon, J.H. (1986). Fluoro-Gold: a new fluorescent retrograde axonal tracer with numerous unique properties. Brain research *377*, 8.

Schonewille, M., Gao, Z., Boele, H.J., Veloz, M.F., Amerika, W.E., Simek, A.A., De Jeu, M.T., Steinberg, J.P., Takamiya, K., Hoebeek, F.E., *et al.* (2011). Reevaluating the role of LTD in cerebellar motor learning. Neuron *70*, 43-50.

Schwarz, L.A., Miyamichi, K., Gao, X.J., Beier, K.T., Weissbourd, B., DeLoach, K.E., Ren, J., Ibanes, S., Malenka, R.C., Kremer, E.J., *et al.* (2015). Viral-genetic tracing of the input-output organization of a central noradrenaline circuit. Nature *524*, 88-92.

Schweighofer, N., Lang, E.J., and Kawato, M. (2013). Role of the olivo-cerebellar complex in motor learning and control. Frontiers in neural circuits *7*, 94.

Sears, L.L., and Steinmetz, J.E. (1991). Dorsal accessory inferior olive activity diminishes during acquisition of the rabbit classically conditioned eyelid response. Brain research *545*, 9.

Shambes, G.M., Gibson, J.M., and Welker, W. (1978). Fractured Somatotopy in Granule Cell Tactile Areas of Rat Cerebellar Hemispheres Revealed by Micromapping. Brain Behav Evol *15*, 47.

Shin, M., Moghadam, S.H., Sekirnjak, C., Bagnall, M.W., Kolkman, K.E., Jacobs, R., Faulstich, M., and du Lac, S. (2011). Multiple types of cerebellar target neurons and their circuitry in the vestibulo-ocular reflex. The Journal of neuroscience : the official journal of the Society for Neuroscience *31*, 10776-10786.

Shinoda, Y., Sugihara, I., Wu, H., and Sugiuchi, Y. (2000). The entrire trajectory of single climbing and mossy fibers in the cerebellar nuclei and cortex. Progress in brain research *124*, 13.

Shinoda, Y., Sugiuchi, Y., Futami, T., and Izawa, R. (1992). Axon Collaterals of Mossy Fibers From the Pontine Nucleus in the Cerebellar Dentate Nucleus. Journal of Neurophysiology *67*, 14.

Smith, B.N., Banfield, B.W., Smeraski, C.A., Wilcox, C.L., Dudek, F.E., Enquist, L.W., and Pickard, G.E. (2000). Pseudorabies virus expressing enhanced green fluorescent protein: A tool for *in vitro* electrophysiological analysis of transsynaptically labeled neurons in identified central nervous system circuits. Proceedings of the National Academy of Sciences of the United States of America *97*, 6.

Song, C.K., Enquist, L.W., and Bartness, T.J. (2005). New developments in tracing neural circuits with herpesviruses. Virus research *111*, 235-249.

Stanley, S., Pinto, S., Segal, J., Pérez, C.A., Viale, A., DeFalco, J., Cai, X., Heisler, L.K., and Friedman, J.M. (2010). Identification of neuronal subpopulations that project from hypothalamus to both liver and adipose tissue polysynaptically. Proceedings of the National Academy of Sciences of the United States of America *107*, 6.

Steinmetz, A.B., and Freeman, J.H. (2014). Localization of the cerebellar cortical zone mediating acquisition of eyeblink conditioning in rats. Neurobiology of learning and memory *114*, 148-154.

Steinmetz, J.E., Lavond, D., and Thompson, R.F. (1989). Classical Conditioning in Rabbits Using Pontine Stimulation as a Conditioned Stimulus and Inferior Olive Stimulation as an Unconditioned Stimulus. Synapse *3*, 9.

Stoodley, C.J. (2014). Distinct regions of the cerebellum show gray matter decreases in autism, ADHD, and developmental dyslexia. Frontiers in systems neuroscience *8*, 92.

Strick, P.L., and Card, J.P. (1992). Transneuronal mapping of neural circuits with alpha herpesviruses. (Oxford: Oxford University Press).

Strick, P.L., and Card, J.P. (2011). Viral Transneuronal Tracing Technology: Defining the Synaptic Organisation of Neural Circuits. In eLS (John Wiley & Sons, Ltd).

Strick, P.L., Dum, R.P., and Fiez, J.A. (2009). Cerebellum and nonmotor function. Annual review of neuroscience *32*, 413-434.

Sugihara, I. (2011). Compartmentalization of the deep cerebellar nuclei based on afferent projections and aldolase C expression. Cerebellum *10*, 449-463.

Sugihara, I., Fujita, H., Na, J., Quy, P.N., Li, B.Y., and Ikeda, D. (2009). Projection of reconstructed single Purkinje cell axons in relation to the cortical and nuclear aldolase C compartments of the rat cerebellum. The Journal of comparative neurology *512*, 282-304.

Sugihara, I., and Shinoda, Y. (2004). Molecular, topographic, and functional organization of the cerebellar cortex: a study with combined aldolase C and olivocerebellar labeling. The Journal of neuroscience : the official journal of the Society for Neuroscience *24*, 8771-8785.

Sugihara, I., and Shinoda, Y. (2007). Molecular, topographic, and functional organization of the cerebellar nuclei: analysis by three-dimensional mapping of the olivonuclear projection and aldolase C labeling. The Journal of neuroscience : the official journal of the Society for Neuroscience *27*, 9696-9710.

Sugihara, I., Wu, H., and Shinoda, Y. (1999). Morphology of Single Olivocerebellar Axons Labeled with Biotinylated Dextran Amine in the Rat. The Journal of comparative neurology *414*, 18.

Sugihara, I., Wu, H., and Shinoda, Y. (2001). The entire trajectories of single olivocerebellar axons in the cerebellar cortex and their contribution to Cerebellar compartmentalization. The Journal of neuroscience : the official journal of the Society for Neuroscience *21*, 9.

Sun, L.W. (2012). Transsynaptic tracing of conditioned eyeblink circuits in the mouse cerebellum. Neuroscience *203*, 122-134.

Svensson, P., Bengtsson, F., and Hesslow, G. (2006). Cerebellar inhibition of inferior olivary transmission in the decerebrate ferret. Experimental brain research *168*, 241-253.

Swanson, L.W. (2004). Brain Maps III: Structure of the Rat Brain, 3 edn (Elsevier, Inc.).

Taylor, J.A., and Ivry, R.B. (2014). Cerebellar and prefrontal cortex contributions to adaptation, strategies, and reinforcement learning. Progress in brain research *210*, 217-253.

Teune, T., Van der Burg, J., De Zeeuw, C.I., Voogd, J., and Ruigrok, T.J. (1998). Single Purkinje Cell Can Innervate Multiple Classes of Projection Neurons in the Cerebellar Nuclei of the Rat: A Light Microscopic and Ultrastructural Triple-Tracer Study in the Rat. The Journal of comparative neurology *392*, 15.

Teune, T., van der Burg, J., and Ruigrok, T.J. (1995). Cerebellar projections to the red nucleus and inferior olive originate from separate populations of neurons in the rat: a non-fluorescent double labeling study. Brain research *673*, 7.

Thompson, R.F. (2013). An essential memory trace found. Behavioral neuroscience *127*, 7.

Thompson, R.F., and Krupa, D. (1994). Organization of memory traces in the mammalian brain. Annual review of neuroscience *17*, 31.

Thompson, R.F., and Steinmetz, J.E. (2009). The role of the cerebellum in classical conditioning of discrete behavioral responses. Neuroscience *162*, 732-755.

Tolbert, D.L., Bantli, H., and Bloedel, J. (1976). Anatomical and Physiological Evidence for a Cerebellar Nucleo-Cortical Projection in the Cat. Neuroscience *1*, 16.

Trott, J., Apps, R., and Armstrong, D. (1998a). Zonal organization of cortico-nuclear and nucleo-cortical projections of the paramedia lobule of the cat cerebellum. 1. The C1 zone. Experimental brain research *118*, 18.

Trott, J., Apps, R., and Armstrong, D. (1998b). Zonal organization of cortico-nuclear and nucleo-cortical projections of the paramedian lobule of the cat cerebellum. 2. The C2 zone. Experimental brain research *118*, 15.

Tsuda, S., Kee, M.Z., Cunha, C., Kim, J., Yan, P., Loew, L.M., and Augustine, G.J. (2013). Probing the function of neuronal populations: combining micromirror-based optogenetic photostimulation with voltage-sensitive dye imaging. Neuroscience research *75*, 76-81.

Tsutsumi, S., Yamazaki, M., Miyazaki, T., Watanabe, M., Sakimura, K., Kano, M., and Kitamura, K. (2015). Structure-function relationships between aldolase C/zebrin II expression and complex spike synchrony in the cerebellum. The Journal of neuroscience : the official journal of the Society for Neuroscience *35*, 843-852.

Tyrrell, T., and Willshaw, D. (1992). Cerebellar cortex: its simulation and the relevance of Marr's theory. Phil Trans R Soc Lond *336*, 19.

Umetani, T. (1990). Topographic organization of the cerebellar nucleocortical projection in the albino rat: an autoradiographic orthograde study. Brain research *507*, 9.

Uusisaari, M., and De Schutter, E. (2011). The mysterious microcircuitry of the cerebellar nuclei. The Journal of physiology *589*, 3441-3457.

Uusisaari, M., and Knöpfel, T. (2008). GABAergic synaptic communication in the GABAergic and non-GABAergic cells in the deep cerebellar nuclei. Neuroscience *156*, 537-549.

Uusisaari, M., and Knöpfel, T. (2010). GlyT2+ neurons in the lateral cerebellar nucleus. Cerebellum *9*, 42-55.

Uusisaari, M., and Knöpfel, T. (2011). Functional classification of neurons in the mouse lateral cerebellar nuclei. Cerebellum *10*, 637-646.

Uusisaari, M., Obata, K., and Knöpfel, T. (2007). Morphological and electrophysiological properties of GABAergic and non-GABAergic cells in the deep cerebellar nuclei. Journal of Neurophysiology *97*, 901-911.

Uusisaari, M.Y., and Knöpfel, T. (2012). Diversity of neuronal elements and circuitry in the cerebellar nuclei. Cerebellum *11*, 420-421.

Varea, E., Nácher, J., Blasco-Ibáñez, J.M., Gómez-Climent, M.A., Castillo-Gómez, E., Crespo, C., and Martínez-Guijarro, F.J. (2005). PSA-NCAM expression in the rat medial prefrontal cortex. Neuroscience *136*, 9.

Voogd, J., and Glickstein, M. (1998). The anatomy of the cerebellum. Trends in neurosciences *21*, 6.

Voogd, J., Pardoe, J., Ruigrok, T.J., and Apps, R. (2003). The distribution of climbing and mossy fiber collateral branches from the copula pyramidis and the paramedian lobule: congruence of climbing fiber cortical zones and the pattern of zebrin banding within the rat cerebellum. The Journal of neuroscience : the official journal of the Society for Neuroscience *23*, 12.

Voogd, J., and Ruigrok, T.J. (2004). The organization of the corticonuclear and olivocerebellar climbing fiber projections to the rat cerebellar vermis: The congruence of projection zones and the zebrin pattern. Journal of Neurocytology *33*, 17.

Voogd, J., Shinoda, Y., Ruigrok, T.J., and Sugihara, I. (2013). Cerebellar Nuclei and the Inferior Olivary Nuclei: Organization and Connections. In Handbook of the Cerebellum and Cerebellar Disorders, M. Manto, D.L. Gruold, J.D. Schmahmann, N. Koibuchi, and F. Rossi, eds. (Springer), pp. 377-436.

Wickersham, I.R., Lyon, D.C., Barnard, R.J., Mori, T., Finke, S., Conzelmann, K.K., Young, J.A., and Callaway, E.M. (2007). Monosynaptic restriction of transsynaptic tracing from single, genetically targeted neurons. Neuron *53*, 9.

Witter, L., and De Zeeuw, C.I. (2015). Regional functionality of the cerebellum. Current opinion in neurobiology *33*, 150-155.

Wojaczynski, G.J., Engel, E.A., Steren, K.E., Enquist, L.W., and Patrick Card, J. (2015). The neuroinvasive profiles of H129 (herpes simplex virus type 1) recombinants with putative anterograde-only transneuronal spread properties. Brain structure & function *220*, 1395-1420.

Woolf, N.J., and Butcher, L.L. (1989). Cholinergic systems in the rat brain: IV. Descending projections of the pontomesencephalic tegmentum. Brain Research Bulletin *23*, 24.

Yang, Y., Lei, C., Feng, H., and Sui, J.F. (2015). The neural circuitry and molecular mechanisms underlying delay and trace eyeblink conditioning in mice. Behavioural brain research *278*, 8.

Yeo, C.H., Hardiman, M.J., and Glickstein, M. (1985a). Classical conditioning of the nictitating membrane response of the rabbit. II. Lesions of the cerebellar cortex. Experimental brain research *60*, 15.

Yeo, C.H., Hardiman, M.J., and Glickstein, M. (1985b). Classical conditioning of the nictitating membrane response of the rabbit. III. Connections of cerebellar lobule HVI. Experimental brain research *60*, 9.

Zemanick, M.C., Strick, P.L., and Dix, R.D. (1991). Direction of transneuronal transport of herpes simplex virus 1 in the primate motor system is strain-dependent. Proceedings of the National Academy of Sciences of the United States of America *88*, 4.